REPORT DOCUMENTATION PAGE		READ INSTRUCTIONS BEFORE COMPLETING FORM
1. REPORT NUMBER SIO REFERENCE 85-23	2. GOVT ACCESSION NO.	3. RECIPIENT'S CATALOG NUMBER

4. TITLE (and Subtitle) SELECTIVE REVERBERATION CANCELLATION VIA ADAPTIVE BEAMFORMING	5. TYPE OF REPORT & PERIOD COVERED Summary
	6. PERFORMING ORG. REPORT NUMBER MPL-U-63/85

7. AUTHOR(s) Dimitrios Alexandrou	8. CONTRACT OR GRANT NUMBER(s) N00024-82-C-6400

9. PERFORMING ORGANIZATION NAME AND ADDRESS University of California, San Diego, Marine Physical Laboratory of the Scripps Institution of Oceanography, San Diego, CA 92152	10. PROGRAM ELEMENT, PROJECT, TASK AREA & WORK UNIT NUMBERS

11. CONTROLLING OFFICE NAME AND ADDRESS Naval Sea Systems Command, Department of the Navy, Code 63R, Washington, D.C. 20362	12. REPORT DATE December 1985
	13. NUMBER OF PAGES 154 pages

14. MONITORING AGENCY NAME & ADDRESS(if different from Controlling Office)	15. SECURITY CLASS. (of this report) UNCLASSIFIED
	15a. DECLASSIFICATION/DOWNGRADING SCHEDULE

16. DISTRIBUTION STATEMENT (of this Report)

Document cleared for public release; distribution unlimited.

17. DISTRIBUTION STATEMENT (of the abstract entered in Block 20, if different from Report)

18. SUPPLEMENTARY NOTES

19. KEY WORDS (Continue on reverse side if necessary and identify by block number)

adaptive beamforming, reverberation cancellation, adaptive algorithm, doppler sonar

20. ABSTRACT (Continue on reverse side if necessary and identify by block number)

The central theme of this thesis is the application of the adaptive beamforming concept to the problem of selective reverberation cancellation, with an emphasis on experimental verification. Oceanic reverberation is often a limiting form of interference in echo detection applications. It may also be the "signal" of interest conveying

DD FORM 1473 EDITION OF 1 NOV 65 IS OBSOLETE
1 JAN 73

S/N 0102-LF-014-6601

valuable information about the scatterers or physical processes influencing their dynamical behavior. Because of stringent limitations imposed by the oceanic medium on the directional characteristics of sonar systems, reverberation is often composite in nature with two or more unrelated reverberation types contributing to the acoustic return. In that setting it would be desirable to selectively cancel the unwanted reverberation component(s) while preserving the component of interest. This signal processing problem whereby both "signal" and "noise" are constituent components of the received reverberation process is the focus of this thesis. The related problem of extracting reflector echoes from a reverberation backround is also considered. Significant contributions of this thesis include:

(1) Exposing relevant reverberation properties. It was shown that the spatial correlation characteristics of volume and boundary reverberation are directly applicable in a reverberation cancellation context.

(2) Critically evaluating a representative cross-section of adaptive algorithmic solutions with special attention to recently developed deterministic least-squares structures. It was determined, based on theoretical predictions substantiated by computer simulations, that lattice filters outperform direct tapped-delay-line implementations and that deterministic least-squares structures are more suitable than stochastic approximation solutions for reverberation cancellation. In addition, the multichannel least-squares lattice was shown to offer a significant advantage over a cascade of scalar filters.

(3) Demonstrating experimentally the feasibility of selective reverberation cancellation with real and simulated data from a shallow-water experiment, a near-surface Doppler sonar deployment and a multibeam bathymetric system. A clear distinction emerged between adaptive noise cancelling with preformed reference beams and spatially adaptive beamforming obtained by operating on array elements with a multichannel joint-process filter. It was shown that significant signal enhancement as well as selective reverberation cancellation can be achieved through constrained adaptive techniques.

SELECTIVE REVERBERATION CANCELLATION
VIA ADAPTIVE BEAMFORMING

Dimitrios Alexandrou

SIO REFERENCE 85-23

December 1985

MPL-U-63/85

MARINE PHYSICAL LABORATORY

of the Scripps Institution of Oceanography,
San Diego, California 92152

UNIVERSITY OF CALIFORNIA, SAN DIEGO
MARINE PHYSICAL LABORATORY OF THE
SCRIPPS INSTITUTION OF OCEANOGRAPHY
SAN DIEGO, CA 92152

SELECTIVE REVERBERATION CANCELLATION
VIA ADAPTIVE BEAMFORMING

Dimitrios Alexandrou

SIO REFERENCE 85-23

December 1985

K. M. Watson, Director
Marine Physical Laboratory

MPL-U-63/85

Table of Contents

List of Figures

List of Tables

ACKNOWLEDGMENTS

This research was supported by the Naval Sea Systems Command, Code 63R14.

VITA

August 23, 1954 — Born — Thessaloniki, Greece.

1976 — B.S. Electrical Engineering, University of Illinois,
Champaign/Urbana, Illinois

1976-1978 — Teaching Assistant, University of Illinois,
Champaign/Urbana, Illinois

1978 — M.S. Electrical Engineering, University of Illinois,
Champaign/Urbana, Illinois

1978-1980 — Member of Technical Staff, Bell Telephone Laboratories,
Naperville, Illinois

1980-1985 — Research Assistant, Marine Physical Laboratory,
University of California, San Diego

1985 — Doctor of Philosophy
University of California, San Diego

PUBLICATIONS

D. Alexandrou, "Sea Beam Interference Cancellation" Proc. OCEANS conference, San Diego, Ca., Nov. 1985

W.S. Hodgkiss and D. Alexandrou, "Power Normalization Sensitivity of Adaptive Lattice Structures", IEEE Trans. Acous. Speech and Sig. Proc., Vol. ASSP-32, No. 4, pp. 925-928, Aug. 1984

W.S. Hodgkiss and D. Alexandrou, "Sea Surface Reveberation Rejection" IEEE Intl. Conf. on Acoust., Speech, Signal Process., San Diego, CA., pp. 33.7.1-33.7.4, March 1984

W.S. Hodgkiss and D. Alexandrou, "Application of Adaptive Linear Prediction Structures to the Prewhitening of Acoustic Reverberation Data", IEEE Intl. Conf. on Acoust., Speech, Signal Process., Boston, MA, pp. 559-602, 1983.

W.S. Hodgkiss and D. Alexandrou, "Applications of Adaptive Least-Squares Lattice Structures to problems in Underwater Acoustics", Proc. of the Society of Photo-Optical Instrumentation Engineers, San Diego, CA., pp. 21-26, Aug. 1983

D. Alexandrou and W.S. Hodgkiss, "Complex Adaptive Joint Process Algorithms", MPL TM-351, 22 November 1982, Marine Physical Laboratory, Scripps Institution of Oceanography, San Diego, CA (MPL-U-93/82)

D. Alexandrou and W.S. Hodgkiss, "Application of Adaptive Linear Prediction Structures to the Prewhitening of the ARL/PSU FY80 Field Test Data," MPL TM-346, 27 September 1982, Marine Physical Laboratory, Scripps Institution of Oceanography, San Diego CA (MPL-U-64/82)

D. Alexandrou and W.S. Hodgkiss, "Complex, Adaptive One-Step Linear Predictor Algorithms," MPL TM-341, 23 June 1982, Marine Physical Laboratory, Scripps Institution of Oceanography, San Diego CA (MPL-U-31/82)

D. Alexandrou and W.S. Hodgkiss, "Initial Processing of Selected Segments of the ARL/PSU FY80 Field Test Data: Run ASP 5.2, "MPL TM-340, 1 June 1982, Marine Physical Laboratory, Scripps Institution of Oceanography, San Diego CA (MPL-U-25/82)

D. Alexandrou and W.S. Hodgkiss, "Initial Processing of Selected Segments of the ARL/PSU FY80 Field Test Data: Run ASP 3.1, "MPL TM-339, 1 June 1982, Marine Physical Laboratory, Scripps Institution of Oceanography, San Diego CA (MPL-U-24/82)

D. Alexandrou and W.S. Hodgkiss, "Computer Programs for the Initial Processing of the ARL/PSU FY80 Field Test Data," MPL TM-338, 1 June 1982, Marine Physical Laboratory, Scripps Institution of Oceanography, San Diego CA (MPL-U-23/82)

D. Alexandrou and W.S. Hodgkiss, "Preliminary Processing of Selected Segments of the ARL/PSU FY80 Field Test Data," MPL TM-333, 28 December 1981, Marine Physical Laboratory, Scripps Institution of Oceanography, San Diego, CA (MPL-U-85/81)

FIELDS OF STUDY

Major Field: Electrical Engineering

Studies in Underwater Acoustics.
Professors Victor C. Anderson and Fred N. Spiess

Studies in Digital Signal Processing.
Professor William S. Hodgkiss

ABSTRACT OF THE DISSERTATION

Selective Reverberation Cancellation via Adaptive Beamforming

by

Dimitrios Alexandrou

Doctor of Philosophy in Electrical Engineering (Applied Ocean Science)

University of California, San Diego, 1985

Professor William S. Hodgkiss, Chairman

The central theme of this thesis is the application of the adaptive beamforming concept to the problem of selective reverberation cancellation, with an emphasis on experimental verification. Oceanic reverberation is often a limiting form of interference in echo detection applications. It may also be the "signal" of interest conveying valuable information about the scatterers or physical processes influencing their dynamical behavior. Because of stringent limitations imposed by the oceanic medium on the directional characteristics of sonar systems, reverberation is often composite in nature with two or more unrelated reverberation types contributing to the acoustic return. In that setting it would be desirable to selectively cancel the unwanted reverberation component(s) while preserving the component of interest. This signal processing problem whereby both "signal" and "noise" are constituent components of the received reverberation process is the focus of this thesis. The related problem of extracting reflector echoes from a reverberation backround is also considered. Significant contributions of this thesis include:

(1) Exposing relevant reverberation properties. It was shown that the spatial correlation characteristics of volume and boundary reverberation are directly applicable in a reverberation cancellation context.

(2) Critically evaluating a representative cross-section of adaptive algorithmic solutions with special attention to recently developed deterministic least-squares structures. It was determined, based on theoretical predictions substantiated by computer simulations, that lattice filters outperform direct tapped-delay-line implementations and that deterministic least-squares structures are more suitable than stochastic approximation solutions for reverberation cancellation. In addition, the multichannel least-squares lattice was shown to offer a significant advantage over a cascade of scalar filters.

(3) Demonstrating experimentally the feasibility of selective reverberation cancellation with real and simulated data from a shallow-water experiment, a near-surface Doppler sonar deployment and a multibeam bathymetric system. A clear distinction emerged between adaptive noise cancelling with preformed reference beams and spatially adaptive beamforming obtained by operating on array elements with a multichannel joint-process filter. It was shown that significant signal enhancement as well as selective reverberation cancellation can be achieved through constrained adaptive techniques.

INTRODUCTION

Oceanic reverberation is the composite echo from a large number of sound scatterers located in the volume and boundaries of the ocean. In the context of signal detection, reverberation is a form of interference which often presents a serious limitation to the useful operational range of an active sonar. Hence, it would be desirable to actively reject reverberation while preserving the signal of interest. Although the view of reverberation as a form of noise is likely to persist, a new outlook has been developing casting reverberation as an information-bearing signal. It possesses information about the nature and distribution of the scatterers and to the extent that the scatterers are influenced by a fluid process about the process itself. In this light, the following signal processing problem arises: Extract from a composite reverberation return the component representing the "signal" of interest. This thesis addresses both aspects of the reverberation cancellation problem. The proposed solution involves the application of constrained adaptive beamforming.

The following general approach is taken: First, the theoretical and experimental evidence on oceanic reverberation is reviewed in order to expose properties of potential relevance in a reverberation cancellation context. Second, the adaptive filtering problem is studied in detail in order to delineate the operational characteristics of existing adaptive structures with particular attention to some recently developed algorithms. Having chosen an "optimum" adaptive processor, real and simulated reverberation data from three active sonar experiments with widely differing objectives are processed through several adaptive beamforming configurations in order to establish the feasibility of the selective reverberation cancellation concept.

This thesis is organized as follows: In the first chapter a review is given of the current state of research on the properties of reverberation. The *physical* and *quasi-phenomenological* approaches are discussed. Some theoretical predictions of the point-

1

2

scattering model regarding the spatial correlation characteristics of reverberation are shown to be applicable in the context of selective reverberation cancellation. A sonar system simulation program (REVGEN) is described.

In the second chapter, adaptive filtering is set in the proper theoretical framework. The adaptive noise cancelling (ANC) concept is presented as a special case of the dual-channel Wiener filtering solution and adaptive beamforming is placed in the context of ANC. The fundamental difference between stochastic approximation solutions and the "exact" deterministic least-squares approach is exposed. Three representative joint-process algorithms are tested through computer simulations. Their behavior in the presence of power disparities in the reference channel and during drastic departures from stationarity is examined, in order to identify the algorithm best suited for reverberation cancellation. An additional simulation demonstrates the advantages of a true multichannel structure over a cascade of scalar filters.

In the third chapter, the selective reverberation cancellation (SRC) concept is applied to shallow-water reverberation data. The effect of adaptive "whitening" on low-Doppler echoes embedded in reverberation is examined. It is shown that significant signal enhancement can be obtained through adaptive noise cancelling with fixed (pre-formed) reference beams. Certain ANC model theoretical predictions as well as the spatial correlation characteristics of reverberation are related to filter performance. It is shown that SRC can be achieved with constrained adaptive beamforming implemented through a multichannel joint-process filter.

In the fourth chapter, data from a near-surface Doppler sonar deployment are used to study the effect of surface reverberation interference on upper-ocean (volume) velocimetry. Based on the intensity/velocity structure of the surface return a hypothesis is presented involving a thin bubble layer just below the surface. Spatial aliasing effects in constrained reference beams are shown to be deleterious to SRC. A

REVGEN simulation of this experiment is used to show that recovery of volume velocity information is possible if the spatial aliasing problem is aleviated.

The fifth and final chapter centers around a REVGEN simulation of the Sea Beam bathymetric system. It is shown that the sidelobe interference caused by the near-specular bottom return can be succesfully removed through ANC, pending a minor modification of the Sea Beam data acquisition system.

CHAPTER I

REVERBERATION IN THE OCEAN

In the active mode of sonar, the regime of interference which usually limits system performance is the sound field created by a large number of unwanted echo returns. The ocean abounds with objects that can intercept and reradiate acoustic energy. Suspended sediment, organic detritus, air bubbles, plankton, fish and minute discontinuities in the thermal structure, are all capable of redirecting sound. Irregularities of the sea surface and the ocean floor are also significant contributors to this reradiation of sound known as *scattering*. The composite echo from all scatterers is known as *reverberation*.

When the objective is signal detection, reverberation is clearly a form of noise. This consideration is largely responsible for the manner in which reverberation has been treated in the scientific literature. The overiding concern has been with the prediction of the reverberation intensity level. This has led to a single-parameter description of reverberation, the *backscattering coefficient* which, combined with geometrical and beam-pattern characteristics gives rise to the *reverberation level* (RL) of the well-known *sonar equations* [Urick, 1975].

Although this view of reverberation as a form of noise will always be valid, a new outlook has been developing casting reverberation as an information-bearing signal. It possesses information about the nature and distribution of the scatterers and to the extent that the scatterers are influenced by a fluid process, about the process itself. The information, if properly extracted, may be used to quantify fishery species of commercial interest [Cushing, 1973; Holliday, 1974], to examine planktonic communities [Greenblatt, 1980], to monitor pollution in industrial dumping sites [Orr and Hess, 1978], to identify ocean bottom types [de Moustier, 1985b] or for remote sensing of oceanic fluid processes [Proni et. al., 1978; Fisher and Squire, 1975; Pinkel, 1981].

4

As reverberation is being reevaluated in terms of its information content, so must the signal processing techniques used vis-a-vis reverberation be reconsidered. For instance, rather than indiscriminate reverberation suppression, the situation may call for the extraction, from a composite reverberation return, of the component created by the class of scatterers associated with the process of interest. In this scenario, "signal" and "noise" are both constituent components of the received reverberation process. This problem has not been previously addressed and is the focus of this thesis.

In the first chapter, we have attempted a brief review of the voluminous bibliography on the physical properties of oceanic reverberation and the mathematical methods used to describe it. The relative advantages of the *physical* versus the *quasi-phenomenological* approach are discussed and a simulation program implementing the latter is described. A direct connection is established between certain model predictions concerning the spatial correlation characteristics of reverberation and the adaptive noise cancelling concept.

1.1 Reverberation types / Scatterer identification

Oceanic reverberation is usually classified as volume, surface and bottom reverberation. The scatterers responsible for volume reverberation are mostly biological in nature [Clay and Medwin, 1977]. Inorganic particles are insignificant contributors and reflections from sound velocity microstructure are effectively masked by biological scattering [Kaye, 1978]. Zooplankton such as copepods are the dominant source of volume scattering in the near-surface region. In deeper water, biological scatterers are often distributed within diffuse Deep Scattering Layers (DSL) consisting of siphonophores, copepods, pteropods, euphausiids and fish. The diurnal migrating cycle of the DSL and its frequency-selective backscattering properties have been studied intensively revealing a complex, multilayered structure [Clarke, 1970; Kampa, 1970; Isaaks,

1974; Hersey, 1962; Gibbs, 1970].

Surface reverberation is generated by the entire spectrum of the rough air/sea interface and is a function of wind speed and the transmitted frequency. [Urick and Hoover, 1956; Chapman and Harris, 1962; Garrison et. al., 1960]. Specular reflections from normally inclined wave facets and scattering from an isotropic layer of bubbles in the near surface have also been suggested as reverberation sources at high and low grazing angles, respectively [Medwin, 1966; Clay and Medwin, 1964]. Shadowing effects by large-scale surface waves may be significant for low grazing angles [Gardner, 1973].

Bottom reverberation is an extremely complex phenomenon owing to the diversity of ocean floor types, lateral inhomogeneity and potential contribution of sub-bottom layers. The complexity is reflected by the disparity among the reported measurements of bottom scattering strength. It appears that both particle size and bottom relief are important factors [Mc Kinney and Anderson, 1964; Buckley and Urick, 1968]

1.2   The theory of scattering from rough surfaces

The theoretical treatment of reverberation poses a formidable analytical problem. In principle, the wave equation could be solved if the boundary conditions, describing the regions where density and sound velocity change discontinuously can be derived. In the real ocean this is an all but impossible task. In fact, even for the simplest of surfaces, the solution is far from trivial. The theoretical solutions to the problem of scattering from rough surfaces can be divided into two groups according to whether deterministic or stochastic surfaces are considered. The scattering of sound by a sinusoidal surface at normal incidence was first treated by Lord Rayleigh [1945]. His view of the sinusoidally corrugated surface as a reflection grating led to an

approximate solution consisting of a discrete set of plane waves travelling away from the surface at angles corresponding to the "orders" of the grating. An exact solution for the sinusoidal surface was obtained by Uretsky [1965] which was substantiated by laboratory experiments on sinusoidal cork surfaces [Barnard et.al., 1966]. Other solutions for periodic profiles of a specific type have been obtained [e.g Twersky, 1951]. In the absence of an exact solution, the Helmholtz formula with the Kirchoff approximation [Baker and Copson, 1939] has typically been used. This approximation is valid for "locally flat" surfaces with irregularities whose radius of curvature is large compared to the wavelength. A good review paper on solutions involving deterministic surfaces is by Lysanov [1958].

A rough surface is more appropriately described as a stochastic process. Most methods used to treat random surfaces are generalizations of the methods developed for deterministic surfaces and are subject to the same restrictive assumptions. The randomized Rayleigh approach whereby the surface is described in terms of random Fourier coefficients was developed by Rice [1951]. Other methods depict a rough surface as a planar array of objects the size, shape, position and separation of which are random variables or, alternatively, through the probability distribution of the slopes of its plane facets [Cox and Munk, 1954]. The Kirchoff method may be used to relate the statistics of the surface to the statistics of the scattered field [Eckart, 1953]. By assuming a Gaussian distribution for the surface scatterers, it is possible to calculate the mean field and mean power scattered in an arbitrary direction. This, in turn, makes it theoretically possible to solve the inverse problem, that is to determine the autocorrelation function of the random surface from measurements of the scattered intensity distribution [Horton, Mitchel, Barnard, 1967]. Eckart's high- and low-frequency solutions were extended to include intermediate frequencies by Proud, Beyer and Tamarkin [1960]. The question of the appropriate form for the surface covariance

function has been examined by Horton and Muir [1967]. A model for a composite rough surface consisting of a superposition of independent, stationary random processes each with its own distribution and covariance function (e.g. "swell", "sea", "ripple") was suggested by Beckman [1965] and the effect of statistical dependence between the component roughness processes was studied by Hayre and Kauffman [1965].

Remarks

This "physical" approach, despite longstanding efforts and the theoretical elegance of many of the solutions, provides at best an incomplete description of scattering from the ocean surface (bottom), because of the restricting assumptions that had to be used in the face of prohibitive analytical difficulties. Only monochromatic incident waves and a single receiver have been considered. The ubiquitous "locally flat" assumption limits the range of transmitted frequencies and surface roughness scales which are amenable to this treatment. In addition, Gaussian statistics with convenient correlation functions must always be used for analytical expediency. Thus, the direct connection of these solutions to the physical characteristics of the ocean boundaries is rather tenuous in general. Still, useful information such as roughness and correlation area may be derived through this approach if these assumptions are satisfied to a sufficient extent. No "physical" solution exists for volume scattering, however.

1.3 The point-scattering reverberation model

An alternative to the *physical* approach is to represent reverberation as a random process constructed by a linear superposition of the individual echoes emanating from a large number of point reflectors located independently in a homogeneous medium. The physical equivalent of the independence assumption is the first Born

approximation which states that secondary scattering is negligibly small. This approach has been developed mainly by Faure [1964], Ol'shevskii [1967] and Middleton [1967 a,b, 1972 a,b] and is known as the *point-scattering* or *quasiphenomenological* model of reverberation. Specifically, the backscattered signal is represented by

$$r(t) = \sum_{i=1}^{n} a_i G_i(t) s[\alpha_i(t - t_i)]$$

The returning echo from each scatterer, indexed by i, is delayed by t_i, the two-way travel time between the source and the ith scatterer. The a_i and α_i are random variables representing distributions of acoustic cross-section and Doppler factor of the scatterers, respectively. For a monostatic sonar,

$$G_i(t) = g B_i^2(\mathbf{r}_i) f(t)$$

where g is a system gain factor, B_i^2 is the two-way beam pattern sensitivity in the direction of the ith scatterer and $f(t)$ represents the two-way propagation loss. $s(t)$ is the transmitted waveform.

Assuming that for a sufficiently large scattering region the mean scatterer density is constant, the number n of scatterers contributing to the reverberation return at any given time may be described as a Poisson-distributed random variable. Based on Poisson statistics, a characteristic function may be derived for the reverberation process and the various moments may be obtained by taking appropriate derivatives. This approach makes it possible to calculate the second order statistics of reverberation for general experimental geometries, beam patterns and transmitted signals.

Remarks

Owing to its general construct, the point-scattering model allows the calculation of some fundamental statistical measures of reverberation for realistic system

parameters. However, no direct connection is established by the model between these measures and the physical characteristics of the scattering region. Any such information must be inserted in the model through a dynamical impulse response function representing the interaction of the incident field and a typical scatterer. Middleton [1967a] suggests that such knowledge must be derived from experiment but he stops short of suggesting appropriate experimental procedures.

The simplest approach is to assume that the point scatterers are perfect point reflectors radiating in all directions and reproducing exactly the incident waveform. Several investigators [e.g. Plemons et. al., 1972] have shown that even this simplest of models predicts temporal and spatial correlation values which are in substantial agreement with experimental estimates, with some interesting deviations. Such deviations may be caused, for example, by departures from isotropic scattering due to "patchy" scatterer distributions or they may be a reflection of the "microroughness" characteristics of a particular scattering region. From an extensive data set, collected in a variety of environmental conditions, the experimentally derived reverberation parameters may be categorized into patterns representing distinct classes of scatterers. Once established with the assistance of independent physical information such as bottom photographs, wind and wave-height measurements or plankton sampling, these patterns could be used to classify scatterer distributions based on reverberation information only. This is the potential solution to the "inverse problem" offered by the point-scattering model, in this case an empirical one. Modest steps have already been taken in this direction [Plemons Shooter and Middleton, 1972,a,b; Wilson, 1982; Wilson and Frazer, 1983; Jackson and Moravan, 1983.] The results tend to support the model predictions on the temporal and spatial covariance properties of reverberation.

No large-scale effort to collect long records of oceanic reverberation data has been reported thus far. Such a project would require a stable ocean-going platform, a multichannel data acquisition system and a powerful computing facility to accomodate the data validation and parameter estimation procedures for the collected reverberation ensembles.

1.4   Spatial correlation of reverberation

Spatial correlation expresses mathematically the fact that returns arriving from widely separated angular directions tend to add out of phase at spatially separated receivers. The point-scattering model of reverberation allows the calculation of the temporal and spatial correlation properties of reverberation independently of "fine structure" morphological information. Although deviations are to be expected for real reverberation data, the model does predict accurately the basic structure of these statistical measures. Based on the predicted structure, good decisions can be reached on experimental configurations conducive to particular signal processing goals. In this context, the point scattering model can be of great value. We will show here that knowledge of the basic spatial correlation structure of the backscattered signal as predicted by the simplest (point reflector) version of the model, can be used directly in the context of selective reverberation cancellation.

The following results on the spatial correlation of volume and boundary reverberation are based the assumptions that the elementary scattered signals reproduce the shape of the transmitted pulses and that the reverberation process has been appropriately stationarized [Ol'shevskii, 1967]. In addition, narrowband (quasi-harmonic) transmit signals and uniform scatterer distributions are assumed.

The geometry for the volume backscattered return is depicted in Figure 1.1a. The two receivers R_1 and R_2 are a distance s apart and vertically aligned. Volume

reverberation arrives from a range of elevation and azimuthal angles determined by the directional characteristics of the transmitting and receiving arrays. For omni-directional transmission and reception, the spatial correlation coefficient of volume reverberation is

$$R_V(s) = \frac{\sin(ks)}{ks} \tag{2a}$$

where

$$k = \frac{2\pi}{\lambda}$$

Thus, the spatial correlation coefficient of volume reverberation is a decaying function and will tend to zero as the transmitted frequency and/or receiver separation increase.

The geometry for the boundary return is described in Figure 1.1b. The two receivers lie in the xz plane and the line connecting them forms an angle ϕ_o with the $x-$ axis. In this case, for omnidirectional transmission and reception and for ranges much larger than the receiver separation, the spatial correlation coefficient is given by

$$R_B(s) = J_o(ks\cos\phi_o) \tag{2b}$$

where J_o is the modified Bessel function of the first kind. For $\phi_o = 0$ (horizontal separation) the result is again a decaying, oscillating function. However, for $\phi_o = \frac{\pi}{2}$ (vertical separation) we have

$$R_B(s) = J_o(0) = 1.$$

Therefore, no loss of spatial correlation is suffered for vertical separation of the receivers. This can be explained intuitively, in terms of the lack of vertical extent of the insonified surface patch. The above relations, are similar to some earlier results on the correlation properties of spatially distributed ambient noise fields [Cron and Sherman, 1962; Jacobson, 1962].

The effect of directional transmission can be readily included. Letting $b_T(\theta,\phi)$ be the beam pattern of the transmitting array, we have for volume reverberation

$$R_V(s) \sim \frac{1}{\Delta\Omega_{eff}} \int_{-\frac{\pi}{2}}^{\frac{\pi}{2}} \int_0^{2\pi} b_T^2(\theta,\phi)\cos(ks\sin\phi)d\theta\cos\phi\, d\phi \qquad (3a)$$

where,

$$\Delta\Omega_{eff} = \int_{-\frac{\pi}{2}}^{\frac{\pi}{2}} \int_0^{2\pi} b_T^2(\theta,\phi)d\theta\cos\phi\, d\phi$$

and for boundary reverberation,

$$R_B(s) \sim \frac{1}{\Delta\theta_{eff}} \int_0^{2\pi} b_T^2(\theta)\cos(ks\cos\phi_s\sin\theta)d\theta \qquad (3b)$$

where,

$$\Delta\theta_{eff} = \int_0^{2\pi} b_T^2(\theta)d\theta.$$

Equation (3b) indicates that the surface return originating at a thin surface layer, will continue to be perfectly coherent between vertically separated receivers ($\phi_s = \frac{\pi}{2}$). However, according to equation (3a), the volume return will become inreasingly correlated with increasing vertical directivity of the transmitting array thus reducing the correlation disparity between the two reverberation types.

Experimental evidence exists supporting these model predictions. Using explosive reverberation data, Urick and Lund [1964] have shown varying degrees of correlation between vertically separated receivers for different reverberation types, with boundary returns displaying decidedly higher values than the volume component. The same investigators [Urick and Lund, 1970a,b] have shown that the spatial correlation of composite reverberation in a shallow water environment is substantially higher in the vertical than in the horizontal. This was confirmed in a more recent experiment

involving a pulsed, high frequency sonar and directional receivers [Wilson and Frazer, 1983].

1.4.1 Spatial correlation and selective reverberation cancellation

Provided that the vertical directivities of the transmitting and receiving arrays are sufficiently low, the predicted disparities in vertical correlation for volume and boundary reverberation may be exploited in order to achieve selective reverberation rejection. It can be shown [Jackson and Moravan, 1983] that the vertical correlation of volume reverberation will be zero for receiver separations larger than the vertical dimension of the transmitting array. If directional receivers are used as well, the "correlation distance" will extend to the sum of the dimensions of the transmitting and receiving array. On the other hand, surface (bottom) reverberation will be highly correlated between the same vertically separated receivers, at least for ranges large relative to the distance of receiver separation. This forms a natural premise for the application of the *Adaptive Noise Cancelling* principle (ANC) whereby the correlated component between two signals is cancelled. In this scenario, boundary reverberation will be cancelled, while volume reverberation (the uncorrelated component) will be preserved at the filter output. Therefore, a vertical array is needed for boundary reverberation rejection.

The ANC concept will be described in detail in Chapter 2 and this idea will be tested with real and simulated reverberation data in Chapter III.

Remarks

i.   The ocean surface will in general have some vertical extent due to the presence of surface waves. This will lead to some loss of vertical correlation for the boundary return and will adversely affect the suggested selective cancellation procedure.

ii.   If indiscriminate reverberation suppression in the presence of a coherent echo return is desired, a horizontal conventional array will be much more effective than a vertical one.

1.5   Reverberation simulation

The point-scattering model of reverberation has the added advantage that it can be readily implemented in software. Several reverberation simulation software systems are available [Princehouse, 1977; Chamberlain and Galli, 1983]. REVGEN, (REVerberation GENerator) [Goddard, 1985] is a direct implementation of the point-scattering model; returns from a large number of discrete scatterers, distributed randomly throughout the volume and the boundaries, are summed coherently at each receiver to abtain a reverberation time-series. The REVGEN output is a dual digital data stream representing the I (in phase) and Q (quadrature) components of the complex-basebanded reverberation signal. A backscattering coefficient for each reverberation type and the densities of their Poisson distributions are specified by the user. Scattering layers, random scatterer motion, platform trajectories, attenuation and reflection losses, arbitrary (multiple) transmitting and receiving beam patterns and several transmitted signal types may be specified through appropriate REVGEN parameters to create realistic experimental settings. In such a controlled environment, a sonar system concept can be tested prior to actual deployment in the ocean thus avoiding the cost and operational difficulties associated with oceanic experiments. REVGEN has undergone an extensive validation process and has been found to be consistent with the theoretical model predictions regarding spectra and correlation functions. A favorable independent assessment was made by Hansen [1984] and we have succesfully repeated the original set of validation tests during the installation of REVGEN on the MPLVAX computer. The current version of REVGEN has been

made available to us by the Applied Physics Laboratory (APL) of the University of Washington.

The REVGEN software package will be used to simulate three oceanic experiments with widely differing objectives. Comparisons with results from available real data will be made in order to determine the extent to which the performance of the adaptive systems in question can be accurately assessed through REVGEN simulated data. Once a reliable connection is established, new experimental procedures can be suggested on the basis of simulated results.

It should be noted that such simulations in no way eliminate the need for further testing through real world experiments as the currently used model is only weakly related to the actual physical scattering process. Other physical phenomena such as sound velocity fluctuations and surface waves are not included in the model. Also not considered are, necessarily, any other unknown factors in the environment of the actual experiment. Therefore, the simulated results are presented only as a useful intermediate step in the process of experimental validation of the adaptive techniques. However, one may conceive a process of continual model update whereby new reverberation measurements (e.g. of second order statistics) are incorporated into the model to eventually produce a more reliable "synthetic" oceanic environment.

1.6   Chapter summary

We have presented a brief survey of the current state of research on the properties of oceanic reverberation. The fundamental differences between the physical and quasiphenomenological methods were discussed. A direct connection was established between the vertical correlation characteristics of volume and boundary reverberation and the adaptive noise cancelling concept. A software implementation of the point-scattering model was described.
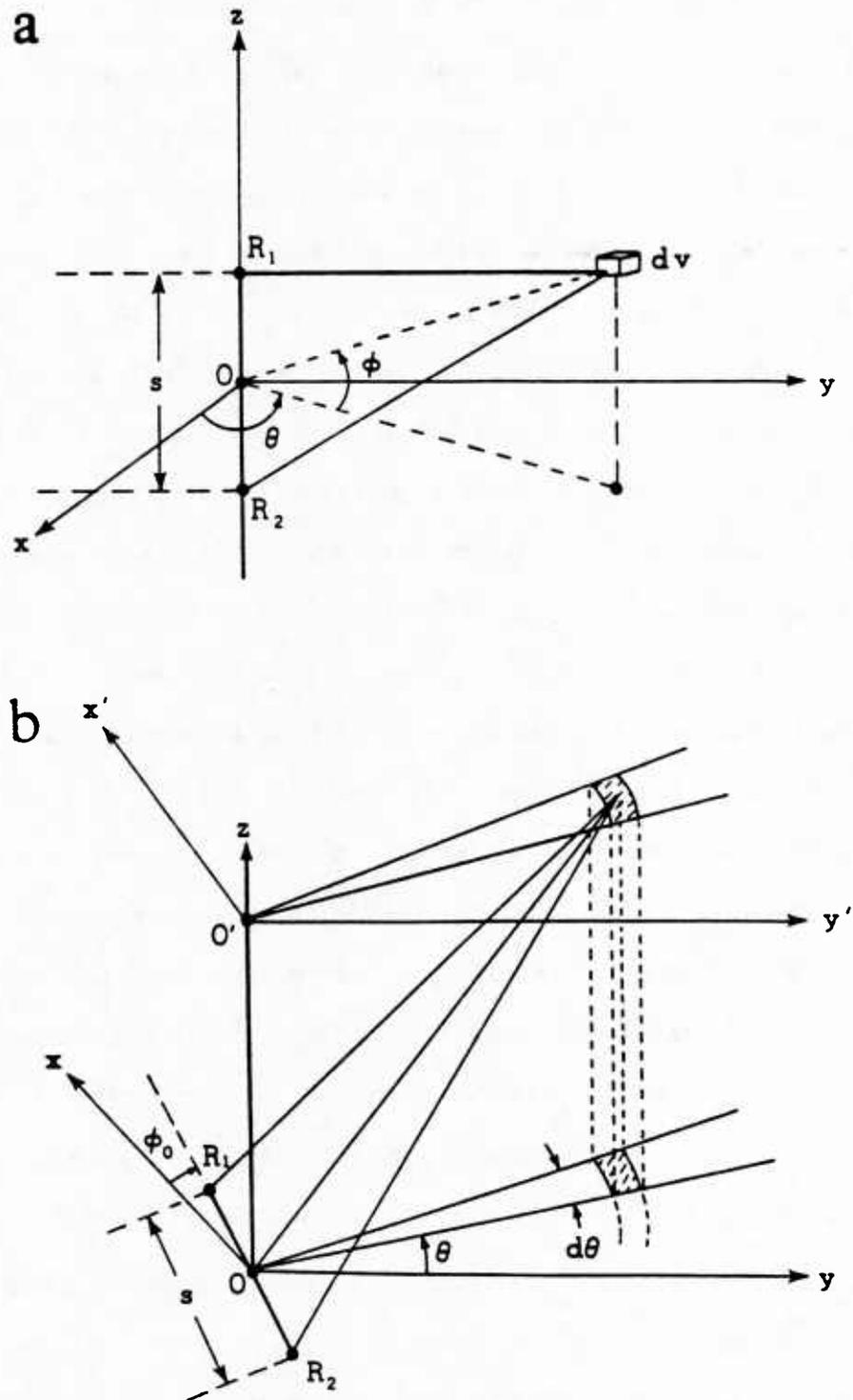
Figure 1.1 *Spatial correlation geometry* (a) volume reverberation, (b) boundary reverberation ($\phi_o = \dfrac{\pi}{2}$ for vertical separation.)

CHAPTER II
ON OPTIMUM ADAPTIVE FILTERING

As their name implies, *adaptive* filters are capable of responding to changing conditions through a rudimentary "learning" process. The filter parameters adjust themselves under the guidance of an appropriate cost function and track the evolving characteristics of the input signal(s). These structures grew out of the demand for systems capable of operating in uncertain, time-varying environments and were made possible by the increasing availability of computational power. The general, underlying problem is the one of designing realizable approximations to optimal Wiener filters when the ensemble of a random process is not available. One is then faced with the problem of extracting the desired information from a single sample function of the process. The problem may be approached from a statistical viewpoint by invoking stationarity and ergodicity and performing time-averaging, or through a deterministic least-squares formulation. Although the two approaches are fundamentally different, they lead to basically equivalent results when wide sense stationarity prevails. Both solutions can be implemented either in a block - processing or a time recursive mode and both give rise to efficient *lattice structures*. Nonstationary processes may be treated as locally stationary by restricting the time interval over which optimization is performed. This is, essentially, the function performed by an adaptive filter of the type considered in this thesis. The Wiener problem, or its deterministic counterpart, is solved over the restricted optimization interval, controlled by an *adaptation coefficient* which provides for a "fading" of past information in favor of recent values.

Rather than evolving from this general mathematical premise, the first adaptive filters were designed to solve some very specific real-time engineering problems. The directions defined by these initial applications have created the various regimes of adaptive filtering and are still evident in current applications, even as a more general

outlook is developing. Among them, *linear prediction* and *high resolution* spectral analysis, *adaptive beamforming* and *adaptive noise cancelling* are most commonly encountered. Central in the development of general adaptive structures has been the "prototype" linear prediction problem. A large and rapidly expanding body of literature has been compiled on linear prediction and its application to speech formant extraction, geophysical signal deconvolution and high-resolution spectral estimation. The solution to this problem, obtained through a *whitening* filter in conjunction with certain modeling schemes for the process of interest, has suggested lattice-form solutions to the more general *joint-process* problem of which noise-cancelling is a special case. Of particular interest throughout this thesis is the class of least-squares lattice filters with exact time-update properties and the potential advantages they enjoy over "noisy" gradient solutions both of direct form and of the lattice type.

In this chapter, the problem of adaptive filtering is set in the proper theoretical framework. A brief presentation of both the statistical and deterministic formulations is given and the evolution of the lattice form is discussed. Next, three adaptive noise-cancelling realizations were chosen to undergo comparison tests through computer simulations. These are the Least-Mean-Square (LMS) algorithm, a direct implementation with a gradient-search mechanism, the Gradient Lattice (GRL), a lattice type also with gradient-based adaptation and the Least-Squares Lattice (LSL), an exact time-update realization not succeptible to "misadjustment" noise. The reported differences in performance represent a significant contribution of this thesis. Specifically, the effect of large eigenvalue spread on the performance of the LMS is shown to extend to its noise-cancelling configuration. In addition, the demonstrated detrimental effect of a "scale-change" in the reference input to the performance of both gradient methods is a new result. Finally, the simulation demonstrating the successful implementation of the multichannel LSL filter and its advantages over cas-

caded processing of individual reference channels is the first reported to the best of our knowledge. In general, it is hoped that future users will benefit from the the exposition of the operational characteristics of these structures in their noise-cancelling mode.

2.1   A historical overview

The initial developments on adaptive filtering proceeded independently within several groups. Howells and Applebaum [1965] designed and built a system for antenna sidelobe cancellation that used a reference input from an auxiliary antenna and a simple two-weight filter. Gabor et al. [1969] designed a "learning" machine, a non-linear adaptive filter implemented as a highly specialized analog computer, capable of approximating a "target" function by successive adjustment of its variable coefficients. The term "adaptive filter" has been used [Jakowatz, Shuey and White, 1960] to describe a structure which extracts an unknown signal from noise, when the signal recurs frequently at random intervals. Davisson [1966] has described an adaptive method for estimating an unknown waveform in the presence of white noise of unknown variance and Glaser [1960] has presented an adaptive system capable of detecting a pulse signal of a fixed but unknown waveform. Adaptive prediction operations to fill telemetry "dropouts" were used by Balakrishnan [1962]. An interference cancelling network using operator-controlled cancellation beams was designed by Anderson [1968].

The work of Widrow et al. [1960] produced the first generalized adaptive structure, based on the mathematical method of steepest descent, the LMS algorithm. The LMS has been used as the central adaptive processor in applications such as adaptive array processing [Widrow et al., 1967; Griffiths, 1969; Frost, 1972], adaptive modeling [Schade, 1971], adaptive channel equilization [Lucky, 1965] and adaptive

noise cancelling [Widrow, 1975]. The development of lattice adaptive filters superior in terms of convergence characteristics to direct-form tapped-delay-line (TDL) implementations such as the LMS, has led to investigations of their performance as the central adaptive element. Adaptive lattice structures were used by Satorius and Alexander [1979] in a channel equilization application and by Hodgkiss and Presley [1981] in frequency tracking simulations. Their potential advantage over the direct form implementation was clearly demonstrated in both cases. Lattice structures for noise-cancelling have been suggested [Griffiths, 1978] but this regime of adaptive filtering is lagging markedly in terms of reported results either simulated or experimental. In particular, the recently developed deterministic least-squares lattice filters [e.g. Lee 1980] have not yet been seriously considered despite their exact time-update and superior convergence properties, achieved with only a moderate increase in algorithm complexity. These structures will be examined in detail in Section 2.6.

2.2   Optimum filtering and prediction

The development of the LMS and its successful application in a plethora of experimental settings, has demonstrated that adaptive structures of considerable diversity can be realized through a central adaptive estimator which is a practical implementation of a Wiener filter. The theory of linear Minimum Mean-Square Error (MMSE) filtering, developed by Kolmogorov [1941] and Wiener [1949], has long been a integral part of estimation theory. Complete treatments may be found in standard estimation theory texts [e.g. Van Trees 1968]. What follows is a statement of the general problem and a brief presentation of the relevant results.

2.2.1 The linear MMSE estimation problem

Given two discrete-time, complex, vector stochastic processes $x(n)$, $d(n)$ we want to operate on the first process (data) to obtain an estimate of the second process (signal). This constitutes the general two-channel (joint-process) *filtering* problem and is the focus of our interest. In addition, the one-step *prediction* problem $d(n) = x(n)$ has played an important role in the development of lattice-type solutions.

We denote the estimate as $\hat{d}(n)$ and choose a processor so that, with $\epsilon_p(n) = d(n) - \hat{d}(n)$, the quantity

$$E\{\epsilon_p(n)\epsilon_p^H(n)\}$$

is minimized.

Restricting our attention to the class of causal linear processors, we express the estimate as

$$\hat{d}(n) = \sum_{i=0}^{p} F_p^{(i)}(n)x(n-i)$$

The unique optimum linear MMSE filter may be obtained through the projection theorem as follows:

$$E\{\epsilon_p(n)x^H(k)\} = 0, \qquad n-p \leq k \leq n$$

equivalently,

$$E\{[d(n) - \sum_{i=0}^{p} F_p^{(i)}(n)x(n-i)]x^H(k)\} = 0$$

or

$$R_{dx}(n,k) = \sum_{i=0}^{p} F_p^{(i)}(n)R_{xx}(n-i,k) \tag{1a}$$

where R_{xx}, R_{dx} are the autocorrelation and crosscorrelation functions of the received signal and between the desired and received signals respectively:

$$R_{xx}(n,k) = E\{x(n)x^H(k)\}, \qquad R_{dx}(n,k) = E\{d(n)x^H(k)\}.$$

The resulting MMSE is given by

$$E_p^d(n) = \min_{\{F\}} E\{\epsilon_p(n)\epsilon_p^H(n)\}$$
$$= E\{\epsilon_p(n)d^H(n)\}$$

or

$$E_p^d(n) = R_{dd}(0) - \sum_{i=0}^{p} F_p^{(i)}(n)R_{dx}^H(n-i,n) \tag{1b}$$

where R_{dd} is the autocorrelation of the desired signal.

The well known time-invariant *Wiener-Hopf* solution, the continuous version of which was derived by Wiener [1949], is a special case of (1) and holds when wide-sense stationarity (WSS) prevails and an infinite observation interval ($p = \infty$) is assumed.

Equation (1a) may be expressed in matrix notation as

$$\mathbf{F}_p^T \mathbf{R}_{xx} = \mathbf{R}_{dx} \tag{2}$$

where

$$\mathbf{R}_{xx} = E\{\mathbf{x}_{[n:n-p]}\mathbf{x}_{[n:n-p]}^H\}$$

$$\mathbf{R}_{dx} = E\{d(n)\mathbf{x}_{[n:n-p]}^H\}$$

with

$$\mathbf{x}_{[n:n-p]}^H = [\ x^H(n), x^H(n-1),...,x^H(n-p)\ ]$$

and

$$\mathbf{F}_p^T = [F_p^{(0)}(n), F_p^{(1)}(n),...,F_p^{(p)}(n)]$$

The solution to the one-step prediction problem, obtained similarly, is given by

$$R_{xx}(n,k) = \sum_{i=1}^{p} A_p^{(i)}(n)R_{xx}(n-i,k), \qquad n-p \le k \le n-1 \tag{3a}$$

and the corresponding MMSE is

$$E_p^i(n) = R_{zz}(0) - \sum_{i=1}^{p} A_p^{(i)}(n) R_{zz}(n-i,n) \tag{3b}$$

Relations (3-a) and (3-b), known as the *Yule-Walker* equations, may be combined to form the so-called *normal* equations:

$$\mathbf{A}_p^T \mathbf{R}_{zz} = [\, E_p^i,\, 0,...,\, 0\,] \tag{4}$$

with

$$\mathbf{A}_p^T = [\, I_m, A_p^{(1)}(n),...,A_p^{(p)}(n)\,]$$

where I_m is the m x m identity matrix.

Remarks

i.   An important property of the optimum linear processor is that, when the processes involved are Gaussian, it is also the best of any type (including nonlinear) for minimizing the MSE. The Gaussian assumption is reasonable for oceanic reverberation as the nature of the physical process that generates it invites application of the central limit theorem.

ii.   The solutions represented by (2) and (4) are valid for general vector, nonstationary processes. It is possible, in principle, to solve them directly by numerical methods given ensemble representations of the processes involved. In applications of practical interest where real-time processing is of the essence, it is often the case that only a single sample function of the underlying random process is available and time-average statistics must be used. When WSS holds at least locally and ergodicity can be safely invoked, this will still lead to the optimum solution. In practice, however, ergodicity is difficult to prove and is routinely assumed. In addition, during periods of transition (departure from WSS), the optimality of the filter will be highly questionable from the probability theory point of view.

iii.   Here we are mainly interested in solving the filtering problem. However, fast and efficient (lattice-type) solutions for (2) can only be obtained in conjunction with the solution of the prediction problem. In that sense, (2) and (4) are intimately related.

2.3   The Adaptive Noise Cancelling (ANC) concept

The set of circumstances which gives rise to the noise cancelling concept is illustrated in Figure 2.1a. The primary channel consists of the signal s, corrupted by a form of additive noise n_o and the reference channel consists of a process n_1 related in some unknown way to the primary noise. The key requirement is that the signal be uncorrelated with both the primary noise and the reference process:

$$R_{sn_o} = 0, \quad R_{sn_1} = 0.$$

We then have

$$R_{ds} = R_{n_o n_1}$$

which leads to the noise cancelling solution as a special case of the general filtering problem solution:

$$R_{n_o n_1}(n,k) = \sum_{i=0}^{p} F_p^{(i)}(n) R_{n_1 n_1}(n,k), \quad n-p \leq k \leq n. \tag{5}$$

Thus, solving the filtering problem in this setting is equivalent to producing the best MMSE estimate of the primary noise process. The ANC output, obtained by subtracting this estimate from the primary input, will consist of the signal component s plus a residual error $n_o - \hat{n}_o$.

A more detailed model for the noise-cancelling structure is shown in Figure 2.1b. The "mismatch" between the primary and reference inputs is represented by a linear transfer function $H(z)$. Additional uncorrelated noise components m_o and m_1 are included in the two channels. This particular model, which is representative of many situations of practical interest, has been studied in detail by Widrow et.al.

[1975]. It was determined that the uncorrelated noise components have a deleterious effect on cancellation, expressed in z-transform notation [Oppenheim and Schafer, 1975] by the following:

$$\frac{\rho_{out}(z)}{\rho_{pri}(z)} = \frac{[\,M_o(z) + 1\,][\,M_1(z) + 1\,]}{M_o(z) + M_o(z)M_1(z) + M_1(z)} \tag{5a}$$

Here, $\rho_{out}(z)$ is the signal-to-correlated noise density ratio at the output, $\rho_{pri}(z)$ is the signal-to-correlated noise density ratio at the primary input and $M_o(z)$, $M_1(z)$ are the ratios of the uncorrelated noise spectrum to the correlated noise spectrum at the primary and reference channels, respectively. It is apparent from (5a) that the ability of the ANC system to reduce noise is limited by $M_o(z)$ and $M_1(z)$ when these quantities are large. When they are small, other factors become important in limiting ANC performance. One such factor is the presence of signal components in the reference channel. Letting $\rho_{ref}(z)$ denote the signal-to-correlated noise density ratio at the reference input and assuming $M_o(z) = M_1(z) = 0$, Widrow et. al. show that

$$\rho_{out}(z) = \frac{1}{\rho_{ref}(z)} \tag{5b}$$

Another relation of potential practical significance is the following, regarding the output noise spectrum $S_{on}(z)$.

$$S_{on}(z) = S_{s_1n_1}(z)|\rho_{ref}(z)||\rho_{pri}(z)|. \tag{5c}$$

Equation (5b) indicates that, although the signal components in the reference input has a detrimental effect on cancellation, it does not render the ANC operation useless if $\rho_{ref}(z)$ is held to reasonably low levels. Equation (5c) makes the somewhat surprising statement that a high signal-to-noise ratio in the primary channel will result in increased ouput noise power. This can be explained intuitively as follows: If $\rho_{pri}(z)$ is low, the filter will be "trained" to cancell the noise rather than the signal and therefore output noise will be low.

2.3.1   Adaptive beamforming via ANC

Conventional arrays are usually designed under the assumption that unwanted noise is spatially disorganized. These fixed-weight arrays suffer a degradation of performance in the presence of directional interference possessing some degree of spatial coherence. Such interference may be due to natural sources, reverberation returns or jamming signals. Other factors, such as array motion, multipaths and constantly changing interference characteristics, contribute to further deterioration. Adaptive arrays, on the other hand, are capable of reducing or eliminating directional noise components and of responding to changing conditions by adjusting their pattern response according to an appropriately chosen error criterion. In general, adaptive arrays are in the form of a space-time filter which can be implemented through the general multichannel filtering structures described in the previous section.

The fields of communications, radar, sonar and geophysics have each contributed to adaptive array development. The exact manner in which control of the available spatial and temporal degrees of freedom is relegated to the adaptive processor and the choice of a performance measure, depend largely on the objectives and priorities of the specific application. For instance, Shor[1966] adjusted the array coefficients to maximize the signal-to-noise ratio (SNR) at the output. Riegler and Compton[1973] and Widrow [1967] minimized the mean square of an error signal equal to the difference between the array output and a reference signal. The total noise power at the output, in the absence of the signal, was minimized by Lacoss[1968], while optimum probability of detection for a fixed false alarm rate was the criterion chosen by Brennan and Reed[1973]. The special case of weak signals in the presence of strong interference was examined by Zahm[1973]. A good tutorial introduction to the adaptive array problem is given by Gabriel[1976] and a more complete treatment is by Monzingo and Miller[1980].

Here we are primarily interested in signal extraction and MMSE is the performance measure of our choice. It is flexible enough to encompass many experimental configurations and it leads to mathematically tractable results. Our objective is to utilize the general adaptive algorithms which have been derived under this criterion in conjunction with the ANC scheme, in order to eliminate reverberation interference entering through the sidelobes and possibly the main lobe of the receiving array. It will be shown that selective reverberation cancellation may be achieved through *constrained* adaptive beamforming.

2.3.2 Adaptive beamforming with constraints

Of crucial importance in any adaptive array application is the utilization of all available a priori information concerning the nature of the signal and the interference, in order to ensure signal preservation at the output. In the early applications of adaptive processing to antenna sidelobe cancellation, the effects of signals on the adapted response were commonly neglected. This was justified by the assumption that the signals of interest were sufficiently low in power and/or duration so that the adaptive control algorithm would not respond to them (e.g. Widrow et. al.[1967].) When such an assumption is unrealistic, the response of the adaptive array must be explicitly constrained to avoid signal cancellation. Constraints may be incorporated into the adaptive algorithm to maintain a chosen frequency response in a desired direction (Frost[1972]). This is computationally expensive and operationally inflexible. "Pilot" signals, simulating actual signals of interest, have also been used to describe a desired "main" look direction, through a two-mode adaptation process [Widrow 1967]. However, accurate replicas of the desired signals are not normally available. An alternative is to impose preadaptation constraints in the time, space and frequency domains [Applebaum and Chapman, 1976]. Restrictions may be effected in the time domain by

allowing the array to adapt only when no signal is present; in the frequency domain by allowing adaptation only to energy received outside the signal band. Finally, preadaptation spatial filtering may be used to remove the signal, whose direction is presumed known, thus protecting it from cancellation. Such prefiltering may range from complete conventional beamforming (Figure 2.2a) to simple element-to-element subtraction (Figure 2.2b). The former can be applied only when the spatial characteristics of the interference, as well as the signal, are known and constant and requires an external steering mechanism. The latter is more appropriate when the directional characteristics of the interference are unknown or variable and results in (constrained) spatially adaptive cancellation beams. These two configurations are compatible with our objectives and will both be used with attention to their relative advantages.

It is interesting to note that such prefiltering operations, by eliminating the signal of interest from the reference channel(s), in effect place constrained adaptive beamforming in the context of ANC and, more generally, of the (vector) Wiener filtering problem. This approach affords us the flexibility of using any efficient solution to the general filtering problem as the adaptive processor controlling the array element weights. It will be shown that significant differences in performance exist between seemingly equivalent algorithmic implementations and that the correct choice is critical to succesful reverberation cancellation.

2.4   Stochastic lattice solutions for optimum filtering

The optimum linear filters described by (2) and (4) can be determined by solving the matrix equation directly. In the stochastic approach, the cost is twofold. First, the needed second order statistics, which are almost always unknown in problems of practical interest, must be estimated from the data and updated periodically, since the statistics are in general nonstationary. The second step involves the inver-

sion of the autocorrelation matrix R. In general, the $p \times p$ correlation matrix can be inverted by standard methods such as Gaussian elimination and Crout reduction [Stewart, 1973], or more robust methods making use of the nonnegative definiteness and/or symmetry properties of R such as Householder transformations or Cholesky decompositions [Lawson and Hanson, 1974]. All of these methods require $O(p^3)$ computations (multiplications of real numbers). The computational requirements can be substantially reduced when R is characterized by certain shift-invariance properties which lead to efficient recursive solutions of the *lattice* or *ladder* type.

For the remainder of this section, we will restrict our attention to scalar processes. This was done for the sake of notational simplicity and does not seriously affect the generality of the presentation.

2.4.1 Levinson's algorithm: The Toeplitz recursion

A faster method of inversion, and therefore solution of the normal equations, exists when R is *Toeplitz*, i.e. of the form

$$R = [r(i-j)], \quad 0 \le i,j \le p \tag{6}$$

It is easy to see that a Toeplitz structure for R is tantamount to the wide-sense stationarity of the input process. In this case, the shift-invariance and symmetry properties of R lead to an inversion technique requiring only $O(p^2)$ computations. The procedure, developed originally by Levinson [1947] and rediscovered by Durbin [1960], consists of using a partial solution and a subsequent correction through a "reversed time" auxiliary solution. The same concept has been used by Szego [1939] in the different but mathematically isomorphic problem of polynomial approximation on the unit circle. Multivariate extensions of the Levinson algorithm have been obtained by Whittle [1963] and Wiggins and Robinson [1965]. Toeplitz recursions exist for both the filtering and prediction solutions. The *auxiliary* Toeplitz recursion solves for the predictors $A_p^{(i)}$

of (4) and the *general* Toeplitz recursion solves for the filter coefficients $F_p^{(i)}$ of (2). These recursions give rise to the *prediction error* and *joint process* lattice structures, respectively. Although Levinson, in his original work, was mainly concerned with the general filtering problem, it was the prediction solution (auxiliary recursion) which has attracted much attention in recent years, in conjunction with certain modeling schemes for the input process. The general Toeplitz recursion can only be achieved through the auxiliary recursion and thus the two procedures are intimately related. The basic structure for the prediction lattice filter is described by the following relations (Figure 2.3a with $k_i^f = k_i^r = k_i$.)

$$e_i(n) = e_{i-1}(n) + k_i(n)r_{i-1}(n-1) \tag{7a}$$
$$r_i(n) = k_i^*(n)e_{i-1}(n) + r_{i-1}(n-1) \tag{7b}$$

where $x(n)$ is the input signal and $e_i(n)$ and $r_i(n)$ are the forward and backward prediction error residuals at stage i.

Levinson's algorithm in its original form requires the external calculation of autocorrelation lags and is sometimes referred to as the "given correlation" algorithm. Alternative stochastic lattice formulations which utilize the input data stream to directly estimate the lattice coefficients are more suitable for real-time processing. One such "given data" structure (GRL) will be considered here as a potential candidate for our central adaptive processor. The original Levinson's algorithm is included in Appendix A for the sake of completeness.

2.4.2   Lattice properties

Levinson's algorithm has implications beyond the original intent of a fast matrix inversion technique. The lattice structures it has created possess properties, summarized below, which can amount to significant operational advantages over direct TDL implementations.

i.   *Stage-by-stage decoupling*

Each lattice stage is independent of all other stages. Increasing the predictor order is achieved by adding one more lattice section, without changing any of the previous sections. Thus, given a lattice implementation of a predictor of order p we have in fact an implementation of all predictors up to that order. Stated somewhat differently, the time-variation of the finite-length filter takes on a simple step-function form in the lattice, whereby each lattice section is turned "on" one at a time. This decoupling or orthogonalization property is directly responsible for the improved convergence properties of the lattice (see Simulation 1.)

ii.   *Stability " by inspection"*

The IIR (inverse) lattice filter is stable if and only if $|k_i| \leq 1$. As a result stability (or lack thereof) of the inverse ("synthesis") lattice filter is easily established by examining these *reflection* or partial correlation (PARCOR) coefficients.

iii.   *AR cut-off*

For an input AR process of order p, the k_{p+i}, $i=1,2,...$ are zero. This property can significantly facilitate AR model identification (see Section 2.4.3)

iv.   *Structural modularity*

The lattice forms are built from a cascade of sections with identical structure, a property attractive from the VLSI implementation point of view.

v.   *Desirable numerical properties*

There is evidence indicating that lattice structures are less sensitive to roundoff noise [Markel and Gray, 1975; Gray and Markel, 1975] and to quantization effects [Bruton, 1976; Fettweis, 1974].

vi.   *Physical interpretations*

The reflection coefficients can be related to parameters of certain models representing physical processes. In particular, models of wave propagation in a stratified medium [Thomson, 1950] and of the human vocal tract [Kelly and Lochbaum, 1962] have been suggested which have lattice-form configurations. The work of Wakita [1973] established a direct connection between the reflection coefficients and the cross-sectional area function of the vocal tract, showing that the vocal tract shape can be estimated directly from the acoustic speech waveform through linear prediction. This parameter estimation technique, coupled with a recent surge of activity in the area of speech signal processing, can account to a large extent for the predominance of the linear prediction solution in the literature. On the other hand, the joint-process lattice solution was largely neglected, leaving direct TDL implementations (e.g. the LMS) unchallenged in filtering applications such as channel equilization and noise-cancelling.

2.4.3 Alternative lattice solutions

The *reflection* coefficients k_i of the lattice prediction filter can be interpreted as a measure of the crosscorrelation between $e_{i-1}(n)$ and $r_{i-1}(n-1)$. This idea has spawned a class of lattice algorithms in which the reflection coefficients are computed directly from the data and differ only in the manner that this quasi-correlation coefficient is normalized. Itakura and Saito [1971] used the *geometric-mean* method of normalization to compute their PARCOR coefficients. Burg [1975], on the other hand, chose the *harmonic-mean* method which satisfied his *maximum-entropy* criterion. A more general class of normalization schemes, of which the above are special cases, has been defined by Makhoul [1977, 1978]. We have chosen the harmonic-mean (maximum entropy) method for our stochastic lattice implementation (GRL) because its derivation was based on a well-defined and intuitively pleasing criterion. Morover, it is the

method of choice for some widely referenced implementations (e.g. Griffiths [1978], Satorius [1979]). Thus, we define k_i as

$$k_i(n) = \frac{2E\{e_i(n)r_i^*(n-1)\}}{E\{|e_i(n)|^2 + |r_i(n-1)|^2\}} \tag{8}$$

where the expectation operator E is approximated in practice by a time average.

Joint-process versions of the *given data* lattice can be easily derived by considering the prediction lattice as a practical implementation of Wold's decomposition theorem [Wold 1939]. In essence, the lattice performs a successive orthogonalization, of the Gram-Schmidt type, on delayed versions of the input signal. The backward residuals are orthogonal $(E\{r_i r_j\} = \delta_{(i-j)}, \ i,j = 1,...,p)$ and constitute an *innovations representation* of the input signal, forming a natural orthogonal basis which spans the signal subspace. The dual-channel filtering problem can be solved by estimating the desired signal with a linear combination of these orthogonal components. A simple application of the orthogonality principle [Satorius and Alexander 1979] leads to the optimum set of cross-correlation coefficients k_i^d thus forming the joint-process lattice structure (Figure 2.3b), suitable for noise-cancelling applications:

$$k_i^d(n) = \frac{E\{e_i^d(n-1)r_i^*(n-1)\}}{E\{|r_i(n-1)|^2\}} \tag{9}$$

These *given data* structures, by implicitly estimating the second order statistics and by making the error signals available at each stage of the lattice, are more suitable for real-time processing than the original *given correlation* Levinson algorithm. In addition, adaptive versions may be easily derived by introducing an exponential data window and an error gradient criterion. It should be emphasized that these structures are still based on a stochastic formulation and are fundamentally equivalent to Levinson's algorithm. They are optimum only when WSS and ergodicity can be safely assumed. They are, however, precursors to purely deterministic least-

squares structures, to be examined in Section 6 of this chapter.

2.4.4   The question of modeling

It is often useful to develop a parametric model for the behavior of a signal or system. The problem of determining the parameters of a hypothesized mathematical model given observations of the signal to be modelled is the subject matter of *parameter estimation* and *system identification*. A variety of estimation techiques have been used in this context, with least-squares methods occupying a prominent position [Astrom and Eykhoff, 1974; Kailath, 1974; Willsky, 1979].

A very successful application of modeling has led to the development of Kalman filters [Kalman and Bucy, 1961] which have proven to be very useful in control applications where *internal* models (or state-space descriptions) are relevant. Parameter identification problems also arise in several digital signal processing applications where *external* models (input/output descriptions) are appropriate, among them seismic signal processing and the analysis, coding and synthesis of speech. The latter application, in particular, has received a great deal of attention in the past 10 years [e.g. Markel and Gray, 1976, Makhoul, 1975]. Modeling, in this context, entails describing the process of interest in terms of the linear (possibly time-varying) system that would generate it when driven with white noise. The most general system of this type is the autoregressive-moving average (ARMA) model, described by the following difference equation.

$$\sum_{i=0}^{p} a_{n,i} x_{n-i} = \sum_{i=0}^{q} b_{n,i} u_{n-i}, \quad n \geq 0, p \geq 0, q \geq 0 \tag{10}$$

In z-transform notation [Oppenheim and Schafer, 1975] we have

$$A(z)X(z) = B(z)U(z) \implies X(z) = H(z)U(z) \tag{11}$$

where

$$H(z) = B(z)/A(z)$$

is a rational transfer function. If $q=0$, then z_n is known as an autoregressive (AR) process and the model is referred to as "all-pole":

$$H(z) = 1/A(z) .$$

The "all-zero" filter which will reduce a given AR process of order p to white noise is known as the *inverse* or *whitening* filter and is identical to the prediction error filter of order p. In fact, parameter estimation can always be regarded as a mathematical modeling process, even if the primary goal is not explicitly stated in this form. Therefore, AR system identification can be effected through the solution of the one-step prediction problem. This procedure is the basis for most *high resolution* spectral estimation techniques, where the spectrum of the input process is modeled as an AR transfer function. In the two-channel filtering problem, on the other hand, it is the cross-spectrum between the two channels which is modelled as an all-pole transfer function and must be compensated for by the all-zero filter represented by the lower section of the joint-process lattice (see Figure 2.1b.) It follows that the optimum choice of filter order is, in general, quite different for the single-channel (prediction error) and the two-channel (joint-process) filters.

2.5   Gradient-based time-recursive algorithms

The coefficients of the whitening (prediction) filter, in either its direct or lattice form, can be obtained by operating on a segment of the input time seriesuntil a white-noise sequence (or as close to white as possible) is produced at its output. In this *block- processing* mode, a new set of coefficients (AR model estimates) is derived per data segment. An alternative approach is to continuously update the coefficients, utilizing the unbroken stream of data and taking into account each new sample. This requires the existence of an updating mechanism with a decaying memory, whereby

"new" samples are emphasized over "old". The resulting filters are known as *time-recursive* or *adaptive* and can be easily derived from block structures of the *given-data* type.

2.5.1   The LMS adaptive filter

The LMS algorithm uses an implementation of the method of steepest descent to provide a time-updating mechanism for the weights of the direct tapped-delay line (TDL) realization of the *linear combiner* which can be used either as a predictor or noise-canceller (Figure 2.4).

The "current" weight vector $a(n)$ (Figure 2.4.b) is set equal to the "past" weight vector $a(n-1)$ plus a change proportional to the negative gradient of the mean-square error surface which is a concave paraboloid with a unique minimum.

$$a(n) = a(n-1) + \mu(-\nabla(n-1)) \tag{12}$$

where μ is the factor that controls stability and rate of convergence.

Since the true gradient of the true MMS error is not known, it is replaced by the gradient of the instantaneous error power $|\epsilon_p^d(n-1)|^2$. This "estimated" gradient is given by Widrow [1975]:

$$\dot{\nabla}(n-1) = -2\epsilon_p^d(n-1)\mathbf{x}^*(n) \tag{13}$$

where

$$\epsilon_p^d(n) = d(n) - \mathbf{a}^T\mathbf{x}(n)$$

$$\mathbf{x}^T(n) = [x(n-1),...., x(n-p)]$$

and forms the basis for the Widrow-Hoff LMS algorithm of adaptive weight updating:

$$a(n) = a(n-1) + 2\mu\epsilon(n-1)\mathbf{x}^*(n-1) \qquad . \tag{14}$$

It has been shown by Widrow [1976] that the expected value of the weight vector converges to the true Wiener solution. It is also shown that the algorithm will

converge in the mean and remain stable as long as

$$1/\lambda_{max} > \mu > 0 \tag{15}$$

where λ_{max} is the largest eigenvalue of the autocorrelation matrix **R**. In addition, the time constant for the "learning curve" corresponding to the ith natural mode of the signal is related to the ith eigenvalue of **R** by

$$\tau_i = 1/4\mu\lambda_i \tag{16}$$

Morover, the ratio of the excess noise power due to weight *misadjustment* over the estimation error power is given by

$$M = \mu tr\mathbf{R} = \mu \; p \; \lambda_{ave} = \frac{p}{4}(\frac{1}{\tau_i})_{ave} \tag{17}$$

Relations (16) and (17) portray the major drawback of the LMS. When the matrix **R** has a large eigenvalue spread, convergence is controlled by the smallest eigenvalue and misadjustment by the largest one. The result is slow adaptation coupled with high misadjustment noise.

It is convenient to introduce a new parameter α_{LMS} [Griffiths, 1976] such that

$$\mu = \alpha_{LMS}/pE_0^s$$

where E_0^s is the power of the reference sequence $x(n)$. Then (15) becomes

$$0 < \alpha_{LMS} < pE_0^s/\lambda_{max} \quad . \tag{18}$$

Since $pE_0^s \geq \lambda_{max}$ it follows that convergence is always achieved for $0 \leq \alpha_{LMS} \leq 1$.

In the algorithm, E_0^s is replaced by the estimate

$$\dot{E}_0^s(n) = (1-\alpha_{LMS})\dot{E}_0^s(n-1) + \alpha_{LMS}|x(n)|^2 \quad . \tag{19}$$

2.5.2   Summary of the LMS algorithm

The scalar, complex joint-process gradient transversal filter (LMS) algorithm is summarized as follows (see Figure 2.4a)

Initialization (k=0,1,...,p)

$$f_k(-1) = 0 \tag{20a}$$

$$E_o^c(-1) = \epsilon_{LMS}, \quad \epsilon_{LMS} = E_o^c(0) \tag{20b}$$

$$x(-k) = x(-p-1) = 0 \tag{20c}$$

$$e_p^d(-1) = 0 \tag{20d}$$

Time update $(n \geq 0 \text{ and } k=0,1,...,p)$

$$f_k(n) = f_k(n-1) - \frac{2\alpha_{LMS}}{(p+1) E_o^c(n-1)} e_p^d(n-1)x^*(n-k-1) \tag{20e}$$

$$e_p^d(n) = \sum_{k=0}^{p} f_k(n)x(n-k) + d(n) \tag{20f}$$

$$E_o^c(n) = (1 - \alpha_{LMS}) E_o^c(n-1) + \alpha_{LMS}|x(n)|^2. \tag{20g}$$

Slightly simplyfying (20a)-(20g), the one-step forward linear predictor complex gradient transversal filter algorithm can be written as (see Figure (2.4b))

Initialization (k=1,2,...,p)

$$a_k(-1) = 0 \tag{21a}$$

$$E_o^c(-1) = \epsilon_{LMS}, \quad \epsilon_{LMS} = E_o^c(0) \tag{21b}$$

$$x(-k) = x(-p-1) = 0 \tag{21c}$$

$$e_p(-1) = 0 \tag{21d}$$

Time update $(n \geq 0 \text{ and } k=1,2,...,p)$

$$a_k(n) = a_k(n-1) - \frac{2\alpha_{LMS}}{p E_o^c(n-1)} e_p(n-1)x^*(n-k-1) \tag{21e}$$

$$e_p(n) = \sum_{k=0}^{p} a_k(n)z(n-k) \quad , \quad a_o = 1 \tag{21f}$$

$$E_o^z(n) = (1 - \alpha_{LMS}) \, E_o^z(n-1) + \alpha_{LMS}|z(n)|^2. \tag{21g}$$

Remarks

Oceanic reverberation is characterized by the rapid onset of components differing widely in intensity. The presence of such components will most likely create this condition of high eigenvalue spread and at the same time the need for extremely fast adaptation. It has been shown in frequency tracking [Hodgkiss and Presley, 1981] and adaptive equilization [Satorius, 1979] applications that adaptive forms of the lattice structure possess significant performance advantages over the LMS, resulting mainly from the orthogonalization and decoupling property between lattice stages. In effect, each stage of the lattice is asigned to a single mode and adapts independently of all other stages. It will be the intent of Simulation 1 to confirm this in a noise-cancelling application.

2.5.3 The gradient lattice filter (GRL)

The same concept of an estimated error gradient may be used to update the reflection coefficients of a lattice filter. Again, the true gradient with respect to the k_i of the sum of the mean square error residuals $E\{|e_i(n)|^2 + |r_i(n)|^2\}$ is replaced by the noisy gradient of the sum of the instantaneous square error residuals $|e_i(n)|^2 + |r_i(n)|^2$. The noisy estimate which can be obtained directly from (8), can be used to estimate the "next" k_i as follows: [Makhoul, 1978; Griffiths, 1977]

$$k_i(n) = k_i(n-1) + \frac{e_i(n-1)r_{i-1}(n-2) + e_{i-1}(n-1)r_i(n-1)}{D_i(n)}, \quad 1 \le i \le p-1. \tag{22a}$$

where $D_i(n)$ is computed recursively from

$$D_i(n) = (1-\alpha_{GRL})D_i(n-1) + |e_{i-1}(n-1)|^2 + |r_{i-1}(n-2)|^2, \quad 1 \le i \le p-1 \tag{22b}$$

The product $\alpha_{GRL} D_i(n)$ where $0 \leq \alpha_{GRL} \leq 1$, represents an exponentially averaged estimate of the power level at the ith stage of the lattice. The normalization by the factor $D_i(n)$ is intended to maintain the same time constant of adaptation at each stage of the lattice. Thus, the overall convergence rate should be unaffected by the eigenvalue spread of $\mathbf{R}$.

The optimum set of the "joint-process" coefficients k_i may be updated adaptively as follows:

$$k_i^d(n) = k_i^d(n-1) + \frac{e_i(n-1)r_i(n-1)}{G_i(n)} \tag{23a}$$

where

$$G_i(n) = (1-\alpha_{GRL})G_i(n-1) + |r_i(n-1)|^2, \qquad 1 \leq i \leq p \tag{23b}$$

Only preliminary results are available concerning the convergence properties and the misadjustment noise of the gradient lattice [Griffiths and Medaugh, 1978].

2.5.4 Summary of the GRL algorithm

The scalar, complex, joint-process gradient lattice algorithm (GRL) is summarized as follows (see Figure 2.3b) with $k_i = k_i^r = k_i^s$).

Initialization (i = 0,1,...,p)

$$k_i(-1) = 0 \quad , \quad i \neq 0 \tag{24a}$$

$$E_i^r(-1) = E_i^s(-1) = \epsilon_{JCGL} \quad , \quad \epsilon_{JCGL} = E_0^s(0) \tag{24b}$$

$$E_i^s(-2) = \epsilon_{JCGL} \quad , \quad i \neq p \tag{24c}$$

$$e_i(-1) = r_i(-1) = 0 \tag{24d}$$

$$r_i(-2) = 0 \quad , \quad i \neq p \tag{24e}$$

$$k_i^d(-1) = 0 \tag{24f}$$

$$e_i^d(-1) = 0 \tag{24g}$$

Time update $(n \geq 0)$

$$e_o(n) = r_o(n) = z(n) \tag{24h}$$

$$e_{-1}^d(n) = d(n) \tag{24i}$$

Order update $(i = 0, 1, ..., p)$

$$k_i(n) = k_i(n-1) - \frac{2\alpha_{JCGL}}{E_{i-1}^r(n-2) + E_{i-1}^e(n-1)} \tag{24j}$$

$$\bullet \, | e_i(n-1)r_{i-1}^*(n-2) + r_i^*(n-1)e_{i-1}(n-1)| \quad , \quad i \neq 0$$

$$e_i(n) = e_{i-1}(n) + k_i(n)r_{i-1}(n-1) \quad , \quad i \neq 0 \tag{24k}$$

$$r_i(n) = r_{i-1}(n-1) + k_i^*(n)e_{i-1}(n) \quad , \quad i \neq 0 \tag{24l}$$

$$E_{i-1}^r(n-1) = (1 - \alpha_{JCGL})E_{i-1}^r(n-2) \tag{24m}$$

$$+ \alpha_{JCGL}|r_{i-1}(n-1)|^2 \quad , \quad i \neq 0$$

$$E_{i-1}^e(n) = (1 - \alpha_{JCGL})E_{i-1}^e(n-1) \tag{24n}$$

$$+ \alpha_{JCGL}|e_{i-1}(n)|^2 \quad , \quad i \neq 0$$

$$k_i^d(n) = k_i^d(n-1) - \frac{2\alpha_{JCGL}}{E_i^r(n-1)} e_i^d(n-1)r_i^*(n-1) \tag{24o}$$

$$e_i^d(n) = e_{i-1}^d(n) + k_i^d(n)r_i(n) \tag{24p}$$

Predictors $(b_l^{(i)}(n) = a_{p-l}^{(i)}(n), l = 0, 1, ..., p)$

$$a_i^{(i)}(n) = k_i(n) \tag{24q}$$

$$a_l^{(i)}(n) = a_l^{(i-1)}(n) + k_i(n)a_{i-l}^{(i-1)*}(n) \quad , \quad 1 \leq l \leq i-1 \tag{24r}$$

2.6   Deterministic least-squares lattice structures

The optimality of the filters discussed in the previous section rests on the assumptions of stationarity and in the *given data* case, ergodicity. During transition periods when the statistics of the signal change drastically, all such solutions are clearly suboptimal. In addition, the misadjustment noise of the gradient methods is often a limiting factor on the algorithm convergence speed. An alternative to those *stochastic approximation* methods is the deterministic least-squares approach. When (WSS) stationarity does prevail, the solutions derived through this approach perform identically to their stochastic (time-average) counterparts. However, they enjoy an important advantage in that they continue to be optimum (in a deterministic least-squares sense) even during abrupt changes in the signal statistics. This fact, together with the "exact" time-update property possessed by one particular realization, contributes to transient behavior superior to the gradient solutions and makes the least-squares structures an excellent candidate for our choice of adaptive algorithm.

The direct form implementation of the exact least squares algorithm was first presented by Morf et al [1977]. The lattice recursions were first reported in [Morf,Lee,Nichols and Viera 1977] and [Morf,Viera,Lee 1977]. A comprehensive presentation of the concept, including Hilbert-space approach derivations, joint process extensions and computer simulations demonstrating the tracking capability of these algorithms, is given by Lee [1980]. Satorius and Pack [1979] and Falconer and Ljung [1978] reported superior performance of the exact least squares algorithms in a channel-equilization application as did Hodgkiss and Presley [1982] in simulated frequency tracking situations and Nehorai and Morf [1982] in a line-enhancement context. Completely absent from the literature are reports on the performance of these structures in their noise-cancelling configuration.

2.6.1 The DLS solution to filtering and prediction

The deterministic least-squares (DLS) problem is formulated as follows: Given two dicrete time series

$$\{\ x(n),\ d(n)\ \}\ ,\qquad N_i \le n \le N_f$$

of dimension m and l respectively, we form the estimate of d(n)

$$\dot{d}(n) = \sum_{j=0}^{p} F_j^{(p)}(n) x(n-j)$$

$$= F_p^T(n) x_{[n:n-p]}$$

and with

$$\epsilon_{p,i,f}(n) = d(n) - \dot{d}(n)$$

we seek to minimize

$$\xi_p^d(i,f) = tr \sum_i^f \epsilon_{p,i,f}(n) \epsilon_{p,i,f}^H(n)$$

where i,f will be specified later $(N_i \le i < N_f\ ,\quad i < f \le N_f\ .)$

The deterministic least-squares (DLS) solution to the filtering problem is obtained through the same arguments used in the stochastic case and is given by:

$$F_p^T(i,f) R_{x,p}(i,f) = R_{dx,p}(i,f) \tag{25a}$$

where

$$R_{x,p}(i,f) = \sum_{n=i}^{f} x_{[n:n-p]} x_{[n:n-p]}^H$$

$$= X_p(i,f) X_p^H(i,f)$$

with

$$X_p(i,f) = \begin{bmatrix} x(i) & \cdots & x(f) \\ \cdots & \cdots & \cdots \\ \cdots & \cdots & \cdots \\ x(i-p) & \cdots & x(f-p) \end{bmatrix}$$

$$R_{dx,p}(i,f) = d_{[i:f]}^T X_p^H(i,f)$$

$$F_p^T = [\ F_p^{(0)},\ F_p^{(1)},\ ...,\ F_p^{(p)}\ ]$$

The minimum least-squares error is

$$E_p^d(i,f) = \min_{\{F\}} \xi_p^d(i,f)$$
$$= R_{d,00}(i,f) - F_p^T R_{dz,p}^H(i,f)$$

(25b)

Similarly, the DLS one-step predictor is given by:

$$A_p^T(i,f) R_{z,p}(i,f) = [\ E_p^c(i,f), 0, ..., 0\ ]$$

(26)

where

$$A_p^T(i,f) = [\ I_m,\ A_1^{(p)}(i,f),\ ...,\ A_p^{(p)}(i,f)\ ]$$

$$E_p^c(i,f) = R_{z,00}(i,f) - A_p^T Q_{z,p}(i,f)$$

$$Q_{z,p} = \sum_{n=i}^{f} x(n) x_{[n-1:n-p]}^H$$

Note that the exact form of $X_p(i,f)$ depends on the choice of i and f. The following choices are most commonly made, resulting in *sample correlation* matrices R with different symmetry and/or shift invariance properties. Such properties are crucial to the development of algorithmic implementations of the above solutions.

(1) Prewindowed case

$$i = N_i,\quad f = N_f$$

(2) Non windowed case

$$i = N_i + p,\quad f = N_f$$

(3) Pre- and postwindowed case

$$i = N_i,\quad f = N_f + p$$

Remarks

An interesting parallelism exists between stationarity conditions in the stochastic formulation and the various windowing schemes in the deterministic least-

squares development. For example, pre- and post-windowing results in a sample correlation matrix **R** which is Toeplitz, in direct analogy with wide-sense stationarity. The Toeplitz recursion is equally applicable here and is known as the "autocorrelation" method of linear prediction in the speech processing literature. The non-windowed case leads to an **R** which is symmetric but not Toeplitz and is known as the "covariance" method. (Clearly such characterizations are unjustified from a statistical point of view.)

The prewindowed case is of particular interest. It leads to a matrix **R** which is not Toeplitz but "close" to it and has shift properties which lead to an algorithmic solution with exact time-update. The statistical analogue would be a process which is not wide-sense stationary but "close" to it, in a sense not explicity defined in standard probability theory. This creates the possibility of treating processes with various degrees of stationarity through the same efficient algorithmic solutions once the appropriate structure for the true autocorrelation matrix has been established.

2.6.2 The "pre-windowed" DLS lattice

In this case, the *sample correlation* matrix **R** of order p is of the form

$$\mathbf{R}_{p,N} = \mathbf{X}_{p,N} \mathbf{X}_{p,N}^{H}$$

where,

$$\mathbf{X}_{p,N} = \begin{bmatrix} x(0) & \cdots & x(p) & \cdots & x(N) \\ 0 & \cdots & \cdots & \cdots & \cdots \\ 0 & 0 & x(0) & \cdots & x(N-p) \end{bmatrix}$$

Note that $\mathbf{R}_{p,N}$ is not Toeplitz but it consists of a product of two (upper- and lower-triangular) Toeplitz matrices and might be thought of as being "near-Toeplitz". In fact, it falls within the class of the so-called α*-stationary* matrices which can be expressed as

$$\mathbf{R} = \mathbf{T} + \sum_{i=1}^{\alpha} \sigma_i \mathbf{U}_i \mathbf{U}_i^{H}, \qquad \sigma_i = \pm 1 \tag{27}$$

where $\mathbf{T}$ is Toeplitz and the $\{\mathbf{U}_i\}$ are upper triangular Toeplitz matrices [Friend-lander, 1979]. These matrices are also known as "low shift rank" matrices [Morf, 1974]. For such matrices, it is possible to derive generalized Levinson-type recursions. Specifically in the pre-windowed case, $\mathbf{R}_{p,N}$ is α-*stationary* with $\alpha = 2$ and satisfies the following recursive identities:

order- and time-update

$$\mathbf{R}_{z,p}(N) = \begin{bmatrix} \mathbf{R}_{z,\infty}(N) & \mathbf{Q}_{z,p}(N) \\ \mathbf{Q}_{z,p}^{H}(N) & \mathbf{R}_{z,p-1}(N-1) \end{bmatrix} \qquad (28a)$$

order-update

$$\mathbf{R}_{z,p}(N) = \begin{bmatrix} \mathbf{R}_{z,p-1}(N) & \mathbf{V}_{z,p}^{H}(N) \\ \mathbf{V}_{z,p}(N) & \mathbf{R}_{z,pp}(N) \end{bmatrix} \qquad (28b)$$

time-update

$$\mathbf{R}_{z,p}(N) = \mathbf{R}_{z,p}(N-1) + \mathbf{x}_{[N-p:N]}\mathbf{x}_{[N-p:N]}^{H} \qquad (28c)$$

where

$$\mathbf{V}_{z,p}(N) = \sum_{n=0}^{N} z(n-p)\mathbf{x}_{[n-1:n-p]}^{H}$$

and all other quantities as previously defined. These identities form the basis for the exact order- and time-update recursions for the pre-windowed DLS prediction lattice. The DLS joint-process lattice can be obtained through an embedding technique, whereby the *joint* sample correlation matrix $\mathbf{R}_{z,p}(N)$ is defined as

$$\mathbf{R}_{z,p} = \mathbf{Z}_p(N)\mathbf{Z}_p^{H}(N)$$

where

$$\mathbf{Z}_p(N) = \begin{bmatrix} d(0) & \cdots & d(p) & \cdots & d(N) \\ x(0) & \cdots & x(p) & \cdots & x(N) \\ 0 & \cdots & \cdots & \cdots & \cdots \\ 0 & 0 & x(0) & \cdots & x(N-p) \end{bmatrix}$$

Then, the filtering normal equations can be re-expressed in terms of $\mathbf{R}_{z,p}(N)$ as follows:

48

$$\mathbf{F}_{jp}^T \mathbf{R}_{s,p}(N) = [\ E_p^s(N),\ 0,\ ...,\ 0\ ] \tag{29}$$

where

$$\mathbf{F}_{jp}^T(N) = [\ I_l,\ \mathbf{F}_p^T(N)\ ]$$

$\mathbf{R}_{s,p}$ has shift properties similar to $\mathbf{R}_{s,p}$. The two sets of recursions can be combined to concurrently solve the forward prediction, backward prediction and filtering problems, giving rise to the complex, multichannel DLS joint-process lattice. The needed algebraic manipulations are presented in Lee [1980] and Satorius and Pack [1979].

Exponential weighting

An adaptive version of the DLS lattice can be easily derived by introducing an exponential "window" in the error norm. Specifically, one may choose to minimize

$$\xi_p^s(N) = tr\sum_{n=0}^{N}\lambda^{N-n}\epsilon_{p,N}(n)\epsilon_{p,N}^H(n)$$

where λ is a constant ≤ 1, so that past errors will have a smaller influence on the estimate. This constant "fade" factor is easily incorporated into the lattice recursions and allows the algorithm to compensate for time variations in the input signals. The "effective" number of points used in this case may be defined in terms of a "time constant" as follows:

$$\lambda^{(N-n)} = \exp{-[\ (N-n)/N_{eff}\ ]}$$

Therefore,

$$N_{eff} = \min\{N,\frac{-1}{\ln\lambda}\}$$

In our implementation $\lambda = 1 - \alpha_{LSL}$.

2.6.3   Summary of the LSL algorithm

The scalar, complex, joint-process, exponentially weighted prewindowed least

squares lattice algorithm is summarized as follows (see Figure 2.3b): (The vector version is presented in Appendix B).

Initialization (i = 0, 1,... , p)

$$r_i(-1) = 0 \quad , \quad i \neq p \tag{30a}$$

$$E_i^r(-1) = \epsilon_{LSL} \quad , \quad \epsilon_{LSL} = 0.001 \text{ and } i \neq p \tag{30b}$$

$$\Delta_i(-1) = 0 \quad , \quad i \neq 0 \tag{30c}$$

$$b_k^{(i)}(-1) = 0 \quad , \quad 0 \leq k \leq i-1 \quad , \quad i \neq 0, \text{ and } i \neq p \tag{30d}$$

$$\gamma_{i-1}(-1) = 0 \quad , \quad i \neq p \tag{30e}$$

$$k_i^d(i-1) = 0 \tag{30f}$$

Time update (n $\geq$ 0)

$$e_o(n) = r_o(n) = x(n) \tag{30g}$$

$$E_o^e(n) = E_o^r(n) = (1 - \alpha_{LSL}) E_o^r(n-1) + |x(n)|^2 \tag{30h}$$

$$\gamma_{-1}(n) = 0 \tag{30i}$$

$$e_{-1}^d(n) = d(n) \tag{30j}$$

Order update (i = 0,1,...,p)

$$\Delta_i(n) = (1 - \alpha_{LSL}) \Delta_i(n-1) \tag{30k}$$

$$- \frac{e_{i-1}(n) r_{i-1}^*(n-1)}{1 - \gamma_{i-2}(n-1)} \quad , \quad i \neq 0$$

$$k_i^e(n) = \Delta_i^*(n) / E_{i-1}^e(n) \quad , \quad i \neq 0 \tag{30l}$$

$$k_i^r(n) = \Delta_i(n) / E_{i-1}^r(n-1) \quad , \quad i \neq 0 \tag{30m}$$

$$e_i(n) = e_{i-1}(n) + k_i^r(n)r_{i-1}(n-1) \quad , \quad i \neq 0 \tag{30n}$$

$$r_i(n) = r_{i-1}(n-1) + k_i^e(n)e_{i-1}(n) \quad , \quad i \neq 0 \tag{30o}$$

$$E_i^e(n) = E_{i-1}^e(n) - |\Delta_i(n)|^2 / E_{i-1}^r(n-1) \quad , \quad i \neq 0 \tag{30p}$$

$$E_i^r(n) = E_{i-1}^r(n-1) - |\Delta_i(n)|^2 / E_{i-1}^e(n) \quad , \quad i \neq 0 \tag{30q}$$

$$\gamma_{i-1}(n) = \gamma_{i-2}(n) + |r_{i-1}(n)|^2 / E_{i-1}^r(n) \quad , \quad i \neq 0 \tag{30r}$$

$$\Delta_i^d(n) = (1 - \alpha_{LSL})\Delta_i^d(n-1) - \frac{e_{i-1}^d(n)r_i^*(n)}{1 - \gamma_{i-1}(n)} \tag{30s}$$

$$k_i^d(n) = \frac{\Delta_i^d(n)}{E_i^r(n)} \tag{30t}$$

$$e_i^d(n) = e_{i-1}^d(n) + k_i^d(n)r_i(n) \tag{30u}$$

Predictors

$$a_i^{(i)}(n) = k_i^r(n) \tag{30v}$$

$$b_e^{(i)}(n) = k_i^e(n) \tag{30w}$$

$$a_l^{(i)}(n) = a_l^{(i-1)}(n) + k_i^r(n) \ b_{l-1}^{(i-1)}(n-1) \tag{30x}$$

$$1 \leq l \leq i-1$$

$$b_l^{(i)}(n) = b_{l-1}^{(i-1)}(n-1) + k_i^e(n) \ a_l^{(i-1)}(n) \tag{30y}$$

The likelihood variable

The parameter which controls the adaptation response of the LSL is $\gamma_{s,p}$, defined by

$$\gamma_{s,p} = \mathbf{x}_{[N-p:N]} \mathbf{R}_{s,p}^{-1} \mathbf{x}_{[N-p:N]} \tag{31}$$

It can be shown [Lee, 1980] that

$$0 \leq \gamma_{s,p} \leq 1.$$

γ has an interesting statistical interpetation as the likelihood of deviation of the p

succesive samples from a joint Gaussian distribution parameterized by $\mathbf{R}_{x,p}$. [Morf and Lee, 1978]. It can be expected to be ~ 0 except when the signal statistics undergo drastic changes, in which case it will approach unity.

Note that in the LSL recursions (Eq. 30s) the "crosscorrelation" quantities Δ_i are weighted by a gain factor equal to

$$\frac{1}{1 - \gamma_{i-1}}$$

which replaces the "smoothed" power estimates of the stochastic gradient algorithms. Clearly, when $\gamma_{i-1} \sim 1$ the algorithm will undergo extremely fast, almost instantaneous, adaptation. It is the presence of this optimum gain factor which sets the "exact" least squares lattice apart from the suboptimum gradient approximations and results in its superior transient response (see Simulation 2.)

On the choice of adaptation coefficient

The proper choice of adaptation coefficient can be made by considering the more general question of resolution *vs* statistical reliability. If WSS holds for all time, then $\alpha = 0$ is the optimum choice and the time-invariant Wiener-Hopf solution is obtained. In cases of practical interest, local WSS if more often encountered and the desired "resolution" is controlled by the time scale of variation of the signal statistics. By that it is meant that one must refrain from averaging over a number of distinct statistical events. Therefore the lower limit of the adaptation coefficients (or the upper limit of the allowable averaging interval) is set by the stationarity properties of the input process. In the gradient descent algorithms (LMS,GRL) the lower bound of α is imposed by the *misadjustment* noise, caused by excessively large steps in the gradient search process (e.g. equation (17)). In the case of the exact deterministic least-squares solution (LSL), there is no misadjustment error. The lower bound of α_{LSL} is strictly a question of statistical reliability.

A complete statistical analysis of the lattice structure has not been pursued in this thesis. However, insight may be gained by considering the variance of the following crosscorrelation estimate between two bandwidth-limited white noise processes $x(n)$ and $y(n)$:

$$\hat{R}_{xy}(k) = \frac{1}{N_{eff}} \sum_{i=0}^{N_{eff}} x(i)y(i+k)$$

where,

$$N_{eff} = \frac{-1}{\ln(1 - \alpha_{LSL})}.$$

The variance of the estimate is given by [Bendat and Piersol, 1971]:

$$Var[\hat{R}_{xy}(k)] = \frac{1}{N_{eff}}(R_{xx}(0)R_{yy}(0) + R_{xy}(k))$$

The above indicates that large, spurious crosscorrelation values can be generated between two uncorrelated processes $(R_{xy}(k) = 0)$, for sufficiently small N_{eff} and/or large autocorrelations within the two processes. Although direct comparison between this simple result and the behavior of the lattice parameters for arbitrary signals is not possible, the LSL joint-process filter has been observed to obey this general rule. Specifically, the filter has shown a tendency towards cancellation of the primary channel when the primary and reference channels consisted of independent white noise sequences, for $\alpha_{LSL} \gg 0.02$. This empirically derived value will be used as the upper bound for α_{LSL} throughout this thesis.

2.7 Computer simulations

The exposition of the theoretical foundation of the LMS, GRL and LSL filters in the preceding sections of this chapter enables us to make certain conjectures regarding their operational characteristics. First, one may expect the LMS to be susceptible to the "eigenvalue spread" condition. On the other hand, a lattice filter (GRL

or LSL) should not be affected owing to their orthogonalization (stage-by-stage decoupling) property. Secondly, the stochastic approximation solutions (LMS and GRL) are clearly suboptimum during transient conditions (i.e. departures from WSS). The exact deterministic LSL solution, on the other hand, remains optimum (in a least-squares sense, not in a stochastic MMSE sense) during such transient states and may be expected to perform better. The simulations of this section were intended to provide support for these mathematical conjectures. They are a representative subset of a large number of simulations performed during the course of this research project [e.g. Alexandrou and Hodgkiss, 1982d,e]. Simulations 1 and 2 were designed to bring out the operational characteristics of the three chosen structures (LMS, GRL, LSL) under transient conditions and in the presence of the "eigenvalue spread" and "scale change" effects, respectively; the third to demonstrate the potential advantage of the multichannel lattice filter over a cascade of single channel filters, when multiple reference signals are available. The scalar, complex versions of LMS, GRL and LSL as well as the vector, complex LSL have been programmed in *Ratfor* [Kernighan, 1975] and used throughout this work.

For the sake of clarity, simple complex exponentials in additive white noise were used, which undergo frequency and/or magnitude "steps" at prescribed points during the iteration. However, the simulated transients do represent conditions which are likely to be encountered in real reverberation signals. Therefore, these results are pertinent to the performance of the chosen algorithms in a reverberation cancellation context. These noise-cancelling simulations have not appeared previously and are a major contribution of this thesis.

2.7.1   Simulation 1 : Eigenvalue spread

The objective here is to examine the performance of the LMS, GRL and LSL

in a noise-cancelling setting, where the reference signal components have widely separated power levels. Both main (primary) and reference channels consist of a pair of complex exponentials corrupted by white noise. The reference channel signals undergo a frequency "step" at iteration number 1536. Table 2.1, below, fully describes the simulation.

Simulation 1	before step		after step	
	main	reference	main	reference
ω_1	$\dfrac{\pi}{8}$	$\dfrac{\pi}{4}$	$\dfrac{\pi}{8}$	$\dfrac{\pi}{8}$
$SNR_1(db)$	20	10	20	10
ω_2	$\dfrac{6\pi}{8}$	$\dfrac{7\pi}{8}$	$\dfrac{6\pi}{8}$	$\dfrac{6\pi}{8}$
$SNR_2(db)$	20	20	20	20

Table 2.1 Summary of Simulation 1

The main and reference channels are displayed in Figure 2.5a and 2.5b respectively, in the form of a Range-Doppler-Map (RDM) created by taking successive, 50% overlapped FFTs of the two time-series. A filter order of p=3 was used and the adaptation parameters were chosen such that the response of all three algorithms to the high power sinusoid was similar. The joint-process error outputs produced by LMS,GRL and LSL are shown in Figures 2.5c,d,e. It is evident that the LMS is lagging substantially in the cancellation of the lower power sinusoid compared to the two lattice filters. The LSL performs marginally better than the GRL which is consistent with previous findings in a frequency tracking application [Hodgkiss, 1981.]

Remarks

The "eigenvalue spread" condition is likely to exist in a real composite reverberation signal since the surface, volume and bottom components are normally characterized by large intensity disparities. The LMS is therefore a poor candidate for

our purposes.

2.7.2 Simulation 2 : Scale change

The fundamental difference between the stochastic approximation realizations (e.g. LMS, GRL) and the deterministic least-squares filter (LSL) is the fact that the latter continues to be optimum within its design even during abrupt changes in the characteristics of the signal(s). The LMS and GRL are, in such cases, clearly suboptimum in either the stochastic (MMSE) or the deterministic least-squares sense. This simulation was intended to bring out the specific consequences of this fact. The complex exponentials in the reference channel perform, in addition to the frequency step, undergo instantaneous magnitude "jumps" of 10,20 and 30 db. The simulation is described in Table 2.2.

Simulation 2	before step		after step	
	main	reference	main	reference
ω_1	$\dfrac{\pi}{8}$	$\dfrac{\pi}{4}$	$\dfrac{\pi}{8}$	$\dfrac{\pi}{8}$
$SNR_1(db)$	20	10	20	20,30,40
ω_2	$\dfrac{6\pi}{8}$	$\dfrac{7\pi}{8}$	$\dfrac{6\pi}{8}$	$\dfrac{6\pi}{8}$
$SNR_2(db)$	20	10	20	20,30,40

Table 2.2 Summary of Simulation 2

The filter outputs for these three cases are shown in Figures 2.6 and 2.7a. The magnitude plots were artificially "clipped" for display purposes.

The GRL proved to be extremely sensitive to this "scale change" effect and became increasingly unstable, failing completely to recover from the transient in the 40 db case. The LMS is similarly succeptible although it appears to be considerably more robust. The LSL was able to adapt immediately to all magnitude jumps. The

likelihood variable can be seen (Figure 2.7b) to approach unity as the severity of the discontinuity inceases. The crosschannel coefficients (k_2^i) of the GRL and the LSL exibit a similar behavior (Figure 2.8).

It is likely that the specific reason for the instability of the gradient filters lies in the "smoothed" power estimate (Eqs. (19), (22b), (23b)) used to normalize the coefficients of these filters. This low-pass filtered power estimate does not change fast enough to compensate for large instantaneous power jumps.

Remarks

The "scale change" condition is also likely to be in effect for real reverberation signals. For instance, the onset of surface reverberation in a volume reverberation backround can readily amount to an abrupt increase in intensity of the order of the simulated magnitude jumps.

2.7.3   Simulation 3: Multichannel vs cascade

In situations where spatially adaptive beamforming is in order and direct control of the spatial transfer function is desirable, the need for the true vector (multichannel) filter is obvious. If, however, the primary channel interference simply consists of a summation of components each of which can be "tapped" individually, one might argue that a valid alternative to the multichannel structure is a cascade of scalar (single-channel) filters where a single interference component is used as the reference channel at each stage of the cascade (Figure 2.9). This simulation will show that although this may in fact be the case when the interference components are mutually uncorrelated, in general the multichannel filter is the better choice because of its ability to compensate for interference components correlated between all reference channels (and not present in the primary channel). In order to clarify this point, consider the case of a scalar primary process $d(n)$ and a two-channel reference signal

consider the case of a scalar primary process $d(n)$ and a two-channel reference signal $\mathbf{x}(n)$,

$$\mathbf{x}(n) = \begin{bmatrix} x_1(n) \\ x_2(n) \end{bmatrix}$$

The matrix form of the solution is (see eq. 2.2)

$$\mathbf{F}^T \mathbf{R}_{xx} = \mathbf{R}_{dx}$$

For the sake of simplicity consider only the 0th order solution (no time lags involved.) For that case, we have:

$$\mathbf{R}_{xx} = E\left\{ \begin{bmatrix} x_1(n) \\ x_2(n) \end{bmatrix} [\, x_1^*(n) \quad x_2^*(n) \,] \right\}$$

$$= \begin{bmatrix} R_{x_1 x_1}(n,n) & R_{x_1 x_2}(n,n) \\ R_{x_2 x_1}(n,n) & R_{x_2 x_2}(n,n) \end{bmatrix}$$

and

$$\mathbf{R}_{dx} = [\, E\{ d(n) x_1(n) \} \quad E\{ d(n) x_2(n) \} \,] = [\, R_{dx_1}(n,n) \quad R_{dx_2}(n,n) \,]$$

$$\mathbf{F}^T = [\, f_1^o \quad f_2^o \,]$$

Therefore,

$$[\, f_1^o \quad f_2^o \,] \begin{bmatrix} R_{x_1 x_1}(n,n) & R_{x_1 x_2}(n,n) \\ R_{x_2 x_1}(n,n) & R_{x_2 x_2}(n,n) \end{bmatrix} = [\, R_{dx_1}(n,n) \quad R_{dx_2}(n,n) \,]$$

or,

$$f_1^o R_{x_1 x_1}(n,n) + f_2^o R_{x_2 x_1}(n,n) = R_{dx_1}(n,n)$$
$$f_1^o R_{x_1 x_2}(n,n) + f_2^o R_{x_2 x_2}(n,n) = R_{dx_2}(n,n)$$

Therefore, the two-channel solution has access to the cross-reference channel components $R_{x_1 x_2}$ and $R_{x_2 x_1}$ and has the option of removing them from either reference channel if they are a major source of output error. This fact can be useful in practice as it can potentially aleviate the effect of additive noise in the reference channels,

described in Section 2.3.

In order to confirm this, two reference channels were created each consisting of a single complex sinusoid in white noise "stepped" in frequency at iteration point 1536 to match the primary input signals. The primary channel of simulation 1 was also used here. A large white noise component ($SNR_w = 10db$) was added to both reference channels to play the role of the cross-channel interference. The simulation is fully described in Table 2.3.

Simulation 3	before step			after step		
	main	ref1	ref2	main	ref1	ref2
ω_1	$\dfrac{\pi}{8}$	$\dfrac{\pi}{4}$		$\dfrac{\pi}{8}$	$\dfrac{\pi}{8}$	
$SNR_1(db)$	20	10		20	10	
ω_2	$\dfrac{6\pi}{8}$		$\dfrac{7\pi}{8}$	$\dfrac{6\pi}{8}$		$\dfrac{6\pi}{8}$
$SNR_2(db)$	20		10	20		10
$SNR_w(db)$		10	10		10	10

Table 2.3 Summary of Simulation 3.

The theoretical evidence (Equation 5a) suggests that the presence of this large white noise component will render noise-cancelling impossible on a single channel basis. The multichannel structure, on the other hand should be able to compensate for such cross-channel noise and proceed with its noise-cancelling task. The simulation results provide support for this assertion. The single-channel LSL with reference channel 1 is unable to perform noise-cancelling (Figure 2.10a,b) and therefore cascade processing of one channel at a time is not possible in this setting. On the other hand, the vector ($m = 2$) LSL is successful in eliminating both the cross-channel white noise component and the sinusoidal interference from the primary input (Figure 2.10c,d,e).

Remarks

This scenario will arise when multiple preformed reference beams are available. When the beams overlap, any component(s) entering through the overlap region (more specifically the part of it which is does not intersect the main beam) will serve as the cross-channel interference components and will have a deleterious effect on cancellation via cascade processing.

2.8   Chapter summary

The adaptive filtering problem was set in the proper theoretical framework. Adaptive beamforming was presented in the context of ANC. The origin of the lattice structure was examined and the relative advantages of the various implementations were considered. The basic differences between the stochastic approximation and the exact deterministic least-squares methods was established. Through computer simulations, the lattice filters were shown to be superior to direct TDL forms in a noise-cancelling setting. The deterministic least-squares lattice was shown to remain stable under drastic magnitude transients that drive the gradient algorithms to instability. Finally, the ability of the multichannel structure to cancel components correlated between reference channels and thus, its superior performance over a cascade of single-channel filters, was demonstrated.

60
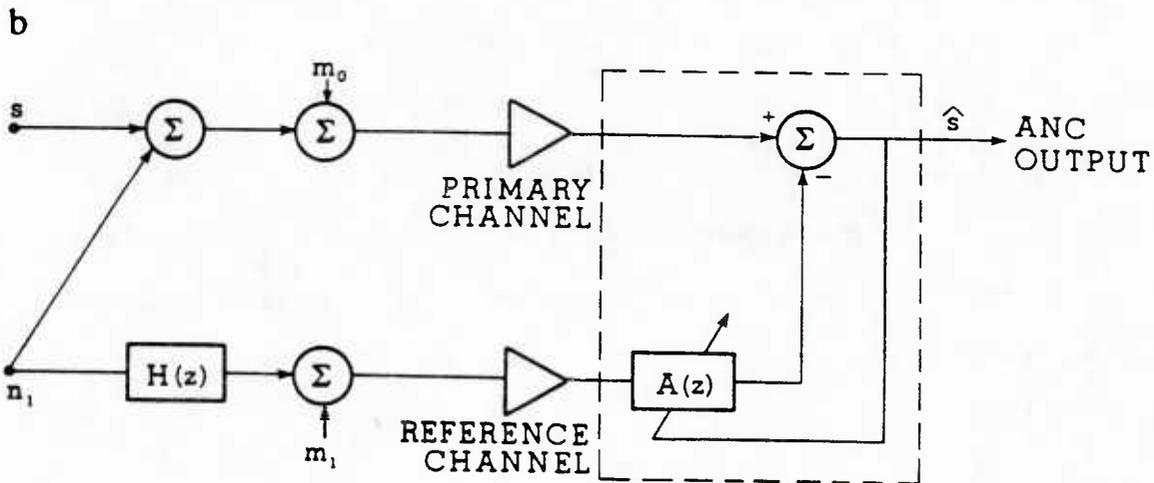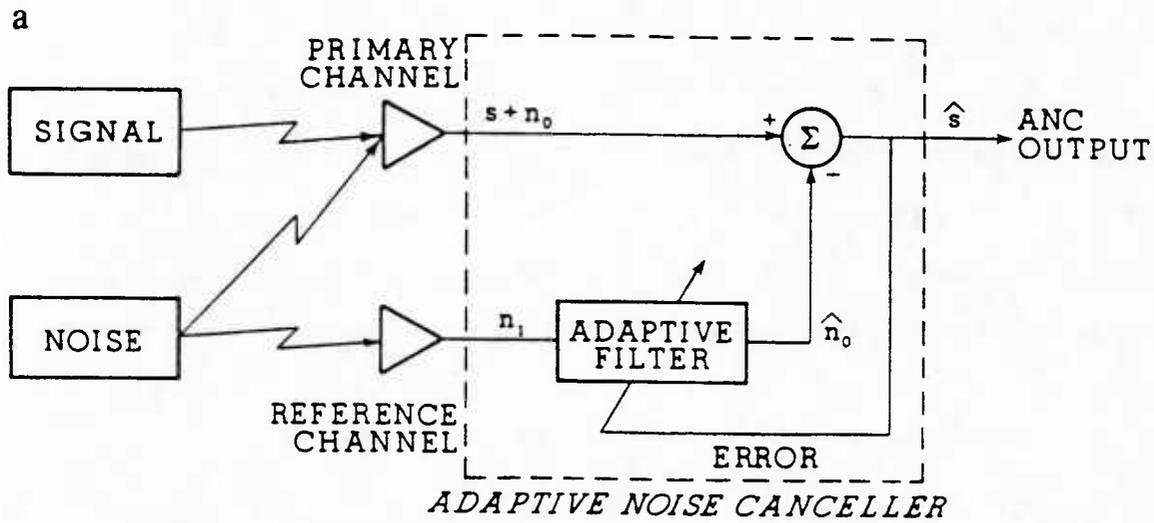
Figure 2.1 *The noise cancelling concept.* (a) General structure, (b) Widrow's linear model. Here m_0 and m_1 represent uncorrelated additive noise components in the two channels. The "mismatch" between the primary and reference channels, expressed by $H(z)$, must be compensated for by the adaptive filter transfer function $A(z)$.
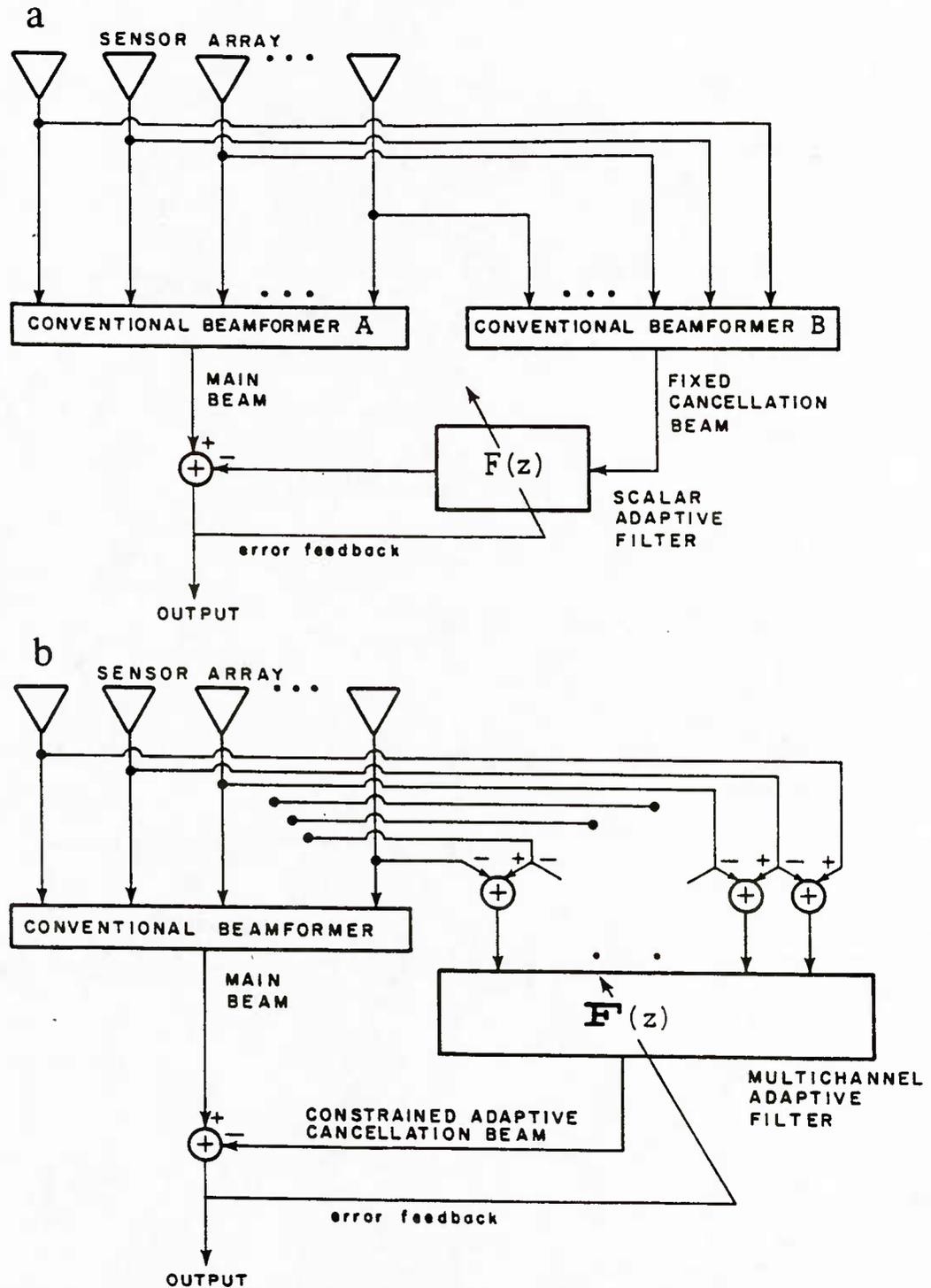
Figure 2.2 *Adaptive beamforming via ANC.* (a) Fixed, preformed reference beam. An external steering mechanism is required to track the changing directional properties of the interference. (b) Constrained adaptive beamformer. The multichannel adaptive filter weights the constrained elements to form a spatially adaptive reference beam.

62
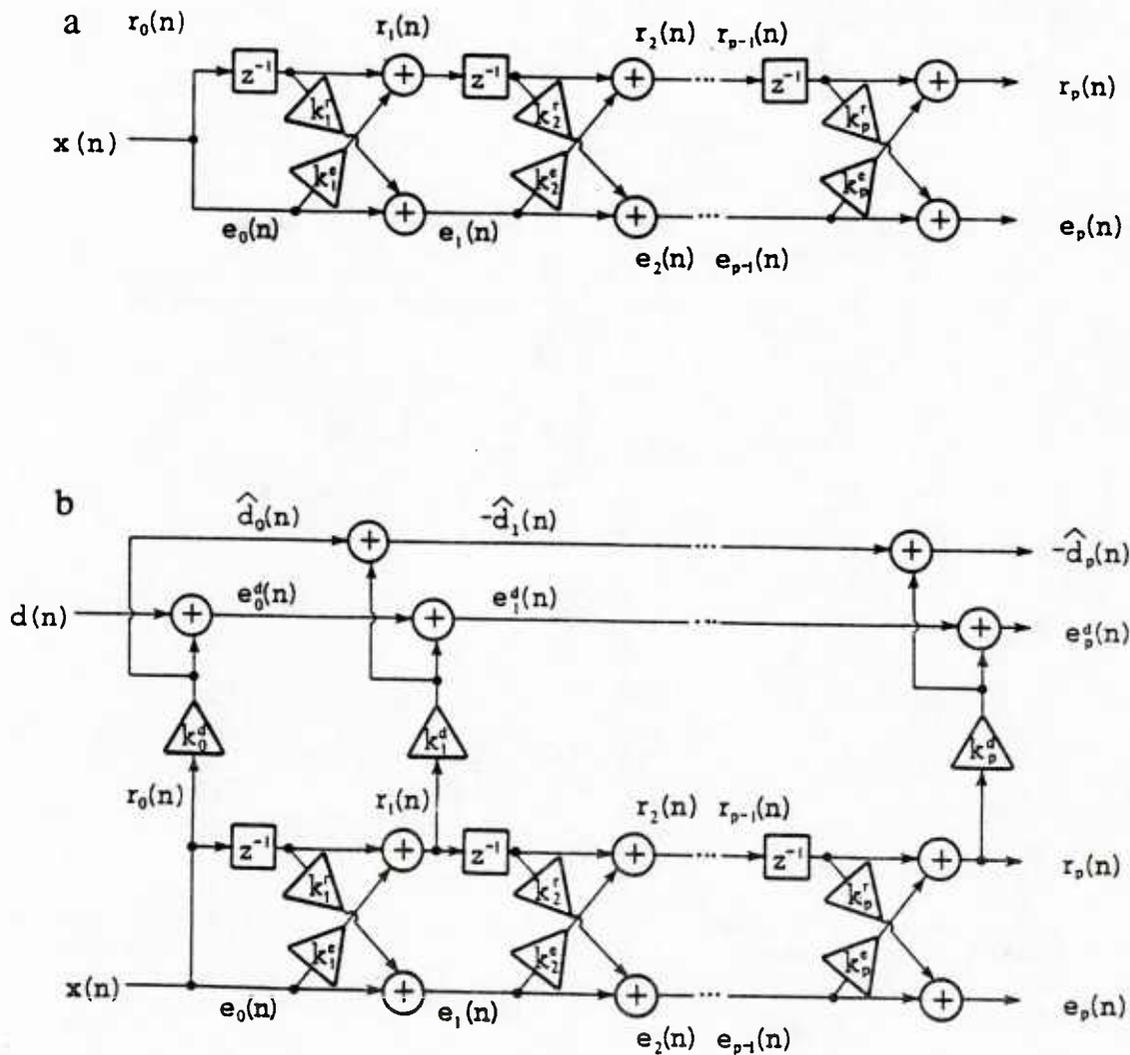
Figure 2.3 *The lattice filter.* (a) Prediction error (whitening) filter; k_i^e and k_i^r are the forward and backward reflection (PARCOR) coefficients; $e_i(n)$ and $r_i(n)$ are the ith order forward and backward prediction error sequences. (b) Joint-process filter; the $r_i(n)$ constitute an orthogonal basis for the reference process $x(n)$ and are weighted by the cross-channel coefficients k_i^d to produce an estimate of the primary process $d(n)$.

a

b
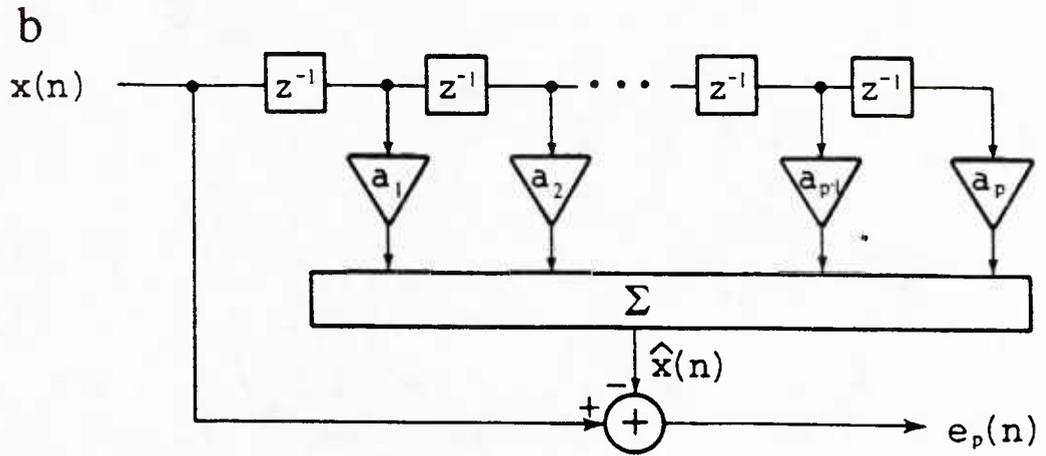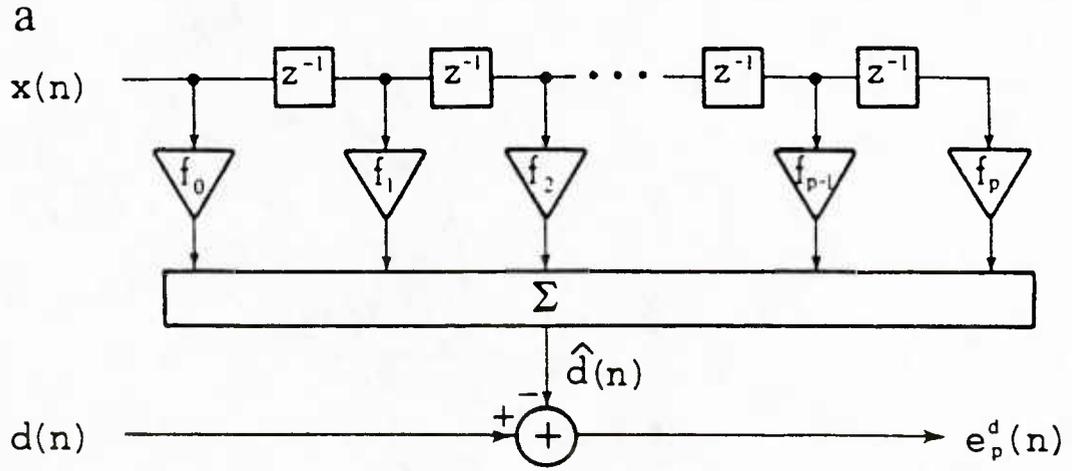
Figure 2.4 *Transversal tapped-delay-line (TDL) filter.* (a) joint-process configuration, (b) one-step forward predictor.
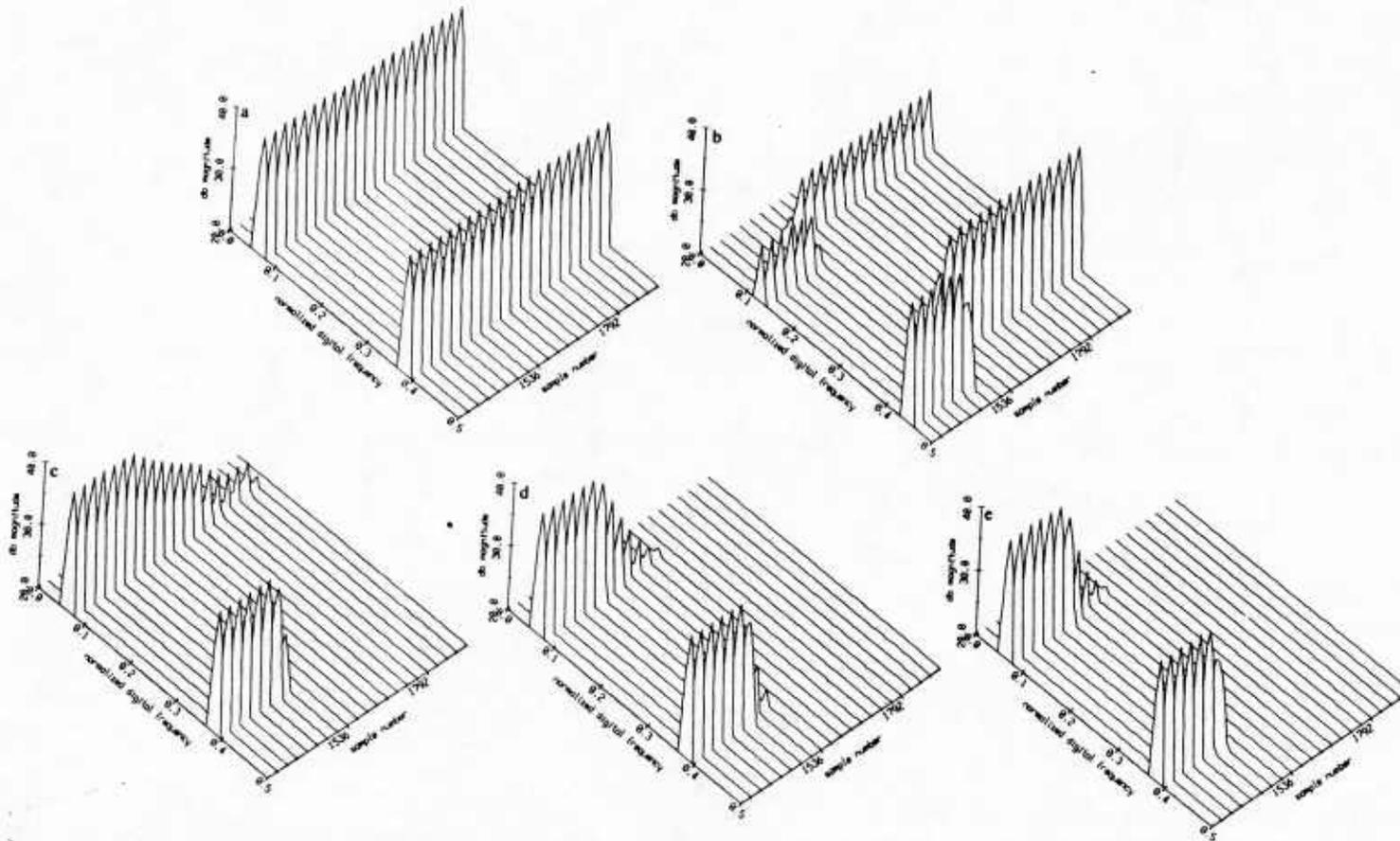
Figure 2.5 *Simulation 1: Eigenvalue spread.* (a) Primary channel input, (b) reference channel input, (c) LMS output, (d) GRL output, (e) LSL output. Not that the LMS lags significantly in cancelling the weak sinusoid.
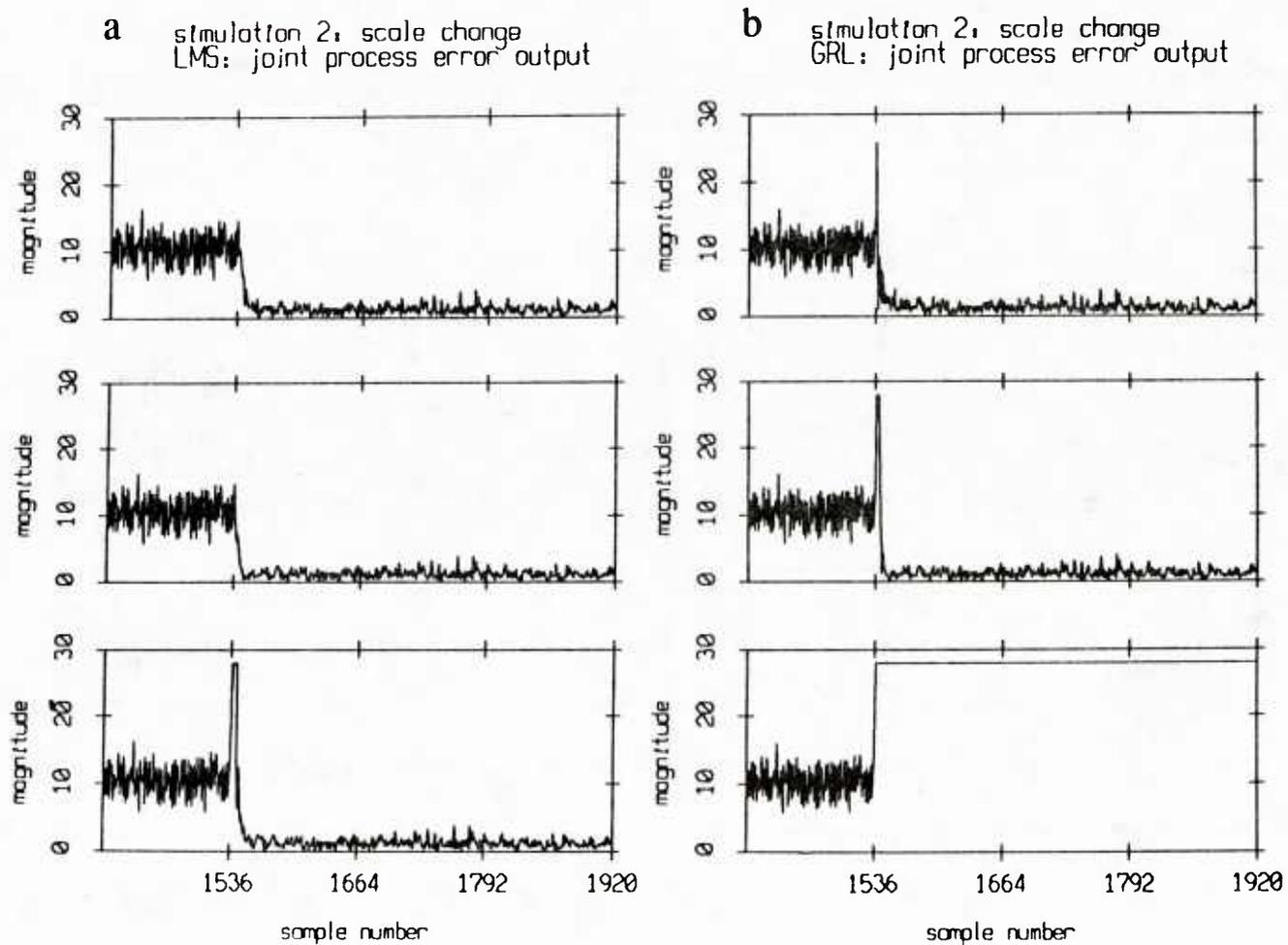
Figure 2.6 *Simulation 2: Scale change.* (a) LMS output (10,20,30 dB jumps) (b) GRL output (10,20,30 dB jumps). Both structures become increasingly unstable as the severity of the scale change increases. (The observed clipping was imposed to facilitate display).
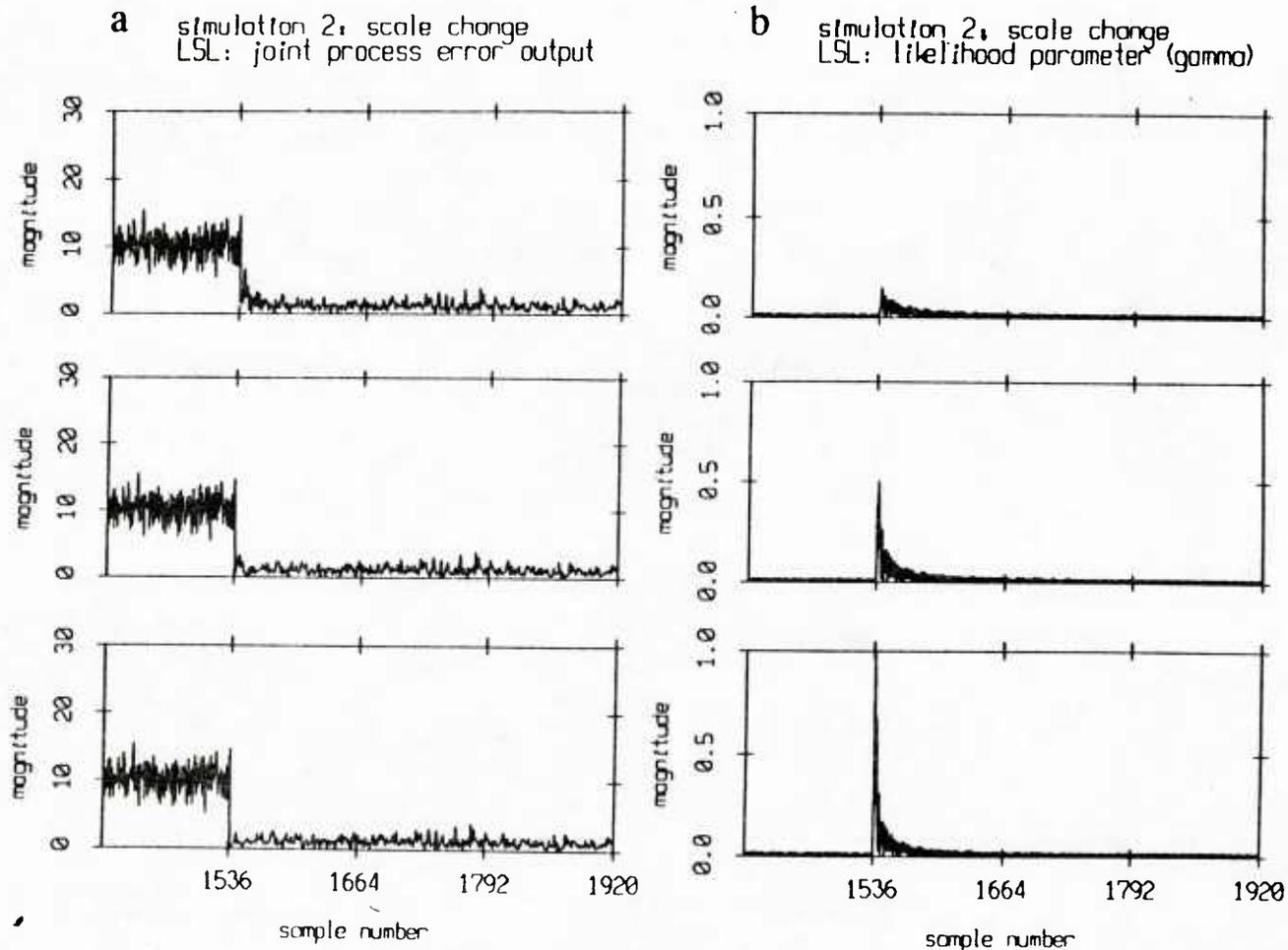
Figure 2.7 *Simulation 2: Scale change.* (a) LSL output (10,10,30 dB jumps) (b) LSL "likelihood parameter" (γ) (10,20,30 dB jumps). Note that the likelihood parameter instantaneously "absorbs" the drastic power transients, allowing the LSL algorithm to adapt gracefully.
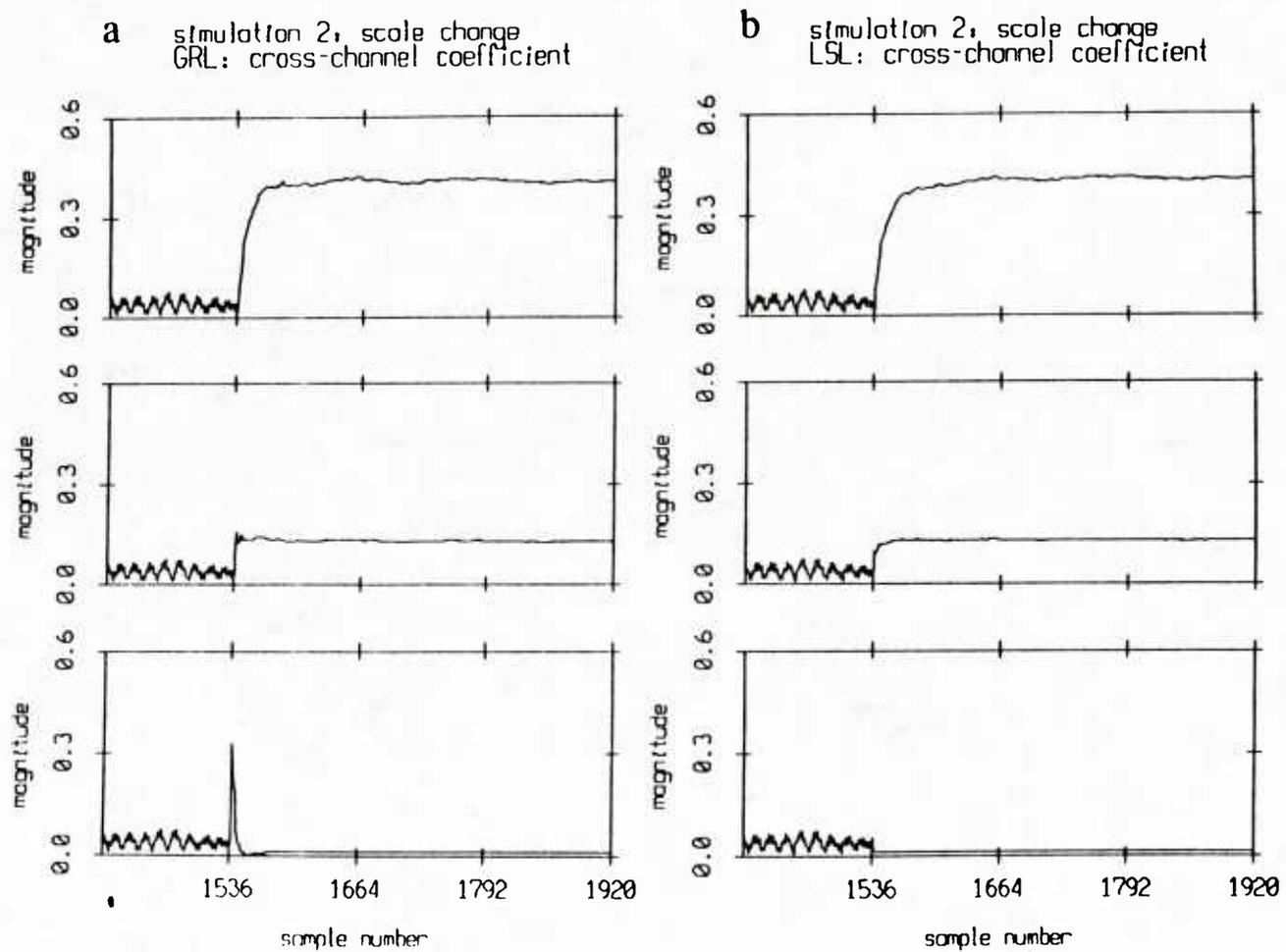
Figure 2.8 *Simulation 2: Scale change.* (a) GRL cross-channel coefficient (k_1^d) and (b) LSL cross-channel coefficient (k_1^d). The instability induced by the power transients is evident in the GRL coefficient, especially for the 30 dB jump. The LSL coefficient exhibits no signs of instability.
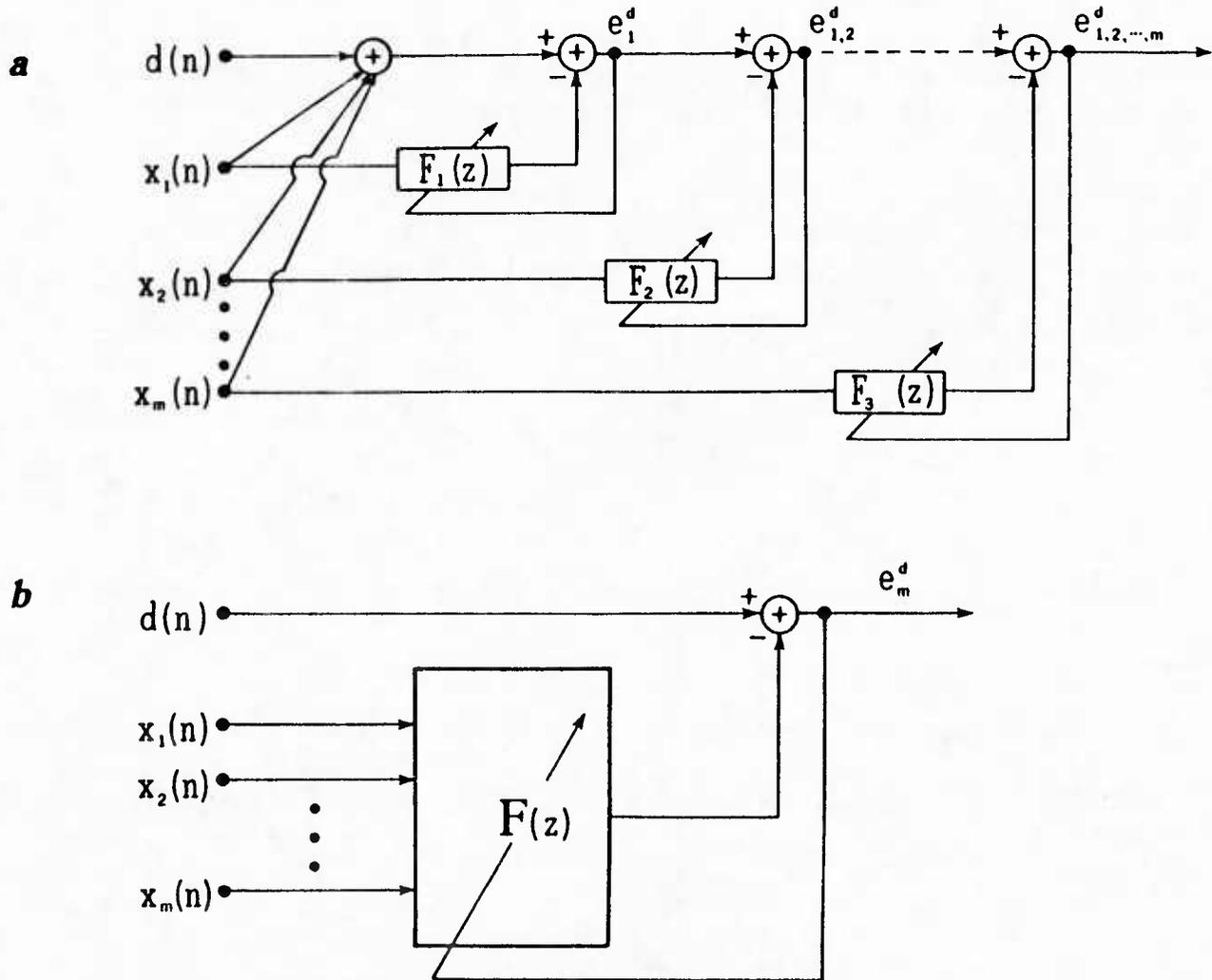
Figure 2.9 *Multichannel vs cascade.* (a) Cascade of scalar filters, (b) multichannel joint-process filter.
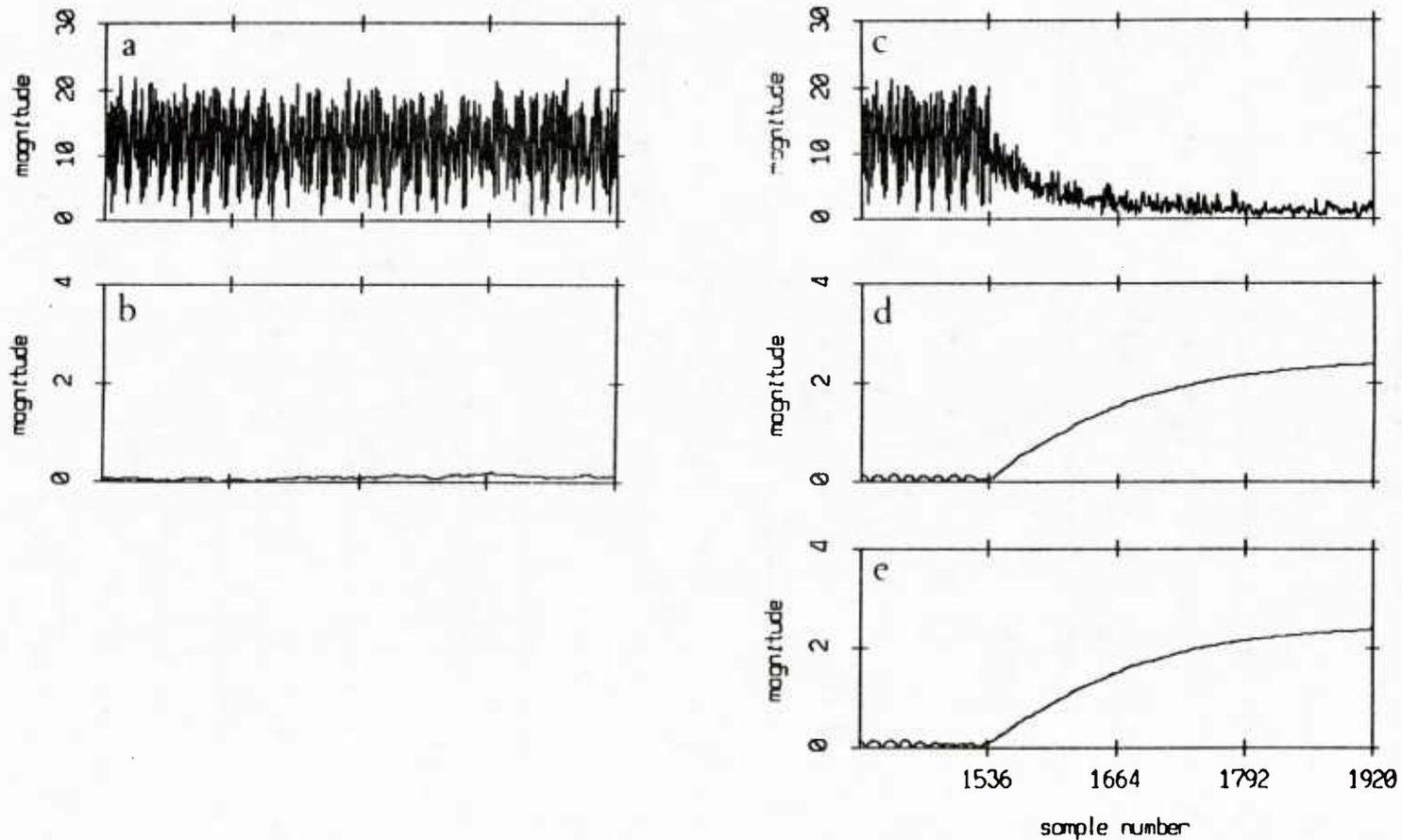
**Figure 2.10** *Simulation 3: Multichannel vs cascade.* (a) Single channel LSL joint-process error output and (b) cross-channel coefficient (k_2^j). The scalar filter is unable to compensate for the presence of a large uncorrelated noise component in the reference channel. On the other hand, the two-channel LSL joint-process error output (c) indicates that the multichannel structure can remove the additive noise component common to both reference channels. This is confirmed by the behavior of the two cross-channel coefficients (d,e).

CHAPTER III
BOUNDARY REVERBERATION REJECTION
IN A SHALLOW WATER ENVIRONMENT

In this chapter, the adaptive beamforming concept will be applied to real reverberation data from a shallow-water active sonar experiment. The shallow-water environment creates some unique difficulties. As opposed to deep-water settings where the acoustic paths are few and identifiable, shallow-water reverberation returns arrive in rapid succession, imposing stringent adaptation requirements on the algorithm and complicating the performance evaluation process.

Two types of problems will be considered here. The first is the detection of acoustic signals embedded in a reverberation backround. This is the problem which may be encountered, for instance, in a fisheries sonar application. The performance of a horizontally directed sonar deployed from a surface vessel is often reverberation-limited. Particularly difficult to detect would be low-Doppler, distributed reflectors such as fish schools moving slowly and/or at an angle to the sonar beam. It will be shown that the detectability of such echo returns can be greatly enhanced through adaptive filtering. The second problem is selective reverberation cancellation (SRC). In this case, signal and noise are constituent components of the received composite reverberation process. Volume reverberation is normally assumed to be the component of interest with boundary reverberation being the interference.

In Chapter 2 we have shown that the correct choice of adaptive processor is of critical importance for succesful reverberation cancellation. However, this choice is not the only factor that merits consideration. Equally important is the decision concerning the filter configuration to be adopted in a particular experiment. In general, this decision will be influenced by the experimental geometry, the degree of control

70

over the spatial characteristics of the system which is afforded by the data acquisition system, the properties of "signal" and "interference" and the objectives of a particular deployment. The most appropriate structure for our purposes is a spatially constrained adaptive beamformer based on the adaptive noise-cancelling (ANC) principle. Given the distinctly different scattering mechanisms responsible for the three reverberation types, the independence assumptions (see Section 2.3) are readily satisfied. No further assumptions need to be made about the relative intensity and duration of signal and interference and no modifications of the algorithm are necessary in order to impose the constraints. The question remains as to the exact manner in which spatial constraints are imposed. Spatial prefiltering can range from complete conventional beamforming designed to encompass the interference and exclude the "signal" component from the reference channel to simple element-to-element subtraction followed by adaptive beamforming controlled by a multichannel algorithm. Both fixed, preformed and spatially constrained adaptive reference beams will be used in this chapter with attention to their relative advantages. The possibility of applying the results on the (vertical) spatial correlation characteristics of boundary and volume reverberation presented in Section 1.4, in conjunction with direct ANC, will also be considered. The Least-Squares Lattice (LSL) in its scalar and multichannel forms will be exclusively used as the adaptive processor, based on theoretical considerations and simulation results presented in Chapter 2.

3.1   The Dabob Bay environment

The experiment was conducted in the deepest part of Dabob Bay, Washington (maximum depth $\sim200m$). The physical, biological and acoustical properties of Dabob Bay have been studied intensively [Helton, 1976]. It is characterized by large fluctuations of temperature and salinity. In addition to the usual seasonal variations

in the top ~30m, cellular inhomogeneities exist in the deeper regions, caused by intrusions of Pacific Ocean water. Water parcels have been detected with distinctly different values of temperature and salinity, with thickness of ~40 m and horizontal extent up to ~1000 m [Ebbesmeyer, 1973], which may remain intact for several weeks before they dissipate. These transient water masses cause wide fluctuations in the sound velocity structure and create the need for up-to-date sound velocity profiling during acoustic experiments. Coring device sampling [Burns, 1962] has shown that the deep regions of Dabob Bay are covered by silt and mud with some sand and fine gravel. A harder, highly reflective, layer consisting of glacial till (a dense mixture of sand, gravel and silt) begins 1–15m below the mudline. A maximum bottom backscattering coefficient of –20db was measured at 30kHz. Correspondingly, the surface backscattering coefficient was found to be in the range of –35 to –25db. Intensive volume sampling and volume scattering measurements over a period of two years has revealed multiple scattering layers with substantial seasonal variations [Anderson, 1981]. The maximum measured volume scattering coefficient is ~–60db.

3.1.1   Experiment Description

The sonar system moved with constant velocity along straight line paths. It carried a transducer array whose elements were combined by a programmable conventional beamformer capable of producing several transmit/receive beam sets. The overall system geometry is depicted in Figure 3.1. The transmit beam pattern choice included a "wide" (60° X 60°) and a "narrow" (15° X 15°) beam. Two receive beam sets were available. The first (beam set 0) consisted of 9 preformed (15° X 15°) beams steered in the directions indicated in Table 3.1. In this coordinate system elevation runs from -90° (up) to 90° (down) and bearing from -180° to 180° relative to broadside (0°).

Beam number	1	2	3	4	5	6	7	8	9
Elevation	0°	-7.5°	-7.5°	-7.5°	-7.5°	7.5°	7.5°	7.5°	7.5°
Bearing	0°	15°	7.5°	-7.5°	-15°	15°	7.5°	-7.5°	-15°

Table 3.1 Steering directions of preformed beam set

It may be noticed that beams 3,4,7,8 overlap partially with the center beam (1). This beam arrangement has good potential as a noise-cancelling configuration. The second receive set (beam set 1) contains the outputs of 9 row sums comprising the array face and constitutes a relatively "raw" data set well-suited for multichannel adaptive beamforming operations. The sonar system transmitted $180ms$ pulses and recorded digitally the complex-basebanded reverberation return. Narrowband calibration returns arriving broadside to the array are occasionally present which are useful "control" signals valuable in assessing the cancellation results. CTD profiles were recorded before each experimental run.

3.2   Adaptive "whitening" of reverberation data

Before we embark on dual-channel ANC operations it would be of interest to examine the effect of single-channel processing with the prediction-error (whitening) filter on real reverberation data. Two potential benefits come to mind. First, time evolving "high resolution" spectral estimates can be obtained or, equivalently, the appropriate AR model for reverberation can be identified. Second, by adjusting the adaptation coefficient, the sensitivity of the filter to transient signals off the main reverberation frequency "ridge" can be substantially reduced. As a result, these signals may be allowed to "leak" in the error output with considerably improved SNR.

The composite reverberation spectrum has a complex and highly variable structure. Boundary reverberation has, typically, an abrupt onset. Morover, surface reverberation is often characterized by Doppler shifts distinctly different from the

volume return [Igarashi and Stern, 1970; Swarts, 1971]. It follows that effective whitening of the reverberation ridge cannot be accomplished with a fixed notch filter. On the other hand, the frequency tracking capability of the adaptive filter should allow it to be more successful to that end.

3.2.1 Data description

Ping EXP3.1 was chosen to undergo adaptive "prewhitening". During this run, the sonar depth was 100 m and receive beam set 0 (9 preformed beams) was in effect. Only the output of the center beam (beam 1 in Figure 3.1b) is considered here. The sound velocity profile measured prior to this run and the associated ray-tracing diagram are displayed in Figure 3.2. The received reverberation is highly composite with both boundaries contributing to the return. Because no real signals are present in this data set, two synthetic echoes (T1 and T2) were inserted in the vicinity of the reverberation ridge in order to demonstrate the degree of signal enhancement attained through adaptive whitening. They are described in Table 3.2 below.

Signal echo	T1	T2
Onset time	1.5 s	2.5 s
Duration	180 ms	180 ms
SNR	~ 0	~ 0
Velocity	0 m/s	0.375 m/s

Table 3.2 Sythetic echo description

The input waveform is displayed in Figure 3.3. The time series plot was made following low-pass filtering and decimation by a factor of 8 in order to facilitate the display of the time-varying features of the data. The Range Doppler Map (RDM) plot is intended to show the time-varying character of the ping in the frequency domain. It was constructed via successive 128-point FFTs of windowed (Kaiser-Bessel, α=2.5)

data segments with 50% overlap. The (dB) magnitude of each transform corresponds to a single line in the pseudo-3d plot. The Time-Varying-Gain (TVG) applied to this ping was designed to compensate for the attenuation factor due to spherical spreading ($\sim r^{-2}$). The fact the cylindrical spreading ($\sim r^{-1}$) is in effect for most of the return in the shallow bay explains the observed rising level with range. The main reverberation ridge occupies the near-DC region, following complex basebanding. The secondary ridge at $\omega_n = 0.25$ is not physically meaningful and could possibly be the result of aliasing suffered during the data acquisition phase. The synthetic signal echoes are well-concealed by reverberation in both the time and frequency domain.

3.2.2   Processing results

The AR-model order for this ping was determined by making use of the AR-cutoff property of the lattice filter (see section 2.4.1). The reflection coefficients of orders (≥ 7) were found to be virtually equal to zero and therefore $p = 6$ was accepted as the appropriate filter order. This is consistent with the findings of Haykin et. al.[1982] in their investigation of radar clutter, the atmospheric counterpart to reverberation and of Hansen [1984] in his study of the oceanic reverberation spectrum. Both have concluded that reverberation (clutter) can be effectively modelled as an AR process of relatively low order.

Three whitening runs were made , each with the scalar LSL prediction-error filter of order $p = 6$ and adaptation coefficients (α_{LSL}) of 0.0002, 0.002 and 0.02 respectively. The results, displayed in Figure 3.4 include the time evolving "high resolution" spectral estimate and the RDM of the prediction error output for these values of α_{LSL}. For $\alpha_{LSL} = 0.0002$, the spectral estimate fails to resolve T2 which, as a result, is not whitened and is preserved at the output with a much improved SNR. For $\alpha_{LSL} = 0.002$, T2 is partially resolved and correspondingly partially removed from the output. For $\alpha_{LSL} = 0.02$, the spectral estimate includes many of the details of the original RDM

and to a large extent, tracks its time-varying behavior. Signal T2 is completely resolved and compensated for. The zero-Doppler signal (T1) was cancelled every time, which is to be expected since it resides in the frequency null induced by the reverberation process.

Remarks

A clear trade-off is evident regarding the choice of adaptation coefficient. If the objective is enhanced detectability of a transient low-Doppler echo in the vicinity of the reverberation ridge, then a relatively small α_{LSL} is in order. In this case, the effective averaging may be excessive for the spectral modeling objective and may result in the "smearing" of certain time-varying spectral features. A larger α_{LSL}, on the other hand, will result in a more realistic spectral estimate at the expense of complete elimination of all signals from the output. It should be mentioned that signal duration is also important with regard to this trade-off. Gradual, persistent echoes from spatially distributed scatterers are more likely to be whitened than transient returns from discrete reflectors. Morover, increased signal cancellation will result as the proximity of the echo to the reverberation ridge is increased. In view of these concerns, the adaptive whitening operation is of limited utility in the context of echo detection.

3.3 ANC with fixed, preformed reference beams

A more promising alternative, for signal detection in a reverberation backround, is dual-channel ANC processing with preformed, fixed reference beams partially overlapping with the main beam. Signal components common between the main and the reference beams will be subject to cancellation. On the other hand, echoes arriving through the angular region covered exclusively by the main beam, will be protected from cancellation. It follows that such echo returns will be enhanced by an ANC

operation between the main and the reference beam. In order to demonstrate this, the same ping (EXP3.1) will be processed with the multichannel, joint-process LSL filter, the (multichannel) reference input consisting of the four interior beams of the multibeam set.

The joint-process error output for $p = 3$ and $\alpha_{LSL} = 0.02$ is shown in Figure 3.5. The reverberation backround is reduced substantially, rendering signals T1 and T2 clearly visible in both the time and frequency domains. Also displayed is a dB-cancellation curve which is the low-pass filtered ratio of the input signal magnitude over the output error magnitude and shows the overall character of cancellation achieved. It is noteworthy that the zero-Doppler echo (T1) is equally well preserved as the other low-Doppler echo (T2). In addition, signal duration is no longer an important factor for signal preservation. The sole requirement is that the echo arrival angles fall within the protected angular region of the main beam. Therefore, even persistent, zero-Doppler echoes from distributed scatterers can potentially be extracted through this process.

Remarks

i.   It should be mentioned that in this case the signal echoes are completely absent from all reference beams. Should a signal component be allowed to enter one of the reference channels, ANC theory predicts potentially serious signal cancellation at the output. Therefore, in designing reference beams, emphasis should be placed in suppressing their sidelobe response in the directions of high main beam response.

ii.   This signal processing technique is likely to be useful in a horizontal fisheries sonar application. The Doppler structure of a fish school is determined by varying degrees of systematic and random motion, including rhythmical

swimming motions, cruising, short-term accelerations and erratic changes in speed and direction [Holliday, 1974]. The aspect between the swimming direction of the school and the main beam axis is also a factor. It follows that the received waveform will be characterized by varying degrees of net Doppler shift and with the exception of fish swimming at high speeds along the beam axis, fish detection with a Doppler sonar is reverberation limited. Reverberation interference is particularly severe in shallow-water applications such as the tracking of migrating species in rivers [Pincock and Easton, 1978; Hendershot and Acker, 1984]. The results of this section indicate that ANC with appropriately formed reference beams offers the potential for improved fish-count estimation in such reverberation-limited environments.

iii. The question remains as to the composition of the residual reverberation signal. It seems unlikely that the particular beam set used is adequate for selective reverberation cancellation. Since the reference beams do not encompass all possible directions of arrival of boundary reverberation components entering the main beam, one may expect the reverberation present at the filter output to be still highly composite. The following REVGEN simulation was intended to resolve this question

3.3.1 REVGEN simulation (RS3.1)

Two simulation runs were performed. In the first run, boundary as well as volume scatterers were placed in the medium. In the second run, only volume scatterers were included in order to create a "desired" signal in the SRC scenario. System parameters were duplicated to the extent possible. Simplified "pencil" beams were used and an isovelocity medium was assumed. A summary of the simulation parameters is given in Table 3.3 below.

Simulation parameter	Symbol	Value
Pulse length	τ	180ms
Shell thickness	T	15 m
No. of volume scatterers per slice	N_{ss}^v	100
No. of surface scatterers per slice	N_{ss}^s	50
No. of bottom scatterers per slice	N_{ss}^b	50
Layer height	H	175
Sound velocity	c	1500 m/s
Volume reverberation coefficient	δ_v	-70 dB
Surface reverberation coefficient	δ_s	-30 dB
Bottom reverberation coefficient	δ_b	-20 dB

Table 3.3 REVGEN simulation RS3.1

The approximate number of scatterers per scattering volume and area for volume and surface (bottom) reverberation respectively, are given by

$$N_{sv} = \frac{N_{ss}^v \beta c \tau}{4\pi T}$$

and

$$N_{sf} = \frac{N_{ss}^s \beta c \tau}{4\pi T}$$

where β is the equivalent horizontal receive beam width in radians. The above computations are based on a "wedge" approximation for the receive beam patterns which is valid at the far ranges, following beam intersection with the boundaries. Here $\beta = 15^\circ = 0.262 rad$. Substituting, we have

$$N_{sv} = 0.375 N_{ss}^v = 37.5$$

and

$$N_{sf} = 0.375 N_{ss}^s = 18.75$$

Therefore, a sufficiently large number of scatterers contributed for the reverberation

return to "converge" to a Gaussian distribution.

No signal echoes were included in this simulation. The composite reverberation data were processed identically to the real case and the results are displayed in Figure 3.6. It can be seen that the ANC output (dotted line) falls between the input (composite) reverberation process and the "desired" volume reverberation signal. Therefore, the output is indeed of composite nature. The dB-cancellation curve shows similar overall cancellation as in the real data case.

3.4   An Application of Constrained Adaptive Beamforming

In this section we focus on SRC. Volume reverberation is the "signal" of interest. The "interference" consists of surface and bottom reverberation entering initially through the sidelobes and eventually through the main lobe of the receive beam. We will examine the possibility of recovering the volume component, normally weak and completely masked by the boundary return, through adaptive processing.

The feasibility of ANC with fixed, preformed beams depends on the sidelobe structure of the particular transmit and receive beam patterns. Two different reference beam sets are in general required for side lobe and main lobe interference cancellation. In constructing a side lobe cancellation beam, great care must be exercised to closely match the side lobe features of the main beam. This may prove difficult for beams with complex side lobe structure. The main lobe cancellation beam, on the other hand, must have a null in the direction of interest in order to protect the volume signal from cancellation. As the interference arrival angle changes with range, the fixed null shape may be a serious limitation to cancellation in the far ranges. Morover, an external decision is needed on the appropriate time for switching from side lobe cancellation to main lobe cancellation mode. The inevitable transient response of the algorithm to such a discontinuous "step" presents an additional problem.

As an alternative, one may allow the adaptive algorithm to directly control the spatial transfer function of the system, provided that spatially separated receive elements are independently available and to, in effect, create its own adaptive reference (cancellation) beam. With appropriately constrained reference elements, this configuration has the potential of cancelling both side lobe and main lobe interference with a graceful transition between the two modes. In addition, it enjoys a significant advantage in operational flexibility as it needs little or no a priori information about the shape of the main receive beam. For these reasons this *Constrained Adaptive Beamforming* operation is especially promising for SRC.

3.4.1   Data description

The experimental data set offers an opportunity for application of this concept. Ping EXP3.2 is a good case in point. The same "wide" transmit beam set is in effect and beam set 1 was used to receive. The latter consists of the individually recorded outputs of 9 array row sums. These rows will be used as the reference elements in the adaptive beamforming process. The basic experimental geometry is unaltered with the exception of sonar depth which now is 30 m. The velocity profile and ray tracing diagram for this run are displayed in Figure 3.7.

A REVGEN simulation (RS3.2) was carried out for this scenario. The simulation parameters of Table 3.1 were used and the receive elements were approximated by rectangular pistons at $\frac{\lambda}{2}$ spacing.

The main beam was constructed by adding the outputs of the 9 rows. The simulated beam pattern is shown in Figure 3.8a. In addition, 8 constrained reference elements were created by pairwise subtraction among the 9 rows, in the manner depicted in Figure 2.2b. The beam pattern of a single constrained element, characterized by a central null, is the dotted curve in Figure 3.8b.

The real and simulated (composite) reverberation signal entering the main beam are displayed in parallel in Figure 3.9. The first plot is the regular RDM display. The second plot, an RDM with ~ 90% overlap, provides a more detailed view of the near ranges where boundary reverberation enters through the sidelobes. The data has been frequency-shifted to compensate for the Doppler shift due to sonar motion. Clearly visible is the typical "hook" pattern of negative Doppler features in the initial ~ 0.5 s of the ping. This pattern is entirely due to high-angle boundary returns which are imparted a lesser net Doppler shift by the velocity of the sonar. With increasing range, as the lower sidelobes and eventually the main lobe become the boundary reverberation outlets, the pattern merges into the main ridge. This artifact is useful for identifying sidelobe returns and establishing their cancellation following adaptive processing. The final plot is the regular time-series diplay.

Although the real and simulated data have similar overall structure, several differences are apparent. The real data are characterized by a somewhat wider "hook" which may be an indication that the real beam pattern has an appreciable side lobe response at a higher angle than the simulated beam or that the actual velocity of the sonar was underestimated in the simulation. In addition, the simulated reverberation is better sustained at long ranges. Two reasons may be cited for this. First, no decaying function of grazing angle was introduced in the simulation for boundary reverberation. This decay with grazing angle is a well-documented fact [Urick, 1975]. The second reason may be inferred from the raytracing diagram (Figure 3.7) and the time of arrival vs angle of arrival plot (Figure 3.10). Because of the well-developed thermocline, a shadow zone is formed in the near surface past a range of ~ 500 m. The surface contribution disappears abruptly at that point. In the simulated case, an isovelocity profile is used and the surface continues to contribute at long ranges. Finally, a high-Doppler calibration signal can be observed in the real data

RDM at $t \sim 1.5s$. It arrives broadside to the array. This signal was not included in the simulation.

3.4.2   Processing with a single constrained reference element

A single constrained reference element, created by subtracting one row element from another, has a beam-pattern (Figure 3.8b) which at first glance appears to be well-suited for SRC. Excluding its broadside null, it is nearly omnidirectional in the vertical, thus covering all possible directions of arrival for boundary reverberation. One may expect it to be effective in cancelling the sidelobe-born boundary returns and to some extent main lobe interference, while protecting much of the volume signal in its null.

Ping EXP3.2 was processed in this manner, using the scalar LSL with $p = 3$ and $\alpha_{LSL} = 0.02$. The single reference channel consisted of rows (5-6). The results for both the real and simulated data are displayed in Figure 3.11. Cancellation is generally low in the near ranges. In addition, the simulated case displays a significant increase in backround noise level for $t \leq 0.5s$. Moderate cancellation was achieved in both cases for intermediate ranges ($1.0 \leq t \leq 2.0$) while the behavior in the far ranges is distinctly different for real and simulated data. For the latter, cancellation continues to improve with range while little or no cancellation is observed for the former.

The low overall cancellation in the near ranges, is a manifestation of the ANC theoretical prediction regarding the effect of uncorrelated noise components in either the primary or the reference channel. This effect, which was outlined in Section 2.2, comes into play here as follows: The transmit beam ensonifies the entire angular region from -60° to +60°. The reference beam, being nearly omnidirectional in the vertical, receives reverberation from the entire range with the exception of the near-broadside. The main beam, on the other hand, has a definite side lobe response which

operates on the high angle returns. Each time boundary reverberation arrives through the nulls between side lobes it is excluded from the primary channel. The same components enter the reference channels without being attenuated and in effect cause the uncorrelated-to-correlated noise density ratio ($M_1(z)$ in Eq. 2.5a) to increase, resulting in reduced signal-to-noise ratio at the filter output. This explains the observed rise of the noise "floor". The somewhat better cancellation apparent for the high angle ($\pm 60°$) returns in the real vs the simulated data, may be an artifact of the RDM displays caused by dynamic range differences, unavoidable in view of the necessarily incomplete model of physical reality which is used in the simulation. The particular side lobe structure of the real main beam, which may be substantially different from the simulated beam, could also explain this difference.

The difference in far-range cancellation performance is due to the grazing angle effect. In the real case, there is simply little boundary reverberation left in the far ranges and therefore the cancellation potential is low. This effect was not included in the simulation and as a result significant cancellation was achieved there. Interestingly, there is a clear trend of improving cancellation performance with range, which is consistent with another ANC theoretical prediction, this one regarding the noise spectrum at the filter output (relation 2.5c). Specifically, the output noise spectrum was found to be proportional to the signal-to- correlated noise ratio at the primary input. In our experimental geometry, this ratio should decrease with range as the boundary returns begin to enter through the main lobe instead of the side lobes. Therefore, one may expect the output noise power to decrease and cancellation to improve. This concept may be tested through the simulated data. Once more, two separate simulation runs were performed with only volume and only boundary scatterers present, respectively. Thus, "signal" and "interference" were isolated. We have calculated the volume to boundary reverberation power ratio at the output of the

main beam and plotted it together with the dB-cancellation curve in Figure 3.12b. It is seen that the two curves are nearly mirror images of each other. The decreasing trend in the main channel SNR corresponds well to the increasing cancellation trend. In addition, many of the large-scale fluctuations seem to obey the same relationship. Figure 3.12a clearly shows that, although cancellation improves with range, this configuration is inadequate for SRC.

Two additional observations can be made, concerning the real data results. First, the high-Doppler "control" signal was virtually unaffected by this processing. This is an indication that the constraining scheme is effective. Second, a large zero-Doppler feature was revealed (marked) at $t \sim 1.0s$. This is probably a volume reverberation feature the origin of which will be speculated upon in a later section.

Remarks

i. Processing with a single constrained reference beam would be more effective in the side lobe cancellation mode, if the transmit beam were identical to the main receive beam. In that case, the "uncorrelated noise" effect would not exist and near-range cancellation would improve.

ii. Regarding the constrained reference cancellation beam, a choice must be made about the width of thr broadside null. It would be desirable to have a wide null initially, when interference arrives through the sidelobes and a progressively narrower null as the main beam begins to intersect the boundaries.

iii. An alternative explanation for the improved cancellation observed in the far ranges is in terms of the increased spatial coherence of boundary reverberation predicted by the point-scattering model (Section 1.4.)

3.4.3   Processing with a spatially adaptive cancellation beam

The results of Simulation 3 indicate that the multichannel joint-process filter can compensate for noise components not present in the primary channel, which are correlated between the reference channels. Therefore, if the multichannel LSL filter were to be used in the present case, with the 8 constrained reference elements comprising the vector reference input, one may expect it to be more effective than the single channel filter by aleviating the near range "uncorrelated noise" effect. Equivalently, the multichannel adaptive algorithm should, in theory, form an adaptive reference (cancellation) beam with the tendency to emulate the side lobe features of the main beam. This adaptive reference beam will still have the central null according to the beam pattern product theorem [Urick, 1975] and therefore, the basic constraining scheme will still be in effect.

The results for the same ping (EXP3.2) processed through the 8-channel LSL filter are displayed in Figure 3.13. Overall, cancellation is substantially improved over the single reference element case. As evidenced by the virtual elimination of the "hook" pattern from the RDM plots, the side lobe boundary interference has been successfully removed. Somewhat surprising is the dramatic improvement in far range cancellation. As a result, in the real data case, volume feature V1 is even more clearly in evidence at $t \sim 1.0$ s and an additional feature (V2) was exposed at $t \sim 1.6$ s.

Figure 3.14a shows that the multichannel constrained adaptive beamformer is generally very successful towards achieving SRC. This is particularly true for $t \geq 1.0$ s. Insight may be gained on the adaptive operation performed by this structure, by considering the adaptive cancellation beam it creates. Vertical "cuts" of this beam, at zero bearing, were calculated from each set of 8 cross-channel reflection coefficients at ~ 0.024 s intervals and are displayed in a "waterfall" plot (Figure 3.14b). Note that the adaptive cancellation beam still has the central adaptive null,

as expected. Morover, it strives to approximate the sidelobe structure of the main beam in the early ranges of high-angle boundary returns. At longer ranges ($t \geq 1.0$ s) when the side lobe activity subsides, the adaptive cancellation beam concetrates on the main lobe boundary returns to the extent allowed by the broadside null.

3.4.4   REVGEN simulation: symmetric case

In order to futher examine the nature of the adaptive cancellation beam, the same processing was carried out in a more benign symmetric experimental geometry. In this REVGEN simulation (RS3.3), the overall depth was set to 300 m and the sonar was positioned at 150 m. The surface and bottom backscattering coefficients were both set equal to -30 db. In the sequence of plots presented in Figure 3.15, it is apparent that the symmetrical arrangement is beneficial to the SRC performance in the near ranges. The adaptive cancellation beam is itself symmetric and its behavior easier to interpret. In its side lobe cancellation mode ($t = 0.5$) it succesfully emulates the side lobe structure of the main beam. As the main lobe begins to intersect with the boundaries, the adaptive filter is seen to adaptively alter the effective width of the broadside null, making it progressively narrower with increasing range (plots for $t = 1.0$ and $t = 2.0$ in Figure 3.15c). This is intuitively satisfying and explains the dramatic improvement in far-range cancellation performance achieved by the adaptive beamformer over single channel (i.e. fixed null shape) ANC.

3.4.5   Volume "feature" interpretation

A number of hypotheses were considered regarding the origin of the volume features (V1 and V2) exposed by the adaptive beamforming operation on the real data. First, the possibility that they are acoustic echoes from schools of fish or cellular water masses within the angular range of the null was debated. This hypothesis was rejected based on the processing results for ping EXP3.3 which preceded ping

EXP3.2 by ∼ 104 seconds. During this time, assuming they were moving slowly relative to the sonar, one whould expect the echoes to be at discernably different ranges for the two pings. This, in fact was not the case; the features appeared at precisely the same ranges.

Alternatively, the features may be explained by the presence of a strong, well-defined scattering layer at a shallow depth. Such a layer, consisting mainly of pre-spawning populations of Pacific herring, has been consistently observed in the spring months [Friedl, 1970; Anderson, 1981; Frost, 1985]. If, due to refraction effects, the near broadside rays residing in the null region intersect this layer at appropriate ranges, they could possibly acount for the features. The high-resolution ray tracing plot created to provide support for this hypothesis, exposed additional evidence (Figure 3.16.) Specifically, two caustics are clearly visible at ranges which correspond well with the feature position. The presence of the caustics in the strong shallow scattering layer can probably account for the intense scattering which produces the volume features.

3.5   Vertical reverberation correlation and ANC

As a final step, the theoretical model predictions presented in Section 1.4 on the vertical correlation characteristics of reverberation will be tested in the context of direct ANC. Row 1 will constitute the main channel. Given the width of the transmitting beam pattern, one would expect the volume component to be decorrelated between row 1 and row 8. A two-channel reference beam will be used, consisting of rows 8 and 9. The processing results for real and simulated data are shown in Figure 3.17. The behavior of the REVGEN data is consistent with the model predictions. Cancellation is virtually zero in the early ranges as both volume and boundary reverberation have low vertical coherence. The cancellation improves gradually and eventu-

ally SRC is achieved as the boundary return becomes increasingly coherent. Cancellation improves with range for the real data as well, although the trend is not quite as clear. This may be construed as evidence of a degree of departure from the spatial correlation structure predicted by the simple point-reflector model.

3.6   Chapter summary

A number of adaptive filtering configurations were applied to the problems of signal detection in a reverberation backround and of selective reverberation cancellation. Adaptive prewhitening, ANC with fixed preformed reference beams and constrained adaptive beamforming were used to treat real and simulated shallow-water reverberation data. It was shown that, although signal enhancement is possible with other methods, only (spatially) adaptive beamforming, implemented through a multichannel joint-process structure, is capable of achieving the SRC objective. Certain model theoretical predictions on ANC performance limitations were shown to be applicable as were the point-scattering model predictions of the spatial correlation characteristics of reverberation. REVGEN simulations were performed to parallel the experimental data and generally good correspondence was observed between the real and simulated processing results.
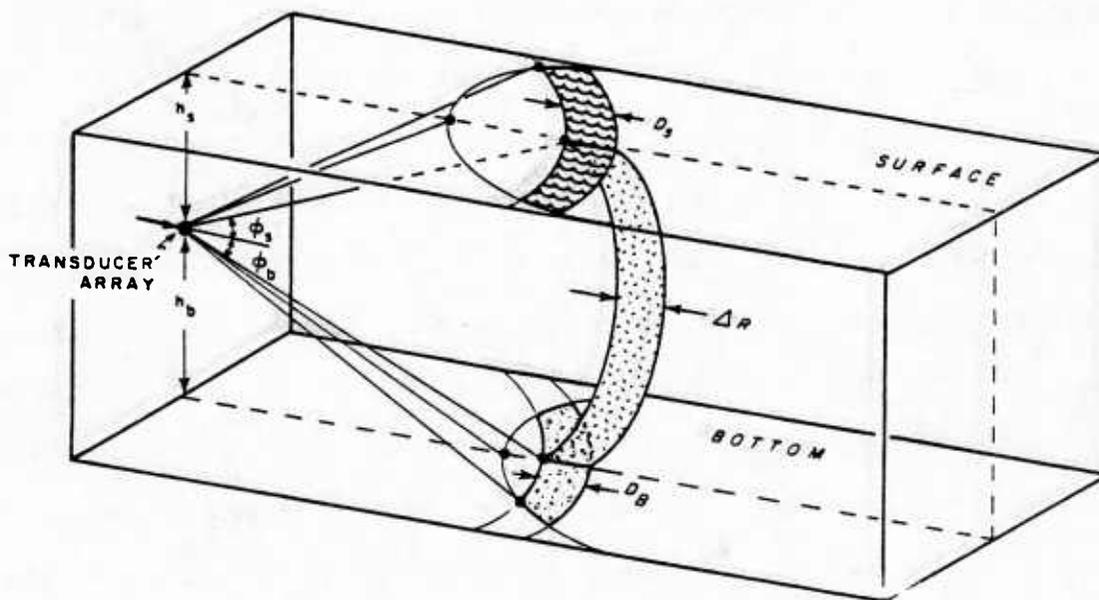
Figure 3.1 *Shallow-water experimental geometry.* The surface, volume and bottom contribute to the backscattered return.
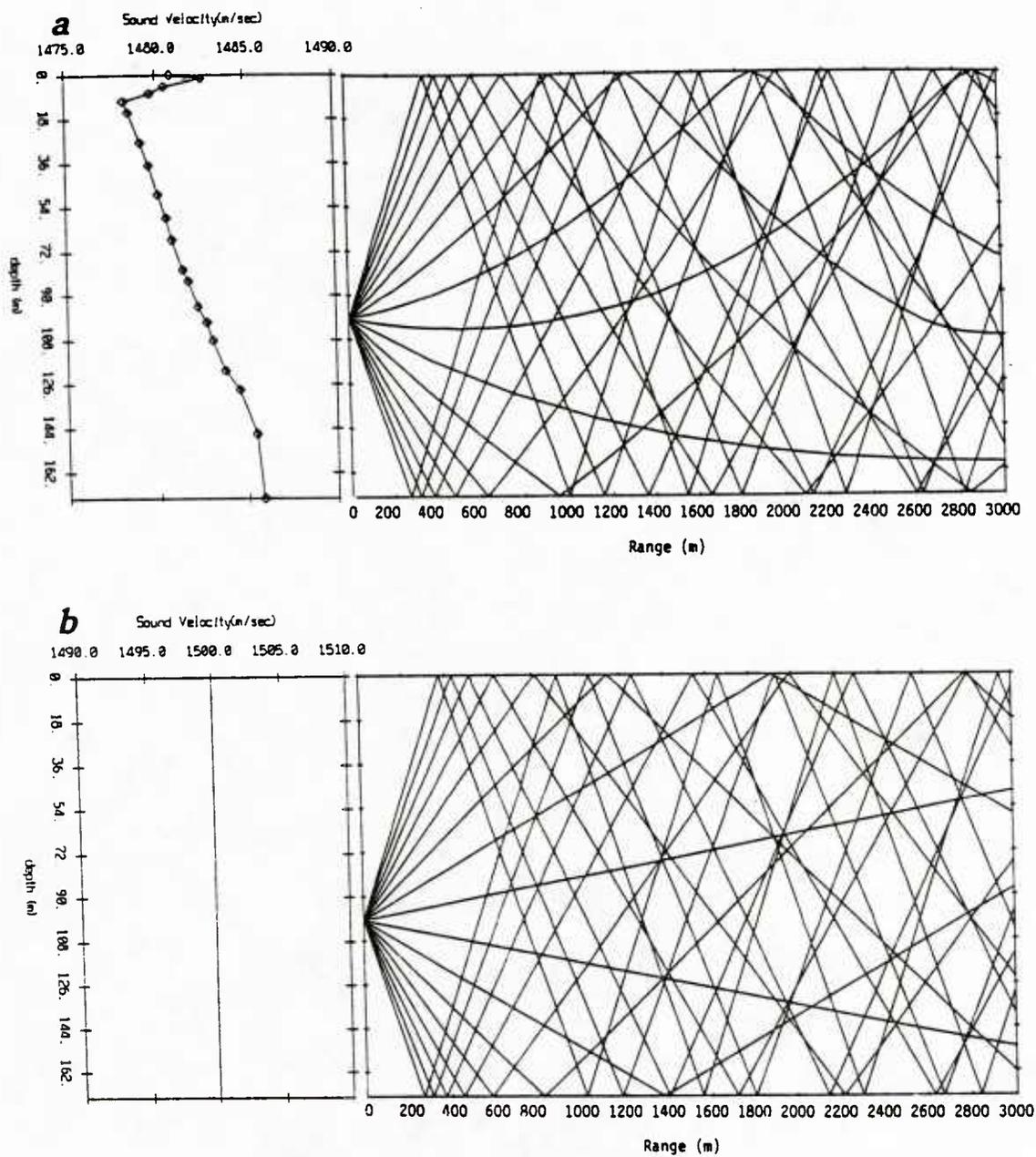
Figure 3.2 *Raytrace: ping EXP3.1.* Velocity profile and corresponding raytrace diagram for real data (a) and REVGEN simulated scenario (b). Both surface and bottom reverberation is produced at all ranges.

a

b

2 synthetic targets: (0 Hz, 1.5 sec), (60 Hz, 2.5 sec)
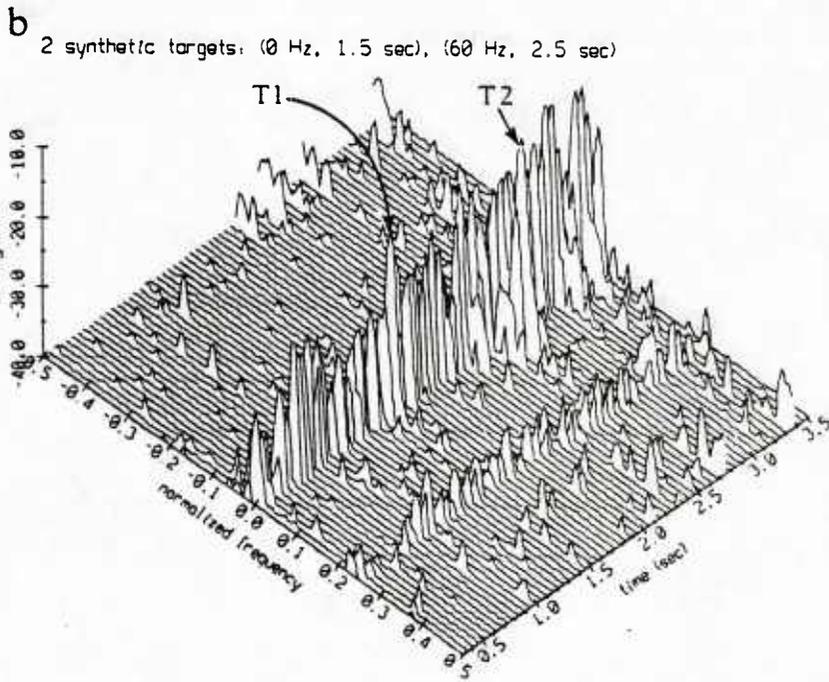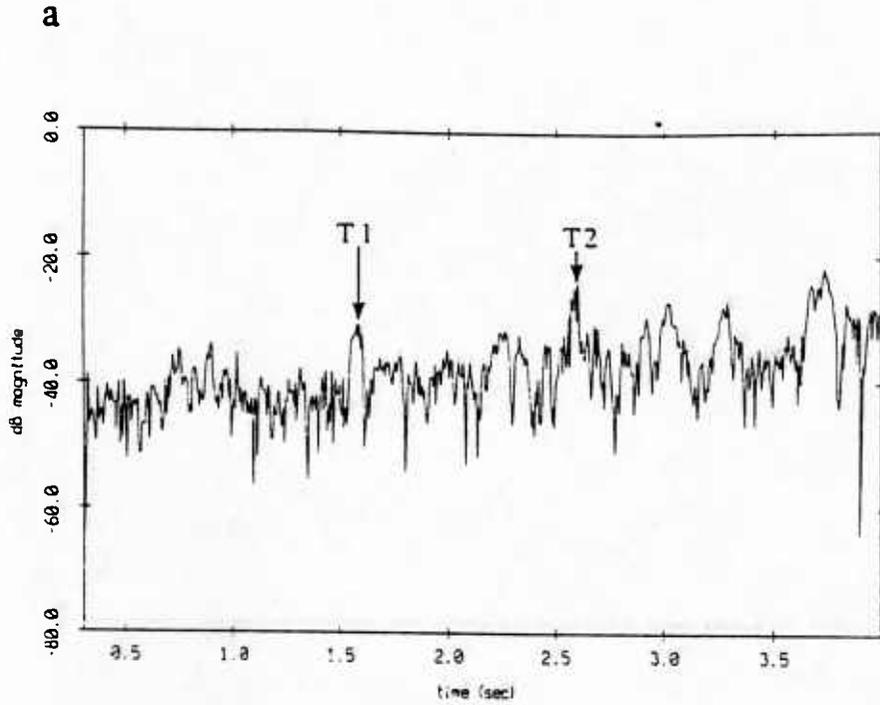
Figure 3.3 *Ping EXP3.1*: Low-pass time series plot (a) and Range-Doppler-Map (b). The two synthetic echos T1 and T2 are masked by reverberation.
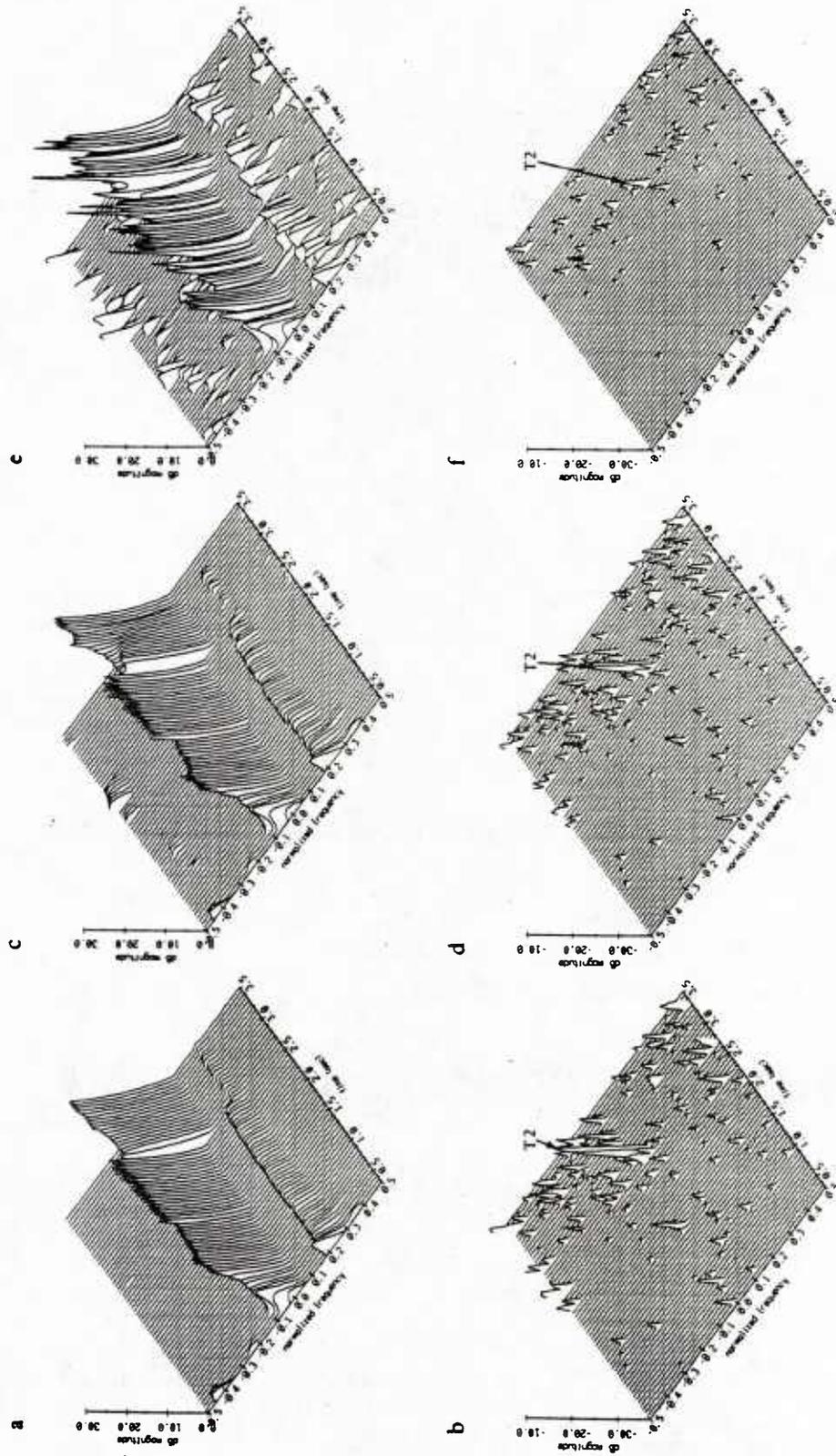
Figure 3.4 *Adaptive prewhitening results.* Adaptive spectral estimate and Range-Doppler-Map of prediction error output for $\alpha_{LSL} = 0.0002$ (a,b), $\alpha_{LSL} = 0.002$ (c,d) and $\alpha_{LSL} = 0.02$ (e,f). As α_{LSL} increases the resolution of the spectral estimate improves and the low-Doppler echo vanishes.
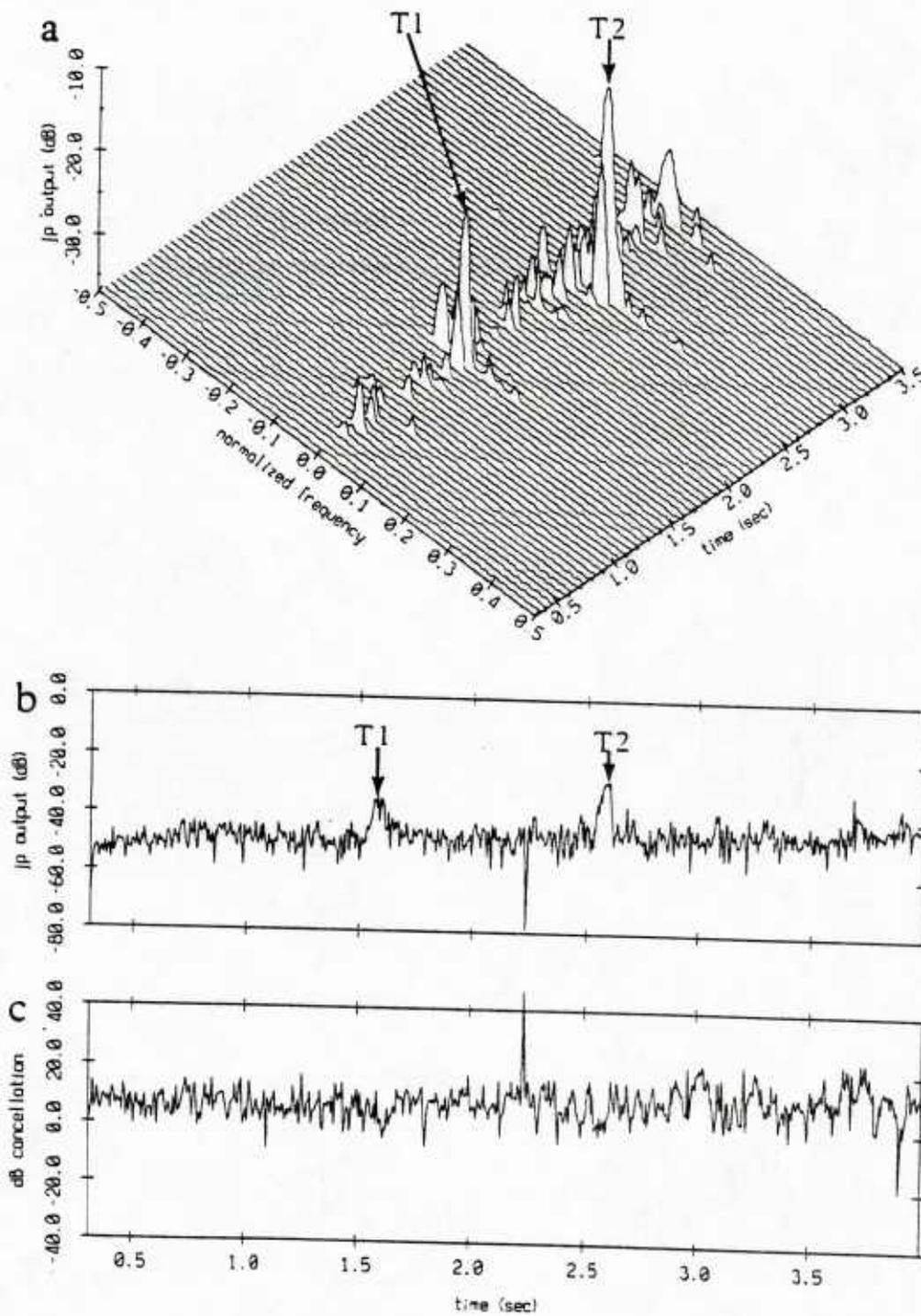
Figure 3.5 *ANC with preformed reference beams.* The Range-Doppler-Map (a) and the time-series (b) displays of the LSL joint-process error output, show the synthetic echo signals T1 and T2 to be greatly enhanced as the reverberation backround subsides. The dB-cancellation curve (c) shows cancellation to improve with range.

a
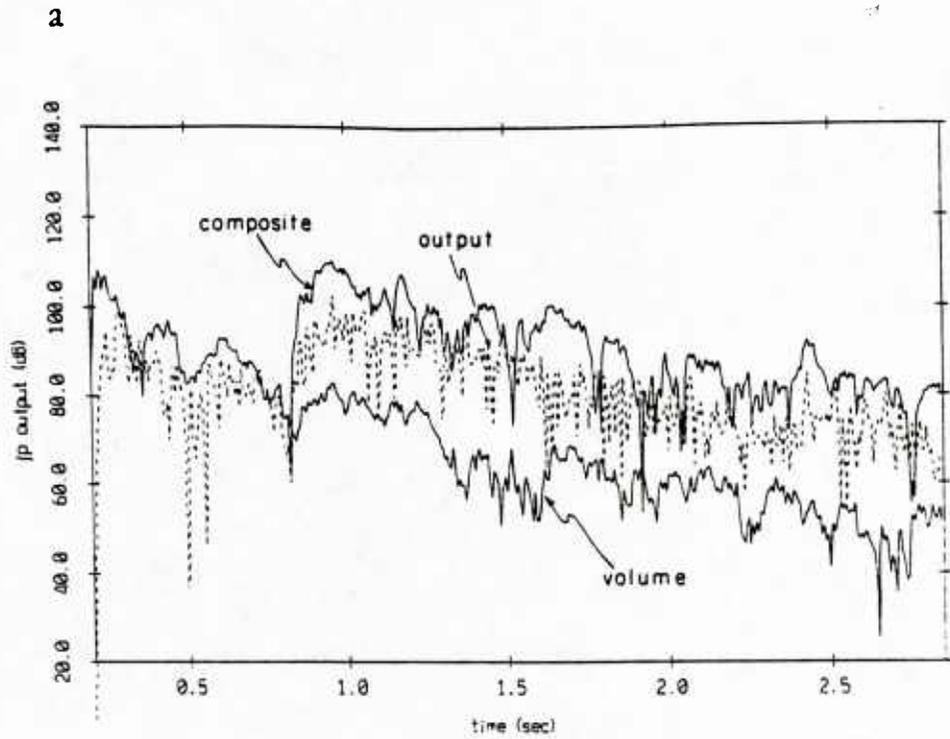
b   DB cancellation
    jmclsl p=3 m=4 alpha=0.22: main(1), ref(3478)
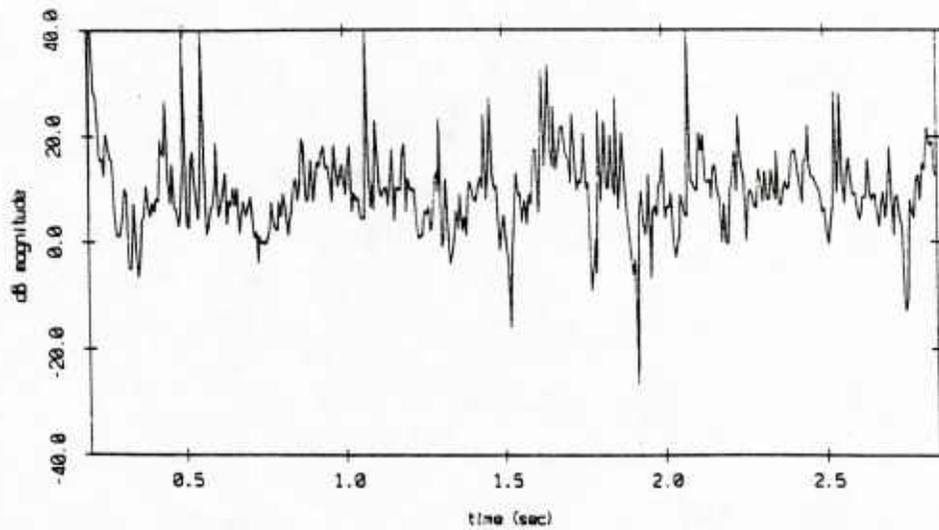
Figure 3.6 *REVGEN simulation of EXP9.1.* The LSL joint-process error output (dotted line in (a)) remains much higher than the "desired" volume signal, indicating that fixed, preformed reference beams are not adequate for SRC despite the fact that substantial cancellation is achieved (b).
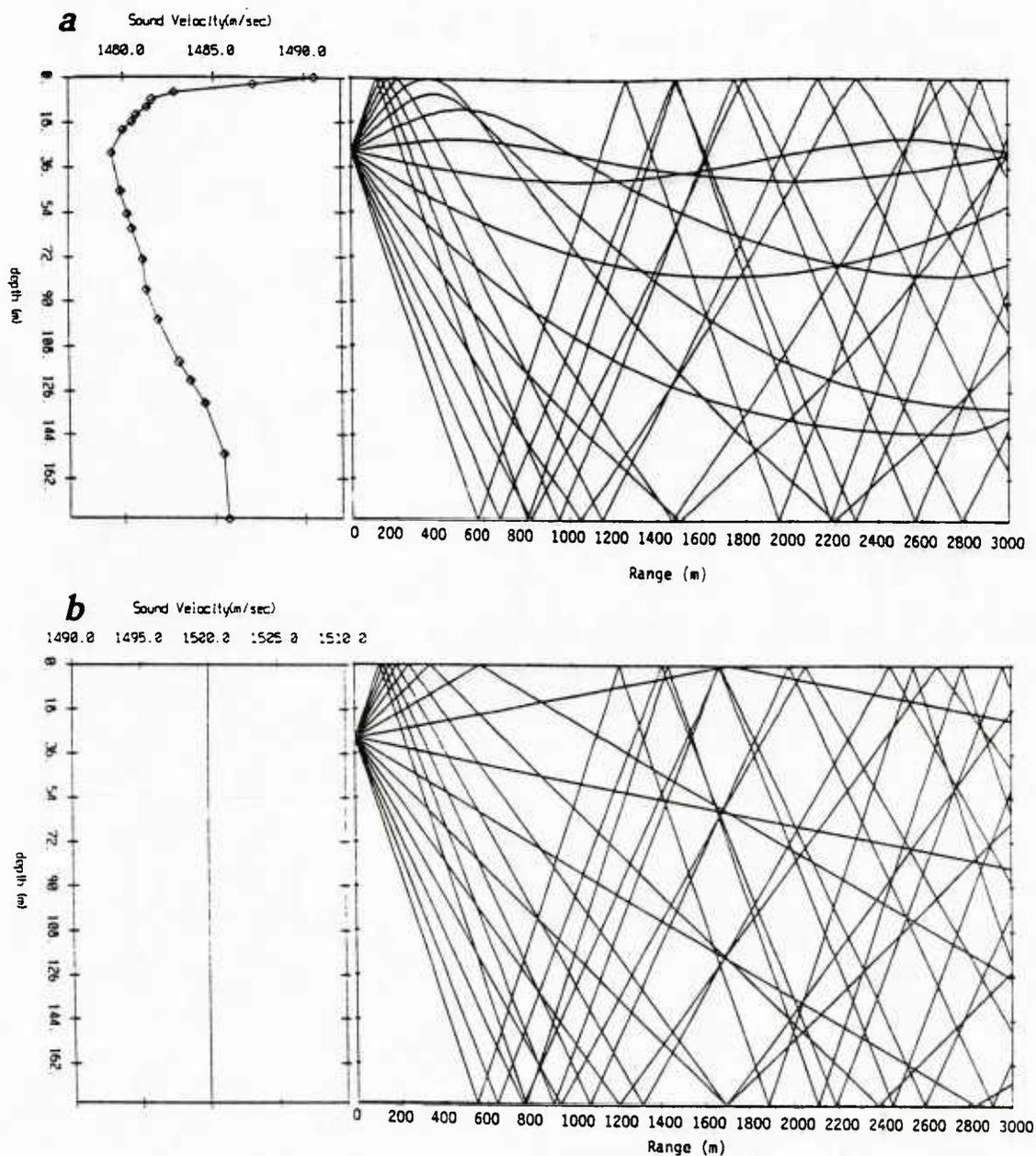
Figure 3.7 *Raytrace: Ping EXP 3.2.* Velocity profile and corresponding raytrace diagram for real data (a) and REVGEN simulated scenario (b). Note that in the real data case a shadow zone is formed in the near surface and no surface reverberation is produced at the far ranges. In the simulated case, on the other hand, surface reverberation continues to be produced at the far ranges.
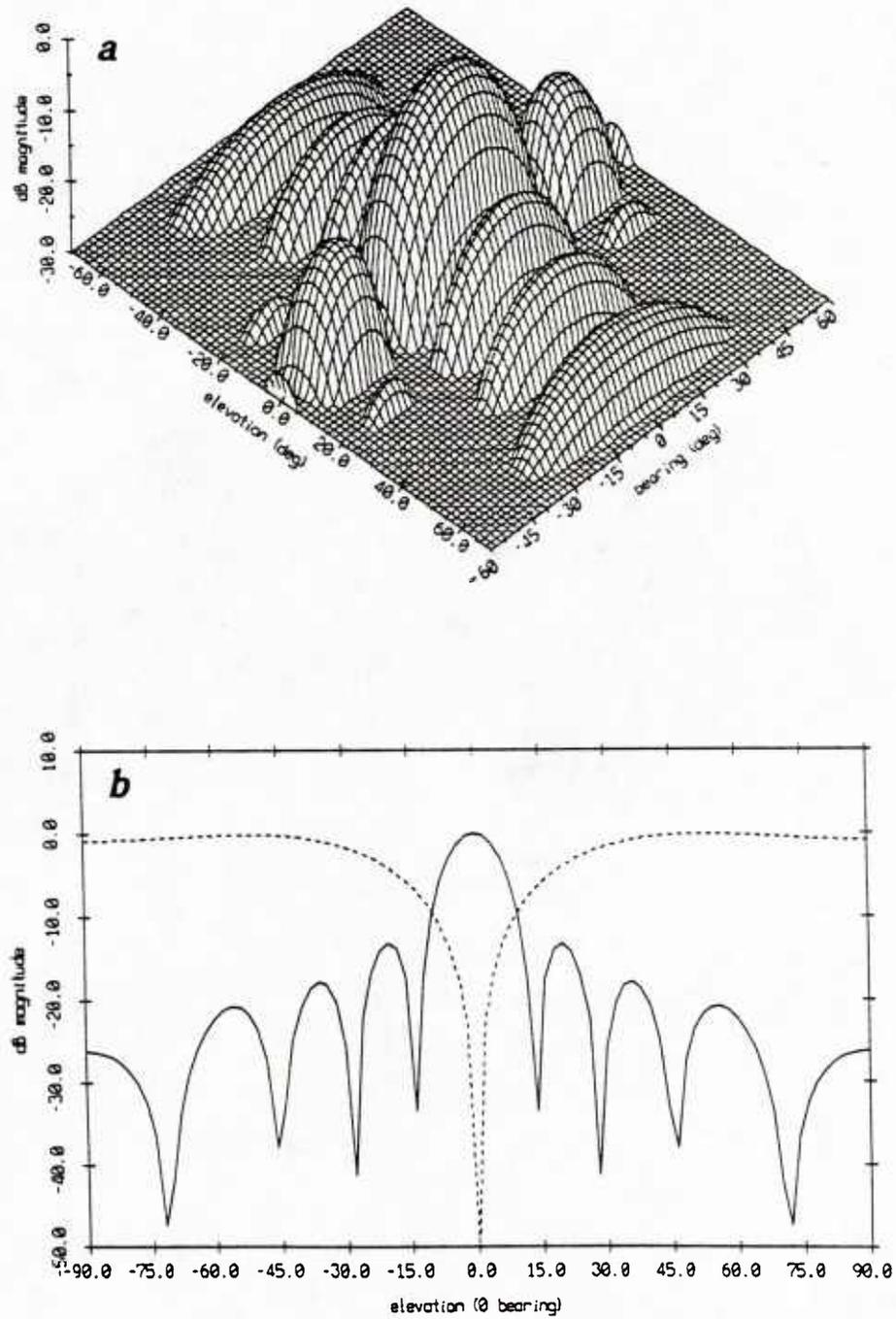
Figure 3.8 *EXP 3.2 beam patterns.* (a) primary beam pattern, produced by adding all 9 rows, (b) single vertical 0° bearing cuts of the primary beam (solid line) and of a single constrained beam pattern produced by subtracting two rows (dotted line.)
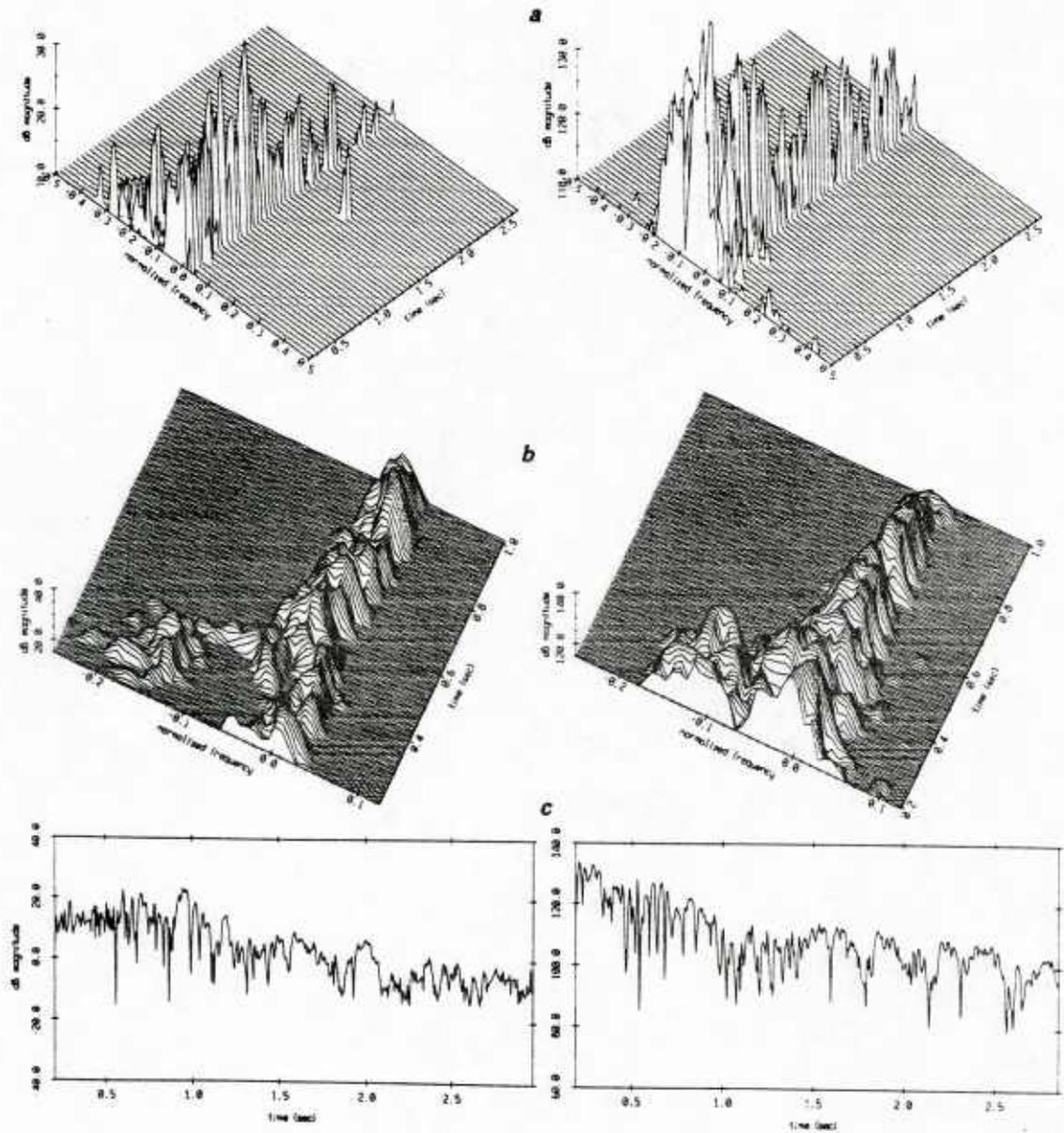
Figure 3.9 *EXP 3.2 data.* Real (LHS) and REVGEN (RHS) primary channel: (a) standard RDM, (b) expanded near-range plot (note the typical "hook" pattern caused by the high-angle boundary reverberation returns) and (c) time-series plot.
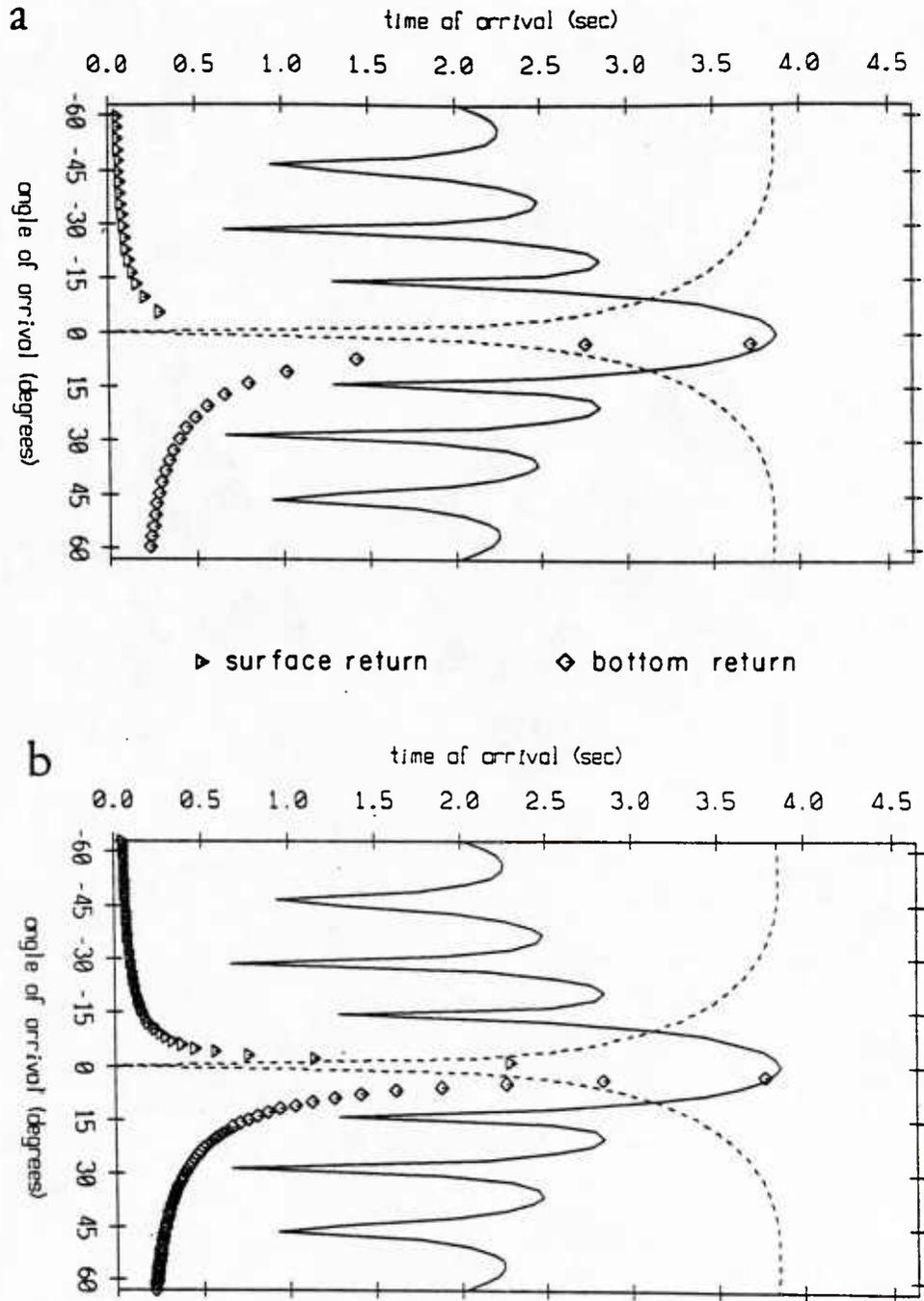
Figure 3.10 *Angle vs time of arrival.* (a) Real (EXP3.2), and (b) REVGEN (RS3.2) data. These plots were intended to illustrate the origin of the "uncorrelated noise" effect. In the early ranges, the constrained reference beam (dotted line) receives reverberation from angular directions where the primary beam (solid line) has a null response.
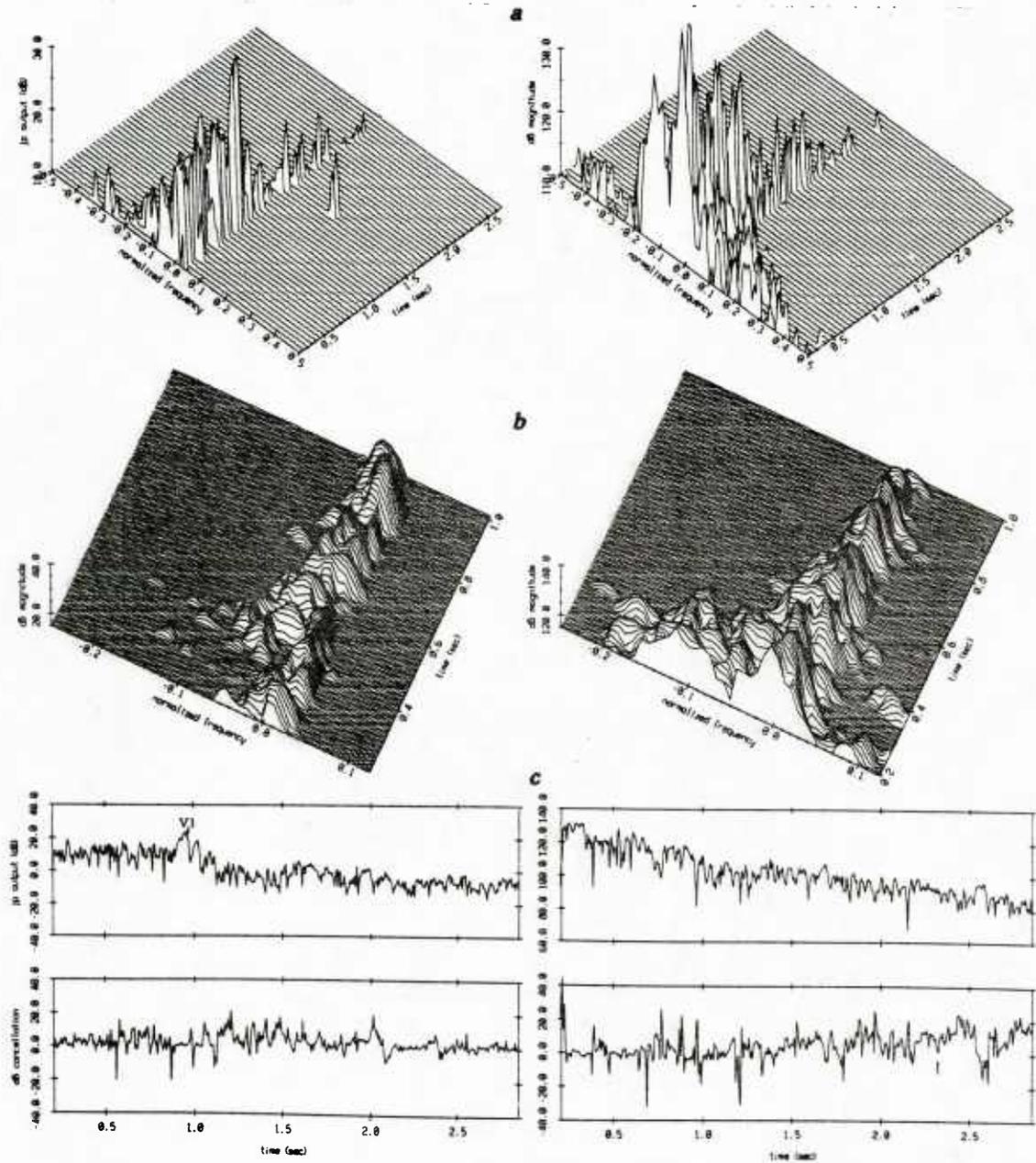
Figure 3.11 *ANC with single constrained reference element.* Ping EXP3.2 (LHS) and REVGEN simulation RS3.2 (RHS): (a) Standard RDM, (b) expanded RDM. Substantial reverberation cancellation is seen for both real and simulated data in the far ranges but near-range performance is marginal. Note increase in noise level in the simulated results. (c) Output time-series and (d) dB- cancellation curve. A volume "signal" (V1) is exposed in the real data output. Cancellation is seen to improve with range for simulated data, level out for real data.

101

a

REVGEN simulation of ASP5.2 ping. 100
db-cancellation and main channel SNR

b
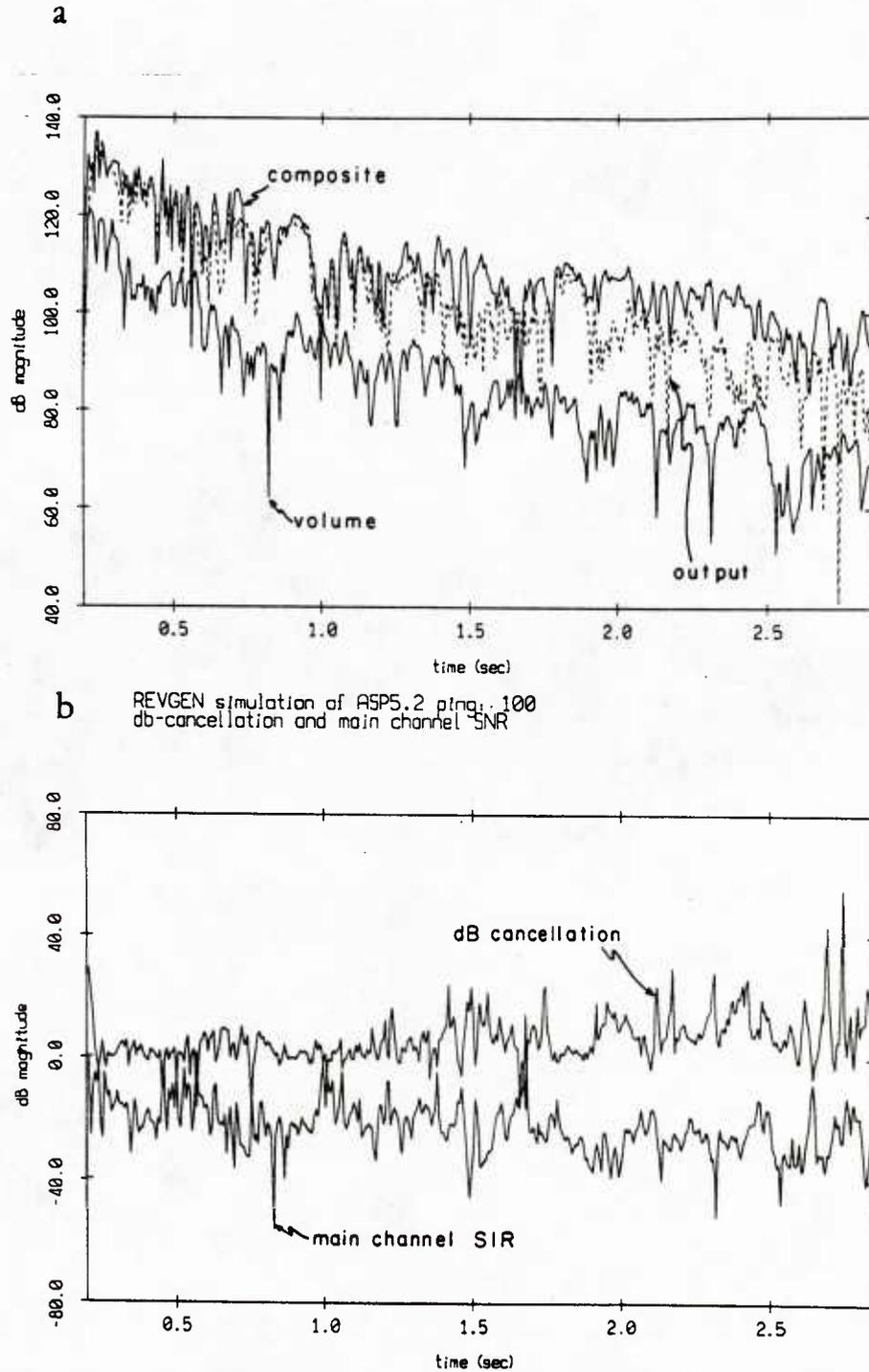
Figure 3.12 *SRC performance of single constrained reference beam (RS3.2).* Composite (top solid line), pure volume (bottom solid line) and joint-process error output for single constrained reference beam (dotted line.) Clearly, the SRC objective is not achieved. (b) dB-cancellation curve and Signal-to-interference ratio in the main channel. The two curves are nearly mirror images of each other.
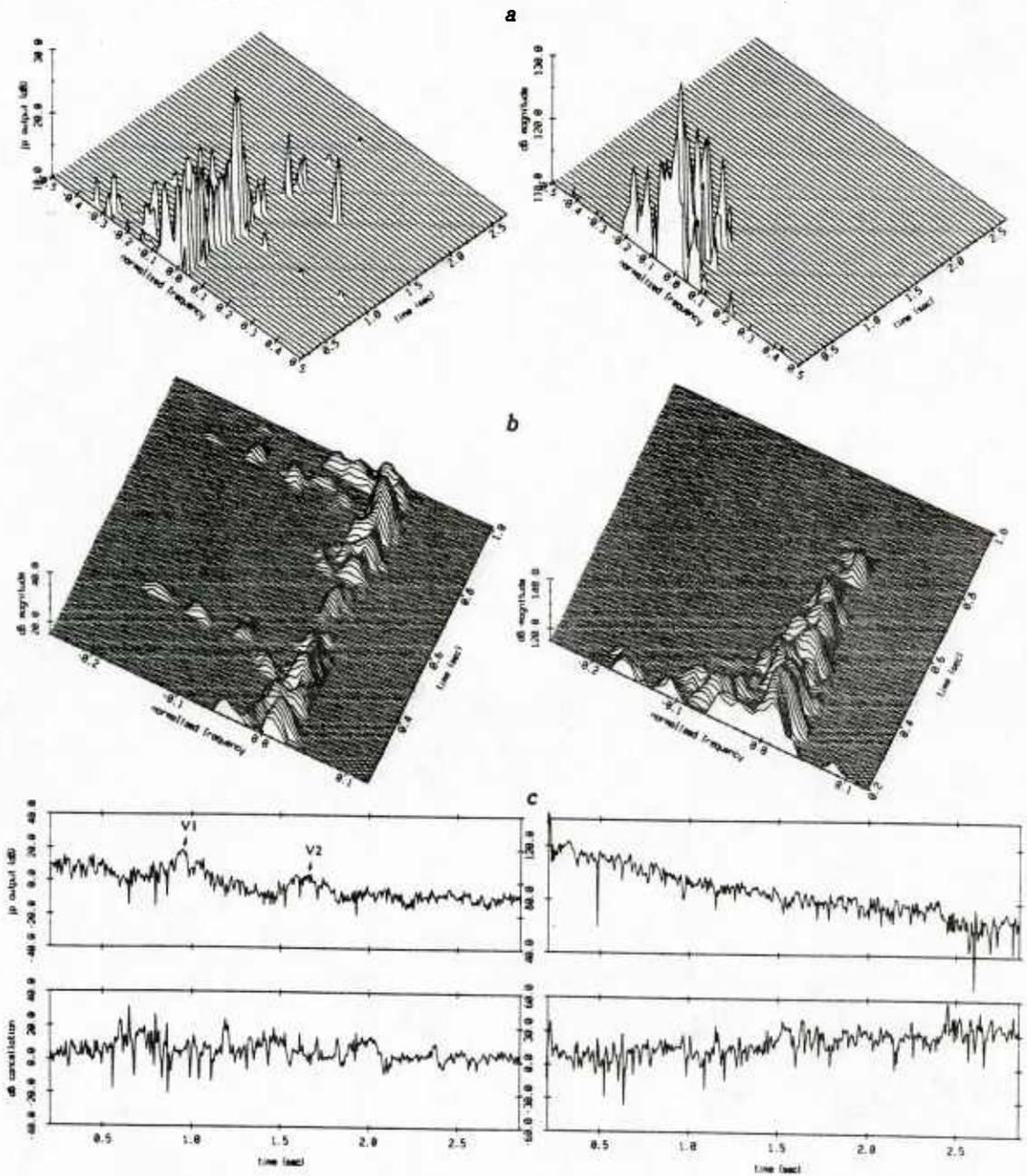
Figure 3.13 *Adaptive beamforming with 8 constrained reference elements.* Ping EXP3.2
(LHS) and REVGEN simulation RS3.2 (RHS): (a) Standard RDM, (b) expanded
RDM. Cancellation improves dramatically for both real and simulated data in
all ranges. (c) Output time-series and dB-cancellation curve. An additional
volume "signal" (V2) is revealed.
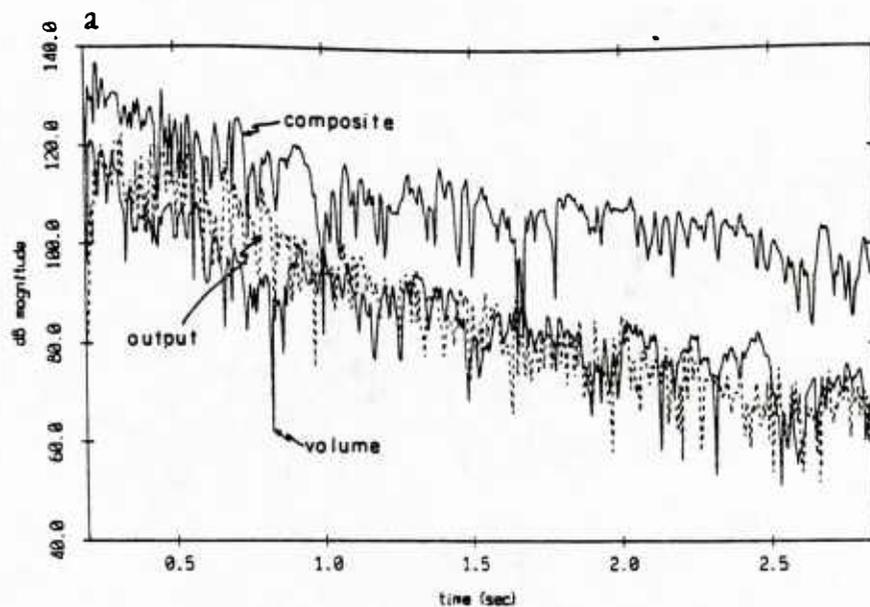
a

composite

output

volume

adaptive cancellation beam (8 reference elements)

symmetric case 1: Wd.1 alpha=0.02

b
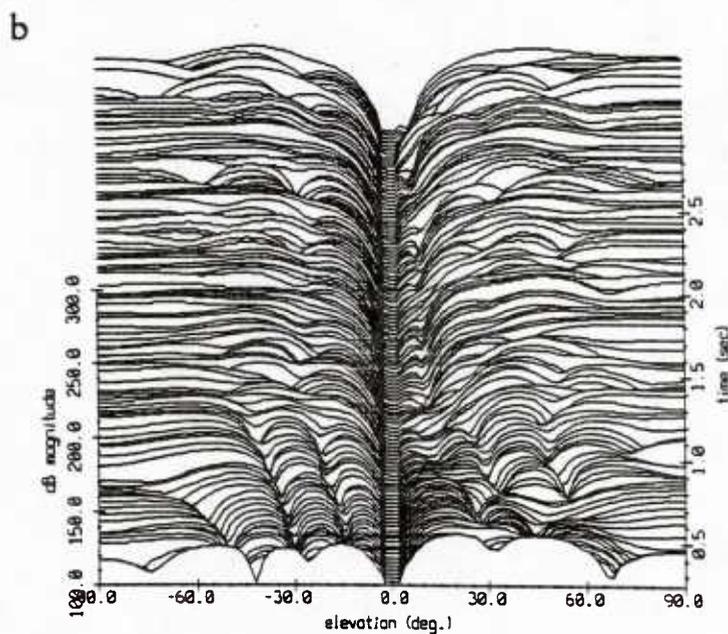
Figure 3.14 *SRC performance of spatially adaptive reference beam (RS3.2).* (a) Composite (top solid line), pure volume (bottom solid line) and output of 8-channel beamformer (dotted line). With the exception of a near-range region (0.5–1.0sec), SRC is achieved. (b) "Waterfall" plot of the adaptive reference (cancellation) beam produced by the algorithm. The adaptive beam strives to emulate the sidelobe structure of the primary beam in the near ranges.

104
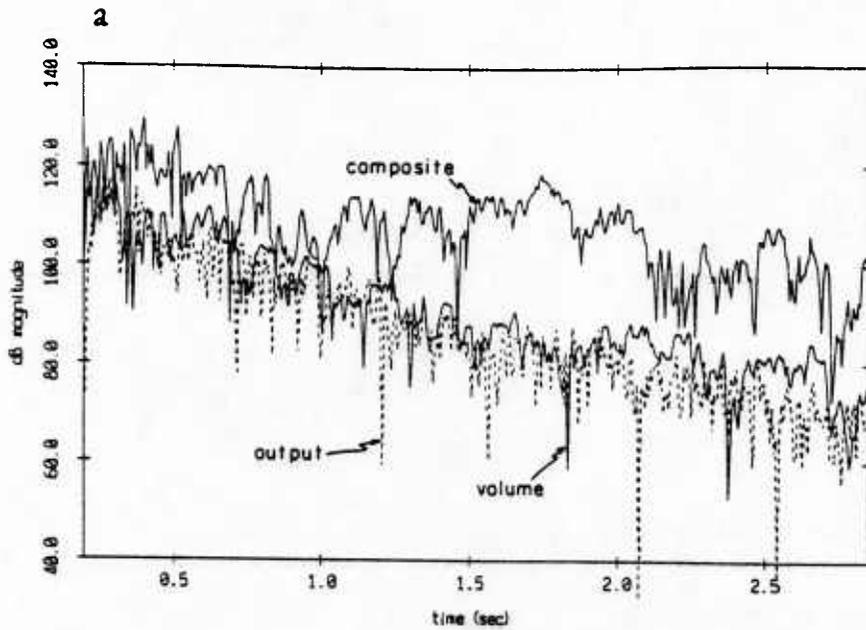
adaptive cancellation beam (8 reference elements)

symmetric case 1, kd.1 alpha=0.02
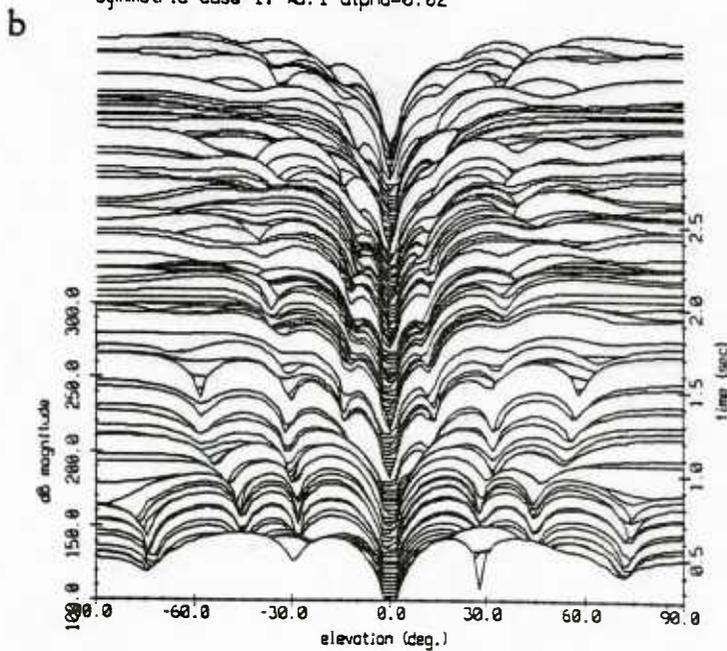
Figure 3.15 *SRC performance of spatially adaptive reference beam (RS3.3): "Symmetric" case.* (a) SRC performance improves in the near ranges and (b) a symmetric adaptive cancellation beam is produced.
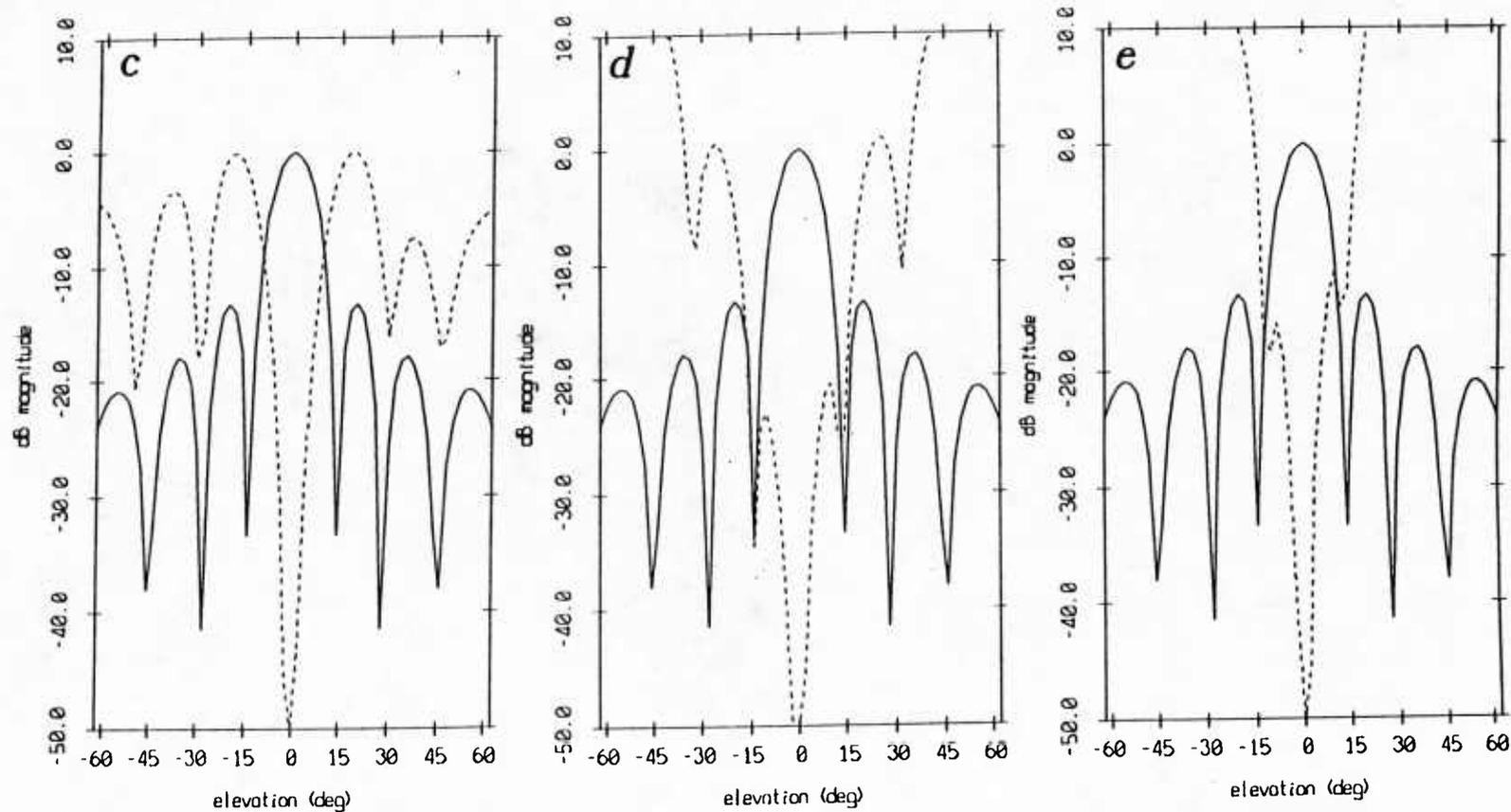
Figure 3.15 (cont.)   Vertical "cuts" of the adaptive beam pattern at $t = 0.5sec$ (c), $t = 1.0sec$ (d) and $t = 2.0sec$ (e) show three stages of the adaptation process. Initially, the reference beam (dotted line) emulates the sidelobe structure of the primary beam (solid line) thus eliminating the near-range "uncorrelated noise" effect. As the high-angle sidelobe returns diminish and boundary reverberation begins to enter through the main lobe, the reference beam progressively narrows its center null to compensate for the near-grazing boundary returns.
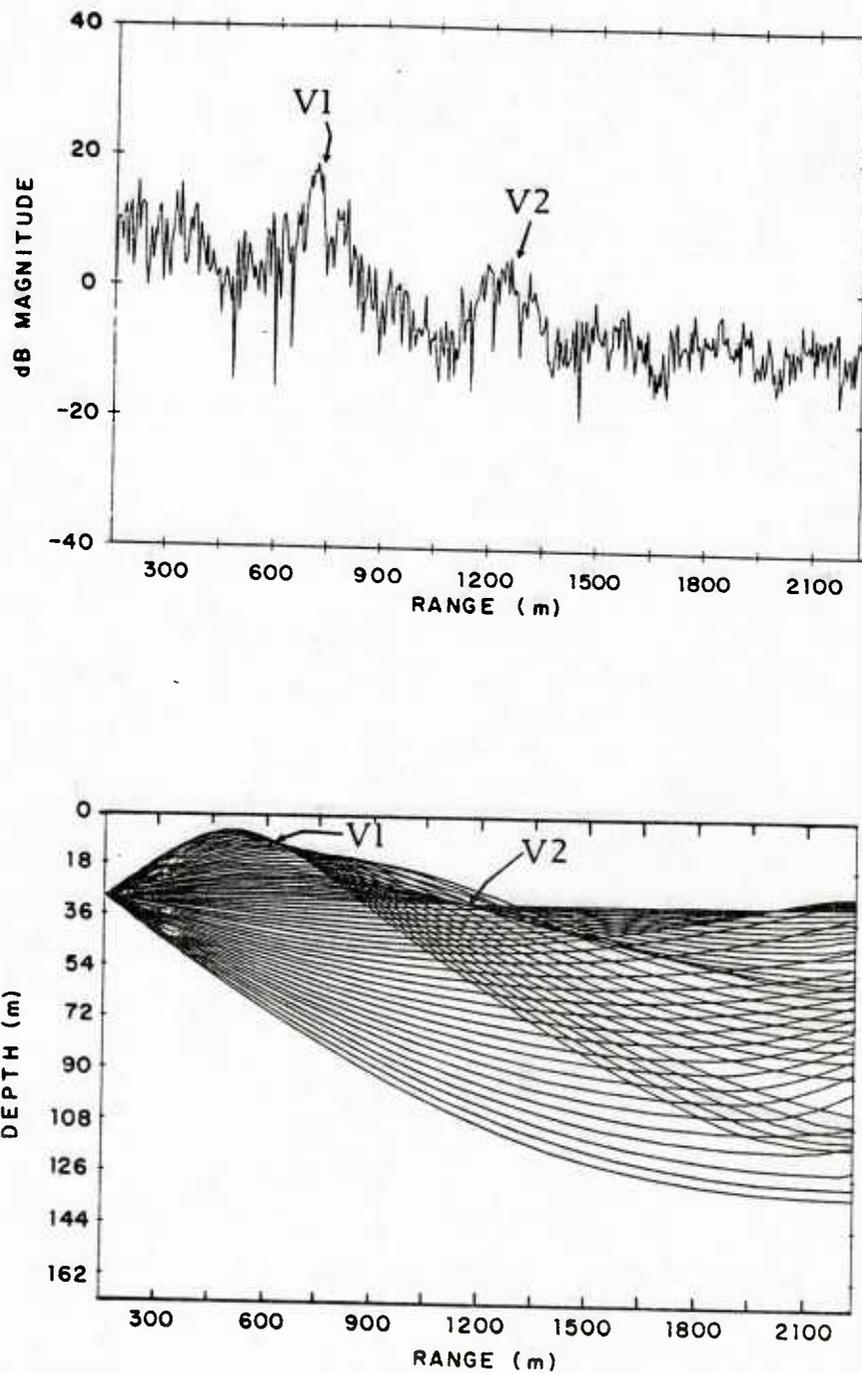
Figure 3.16 *Volume "feature" interpretation.* The two volume "signals" exposed in the data
(EXP3.2) by the adaptive beamforming operation (a), correpond well in range
with two caustics resulting from the sharp velocity gradient in the near-surface.
The raytrace diagram (b) covers an angular range of ±3 ˚ which is covered by
the null of the reference channel. Therefore, the strong volume reverberation
returns originating at the caustic regions are protected from cancellation and
preserved at the filter output.

a
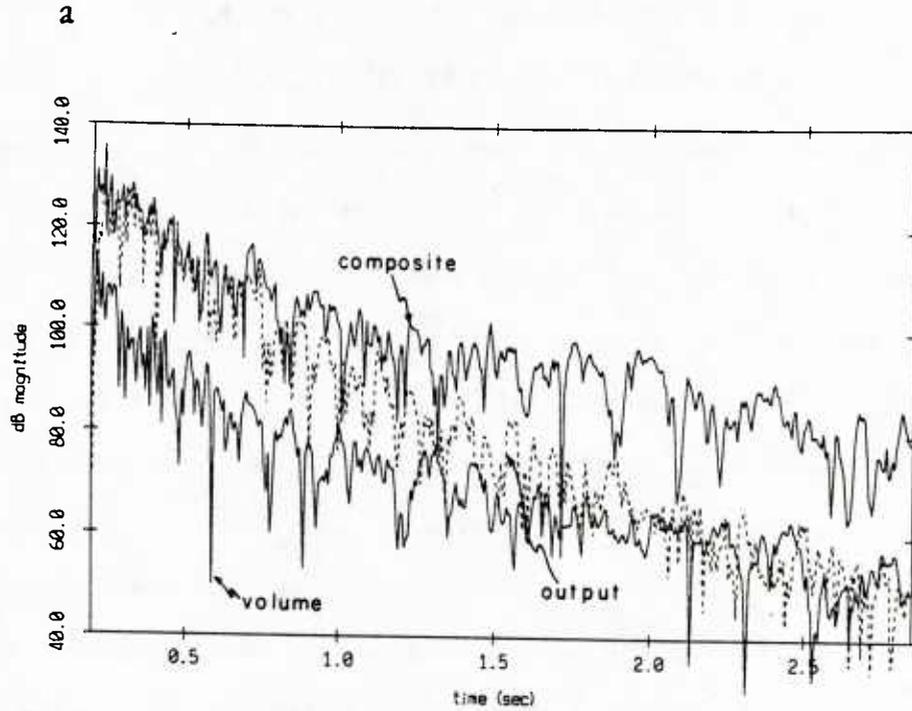
ASPS.2 ping:100
LSL m=2 p=3 alpha=0.02 main(1+2+...+9), ref(8,9)

b
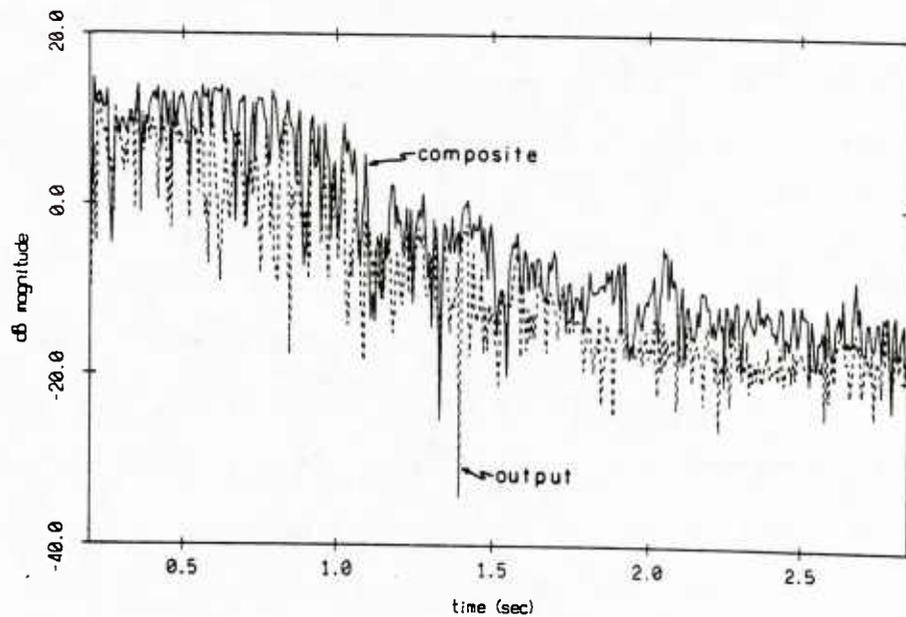
Figure 3.17 *Vertical correlation and ANC.* Real (EXP3.2) (a) and simulated (RS3.2) data (b). The main and reference channels are the outputs of rows 1 and 9 respectively. Cancellation improves with range for the simulated data as predicted by the point-scattering model. The real data results are not as conclusive.

CHAPTER IV

SURFACE REVERBERATION INTERFERENCE
IN UPPER OCEAN VELOCIMETRY

Doppler sonar systems offer significant operational advantages over mechanical flow meter devices and are becoming increasingly popular within the oceanographic community as remote velocity sensing tools. Typically, they are narrow-beam sonars which transmit short pulses of sound at carrier frequencies ranging from several kHz to $\sim$ 10 MHz. The Doppler shift of the volume backscatter has information about the relative radial velocity between the platform and the scatterers. Assuming that the primarily biological scatterers are passive tracers of water motion and that platform motion is insignificant on the velocity scales of interest, or independently measured and compensated for, this estimate may be interpreted as water mass velocity. Doppler sonars are most frequently categorized into pulse-to-pulse *coherent* and *incoherent* types. In a coherent system the velocity is estimated from the pulse to pulse variations of the echo phase. In an incoherent system, each return is considered to be an independent realization (sample function) of a random process and the velocity determination problem is essentially one of spectral estimation. A classification of Doppler sonar types is given by Pinkel [1980].

Sidelobe interference from the surface, bottom or a strong scattering layer is a definite concern during a Doppler sonar experiment; it can distort the volume velocity information or completely mask the volume reverberation component. This problem has been cited explicitly by Pinkel [1980], Lhermitte [1983] and Zedel [1985] and is very likely to arise during a near-surface deployment of a horizonally directed Doppler sonar. The near-surface region and the mixed layer in particular, is characterized by dynamic velocity features which are related to the air-sea interaction process and may represent important momentum transfer mechanisms [e.g. Pollard, 1970; Weller et.al.,

1985]. For these reasons, it is a region of great interest to the physical oceanographer. Currently, limited sampling of the mixed layer velocity field can be obtained by downward-looking Doppler sonars [e.g. Regier, 1982]. A horizontal sonar would be considerably more efficient for that purpose if not for the surface reverberation interference problem which is made more acute by the upward refraction typically encountered in the mixed layer.

This situation is a potential candidate for SRC. Succesful application of the adaptive techniques described in the previous sections may significantly extend the useful operational range of a horizontal Doppler sonar. In this chapter, real and simulated data from a pulse-to-pulse incoherent sonar will be used to examine the potential of recovering the volume velocity information by eliminating the contamination due to sidelobe-born surface interference.

4.1   Experiment description

The data were collected in May 1983 off the coast of San Diego, from Research Platform FLIP and through the pulse-to-pulse incoherent sonar system of the Internal Wave Group (SIO). A six-panel array was mounted at a depth of 38 meters on the port side of FLIP's hull, its normal axis forming $\sim 45°$ angle with the fore-aft direction. Each trapezoidal panel consisted of 210 transducer elements which were combined to produce a narrow ($\sim 2°$) beam. A maximum of 3 receive channels was available at 75 khz. Panel A was the transmitting array and panels B,C,D were used to receive. The experimental geometry and the panel arrangement are depicted in Figure 4.1. The beam pattern of a single panel, calculated by approximating the hexagonal transducer elements by circular pistons, is shown in Figure 4.2. It was found to be in good agreement with the available calibration measurements. Because the element spacing is somewhat larger than $\lambda/2$, spatial aliasing occurs giving rise to

three families of grating lobes which are ~15 dB down from the main lobe. The upper two grating lobes (elevation ~37° and bearing ~ ± 26°) were expected to let an amount of surface reverberation in the receive channels during the experiment.

Two data sets were collected, one with the array pointed horizontally (run 12A) and the other with the array rotated up ~ 3° (run 11A). A pulse length of 20 ms was used. Each transmission was followed by a 2 sec "listen interval" and the complex basebanded signal, sampled at 500 Hz, was digitally recorded. A step gain of 40 db was applied at ~ 0.3 sec following each transmission in order to preserve the backscattered return at long ranges.

During data collection, the wind speed was ~25 kn and the sea surface displayed a large swell with "chop" and "whitecaps." The estimated wave height was ~ 4 m. The diagram in Figure 4.3 shows the orientation of FLIP relative to the wind direction as recorded during data collection. It is evident that the main lobe axis of the port horizontal sonar nearly coincides with the direction of the wind.

4.2   Velocity estimation procedures

In the case of a pulse-to-pulse incoherent Doppler sonar, the velocity information is embedded in the spectrum of the reverberation return. Normally, the entire spectrum cannot be resolved in the spatial scales of interest. However, much useful information resides in the first and second moments of the spectrum (mean and spectral width, respectively). Because the autocorrelation and the spectrum are Fourier transform pairs, these moments may be estimated in the time-domain based on a well-known transform property. Namely, the spectral moments are equal to the derivatives of the autocorrelation function evaluated at zero lag. The derivatives may be determined by evaluating the autocorrelation function at one additional non-zero lag. This forms the basis for the Spectral Moment Estimation (SME) method

[Rummler, 1968; Miller and Rochwarger, 1972] which is widely used in oceanic Doppler sonar applications [Pinkel, 1980] and will be employed here. Specifically, the first spectral moment (mean frequency) is given by:

$$f_d(t) = \frac{1}{2\pi\Delta\tau}\tan^{-1}\left[\frac{\text{Im } R(t,\Delta\tau)}{\text{Re } R(t,\Delta\tau)}\right] \tag{4.1}$$

where $\Delta\tau$ is a suitably "small" time lag and R is the reverberation autocorrelation function. The velocity can then be estimated through:

$$\hat{v}(t) = \frac{cf_d(t)}{2f_c} \tag{4.2}$$

where c is the speed of sound in the ocean and f_c is the carrier frequency.

Remarks

i. The SME method will be effective when the Doppler spectrum is unimodal. If multiple spectral peaks exist, reflecting distinct velocity "events", this method will produce a meaningless "average" estimate. It is likely that *high resolution* AR (or ARMA) spectral estimation techniques may offer significant advantages over SME by resolving the multiple Doppler features. For example, Hansen [1984] has shown that velocity anomalies in the volume signal, presumably caused by fast-swimming fish, can be detected through AR modeling. It may be that surface reverberation can be equally well detected by such a spectral modeling scheme and the volume and surface velocity components thus isolated.

ii. Although several different autocorrelation estimators exist, the work of Hansen [1984] indicates that they result in essentially equivalent velocity estimates in terms of estimate variance [Theriault, 1981]. Here, the following estimate will be used:

$$R(t,\tau) = \frac{1}{N}\sum_{i=1}^{N} z_i(t)z_i'(t+\tau)$$

where i is the ping (sample function) index.

4.3 Data description

Relative intensity profiles from a representative $\sim$6 min long data segment are displayed in Figure 4.4. Each profile is a 20 ping average. Two surface reverberation features are clearly visible in this plot. First, a near-range ($\sim$ 65 m) peak is observed which corresponds well in range with the distance to the surface in the direction of the upper grating lobes. Evidently, the surface return is strong enough to overwhelm the volume signal by $\sim$20 dB despite the reduced response of the sidelobes. As the sidelobe surface hit ends, the volume component reappears until a grazing main lobe surface hit, probably the result of upward refraction, occurs at $\sim$400-600 m and dominates the return. The data are significantly different for the two runs in the far ranges. It appears that for the horizontal deployment (run12a) FLIP's motion causes the beam to periodically miss the surface. This seems to occur with a $\sim$ 1 min period. The "glitch" at $\sim$300 m is a remnant of the step gain correction.

Expanded intensity plots of the near-ranges (prior to the gain change) together with the corresponding velocity profiles calculated through SME are displayed in Figure 4.5. Striking velocity "anomalies" are observed in the vicinity of the intensity features. They are mostly negative which is consistent with the downwind orientation of FLIP during the experiment and display a complex, variable character. The volume velocity estimates are of the order of several cm/s as expected. A substantial increase in the variance of the velocity estimate is observed in the 200-300 m range which can be attributed to low SNR.

4.3.1 The Doppler shift of surface reverberation

Doppler shifts from the ocean surface have been observed in experiments involving both electromagnetic and acoustic wave transmission. [Crombie and Watts, 1967; Pidgeon, 1968; Valenzuela and Laing, 1970; Igarashi and Stearns, 1971; Swarts, 1972]. Most frequently, the mean Doppler frequency of surface reverberation (clutter) corresponds to the phase velocity of surface waves that satisfy the Bragg resonant condition (i.e. water waves of wavelength half the transmitted wavelength for grazing incidence). This "diffraction grating" effect was clearly demonstrated in a laboratory experiment by Liebermann [1963]. By insonifying a randomly rough surface, he showed that monochromatic acoustic radiation is preferentially scattered from travelling surface waves with the appropriate wavelength, resulting in Doppler shifts characteristic of the wave phase velocity. Other possible Doppler shift mechanisms cited in the literature are orbital velocities associated with gravity waves and "whitecaps" travelling in the direction of the wind [Hicks et. al., 1960].

4.3.2 Surface "roughness" vs bubble layer: A hypothesis based on observation

The single (180 ping average) intensity and velocity estimates plotted together in Figure 4.7 reveal an interesting discrepancy: The surface velocity "anomaly" does not coincide in range with the surface reverberation intensity peak. Specifically, the velocity feature develops during the second half of the intensity feature. This may indicate the presence of two distinctly different scattering mechanisms at or near the surface. We offer the following hypothesis based on the geometry of the sidelobe hit (Figure 4.6) and the postulated presence of a layer of bubbles entrained by turbulence just below the surface. Such a bubble layer has been consistently detected in moderate to high sea states [e.g. Thorpe, 1981] and can cause

intense scattering. If this layer undergoes a random (chaotic) motion it can be expected to contribute mainly to the broadening of the Doppler spectrum rather than result in a net Doppler shift. At the same time, a surface insonified "patch" develops which may cause net Doppler shifts associated with capillary wave velocity or whitecap drift. Initially (aa' in Figure 4.6) the zero-mean spectral broadening due to the bubble layer return may obscure the surface velocity information. In the latter stages of the sidelobe hit (bb' in Figure 4.6), on the other hand, the volume component of the combined return diminishes and the surface return dominates. In that region, the SME velocity estimate is in the range of 15 to 30 cm/s.

The wavelength of the capillary waves which selectively scatter the 75 kHz ($\lambda = 2cm$) incident acoustic radiation will be, according to the diffraction grating concept:

$$L = \frac{\lambda}{2\cos\theta} = 1.252 \ cm.$$

where θ is the grazing angle (here $\sim 37^\circ$). The corresponding capillary wave phase velocity is given, to a linear approximation, by:

$$v_L = \left[\frac{gL}{2\pi} + \frac{2\pi T}{L\rho}\right]^{1/2} \tag{4.3}$$

where T is the surface tension, ρ is the water density and g is the acceleration of gravity. Taking $T = 73.82 dyn/cm$ and $\rho = 1.025 \ g/cm^3$ [Neuman and Pierson, 1966] we have,

$$v_L \sim 23.60 \ cm/s.$$

This value is in good agreement with the surface velocity estimate and provides support for the "diffraction grating" effect.

Further support for the present hypothesis is provided by the velocity estimate in the ranges of the grazing main lobe surface hit. In such a low grazing angle

scenario, a subsurface layer of bubbles has often been suggested as the dominant scattering mechanism. This and the fact that no large velocity "anomalies" were found in that region are consistent with our hypothesis.

4.4   Sidelobe interference cancellation

An attempt was made to utilize the limited beamforming potential of this system to create a reference beam suitable for surface reverberation cancellation. A fixed constrained beam may be produced by subtracting two neighboring panels (e.g. B and C). Let this be known as configuration C1. The "uncorrelated noise" effect cited in Section 3.4.1 will not be present here because the transmit and receive beams are identical. However, a potential difficulty lies in the large separation distance between the centers of any two panels which is $d = 0.526m$ or $d = 26.3\lambda$. Panel-to-panel subtraction will cause severe spatial "aliasing" resulting in a finely structured "grating null" pattern which may seriously distort the sidelobe structure of the reference beam. This may in turn destroy the ANC potential of this particular configuration.

4.4.1   Spatial aliasing in constrained reference beams

In order to quantify the grating null effect, consider two identical omnidirectional transducers spaced a distance d apart and suppose that a signal $x(t)$ impinges on the two-element array at an angle θ relative to broadside. The phase delay between the two elements will be

$$\phi = 2\pi(d/\lambda)\sin\theta$$

and the output of the constrained array formed by subtracting one element from the other will be

$$x_c = x(t) - x(t)e^{j\phi}.$$

In addition to the obvious broadside null corresponding to $\theta = 0°$ (representing the

desired constraint), additional "grating" nulls will appear for

$$d/\lambda \sin\theta = n, \quad n = 1,2,...$$

In our case, $d/\lambda = 0.526/0.02 = 26.3$ and the first grating null will appear at $\theta = \sin^{-1}(1/26.3) \sim 2.18^\circ$. Therefore, according to the beam pattern multiplication theorem [Urick, 1975], one may expect a large number of closely spaced grating nulls in the reference beam formed by subtracting the elements of two panels.

The effect of panel separation on the resulting reference beam is illustrated in Figure 4.8. The first plot (4.8.a) is of a vertical "cut" of the beam pattern produced by omnidirectional elements separated by ~ 0.526 m, the distance between two neghboring panels. Note the finely structured grating null pattern. The second plot (4.8.b) displays a 0° bearing cut of the resulting reference beam and shows the broadside null in the main lobe, representing the desired constraint. The third plot (4.8.c) in the sequence is of a -26° cut and shows the original grating lobe to be disected by one of the grating nulls. Since the preservation of this sidelobe, the main interference outlet, is crucial for succesful ANC the reference beam created by panel-to-panel subtraction is a poor one for our purpose.

The situation can be remedied by effectively bringing the two arrays closer together. For instance, by allowing sections of the arrays to overlap, two offset-phase-center beams may be constructed which are sufficiently close to prevent the formation of deleterious grating nulls. The series of plots in Figure 4.8.d,e,f demonstrates the effect of reducing the distance between the array phase centers to $\sim \frac{\lambda}{2}$. The single wide broadside null is seen to virtually eliminate the main lobe while leaving the original grating lobe undisturbed in the reference beam. This configuration (C2) is nearly ideal for sidelobe interference cancellation and will be tested through a REVGEN simulation.

4.4.2 Processing results

Segments of the real FLIP data from both experimental runs were processed with the joint-process LSL filter ($p=3$, $\alpha_{LSL} = 0.02$). The results (Figure 4.9) are consistent with the predictions of the previous section regarding the experimental panel arrangement (C1). Although substantial cancellation ($\sim$10 dB) is achieved in the range of the surface sidelobe hit, a large surface reverberation component remains in the ANC output. Lesser ($\sim$ 3 dB) cancellation of the volume signal is observed owing to the fact that the main lobe is not completely eliminated from the reference beam by the narrow broadside null. Cancellation improves once more (to $\sim$10 dB) following the onset of the main lobe grazing surface hit but it is unlikely that SRC is achieved; this is a situation analogous to the one described in Section 3.4.1 , where the fixed null width proved to be a serious limitation in maintaining a high interference-to-signal ratio in the reference channel and consequently achieving SRC.

4.4.3 REVGEN simulation

Two simulations were performed. In the first simulation (RS4.1) the experimental panel arrangement (C1) was used. In the second (RS4.2) the "ideal" configuration (C2) was implemented. In both simulations the experimental geometry was slightly altered in order to contain the computational burden imposed by the narrow beam patterns. Specifically, a very high density of scatterers is required to achieve near-Gaussian reverberation statistics. By moving the arrays deeper, to 240 m, and thus allowing the scattering volume to expand prior to the initial surface hit, a lower density is required and substantial computational savings are gained. This alteration does not constitute a serious departure from the experimental setting with regard to our objective. The volume and surface layers were assigned distinctly different velocities in order to facilitate the performance evaluation process. The simu-

lation parameters are summarized in Table 4.1

Simulation parameter	Symbol	Value
Carrier frequency	f_c	75.0 kHz
Pulse length	τ	20ms
Sampling rate	f_s	500 samples/s
Shell slice thickness	T	5 m
No. of volume scatterers per slice	N_{ss}^v	3000
No. of surface scatterers per slice	N_{ss}^s	1000
Layer height	H	260 m
Sound velocity	c	1500 m/s
Volume reverberation coefficient	δ_v	-70 db
Volume velocity (μ,σ)	v_v	(5,1) cm/s
Surface reverberation coefficient	δ_s	-20 dB
Surface velocity (μ,σ)	v_s	(200,20) cm/s

Table4.1 REVGEN simulation (RS4.1)

In addition, the calculated FLIP panel beam pattern was inserted in the simulation.

Intensity and velocity profiles from the simulated data are displayed in Figure 4.10 a,b. Note that the intensity and velocity surface "events" coincide in range in the absence of a simulated subsurface zero-mean-velocity layer. The processing results for Simulation RS4.1 are shown in Figure 4.10 c,d. Marginal intensity cancellation is obtained, similar to the real data results. Virtually no improvement in the velocity estimate is seen. The results for Simulation RS4.2, shown in Figure 4.10 e,f, are dramatically different. No evidence of the surface reverberation intensity feature remains and nearly complete recovery of the volume velocity information is achieved.

Remarks

i.   The "ideal" beam resulting from configuration C2 is not suggested as the best possible practical implementation of an adequate reference beam for this application. External transducer elements emulating the sidelobe structure of the main beam should be equally effective.

ii.   No simulations were performed for the main lobe grazing surface hit. The results of Section 3.4 apply equally well here. SRC can be achieved and therefore volume velocity recovered only via spatially adaptive beamforming implemented through a multichannel joint-process structure.

4.5   Chapter summary

Data from a horizontal pulse-to-pulse incoherent Doppler sonar system were used to estimate the velocity features of surface reverberation. A hypothesis involving the presence of a thin layer of bubbles just below the surface was found to be consistent with the observed intensity/velocity structure of the surface return. Spatial aliasing in constrained reference beams was found to be detrimental to SRC. REVGEN simulations of this experiment were used to show that SRC and volume velocity recovery are possible if the spatial aliasing problem is aleviated.
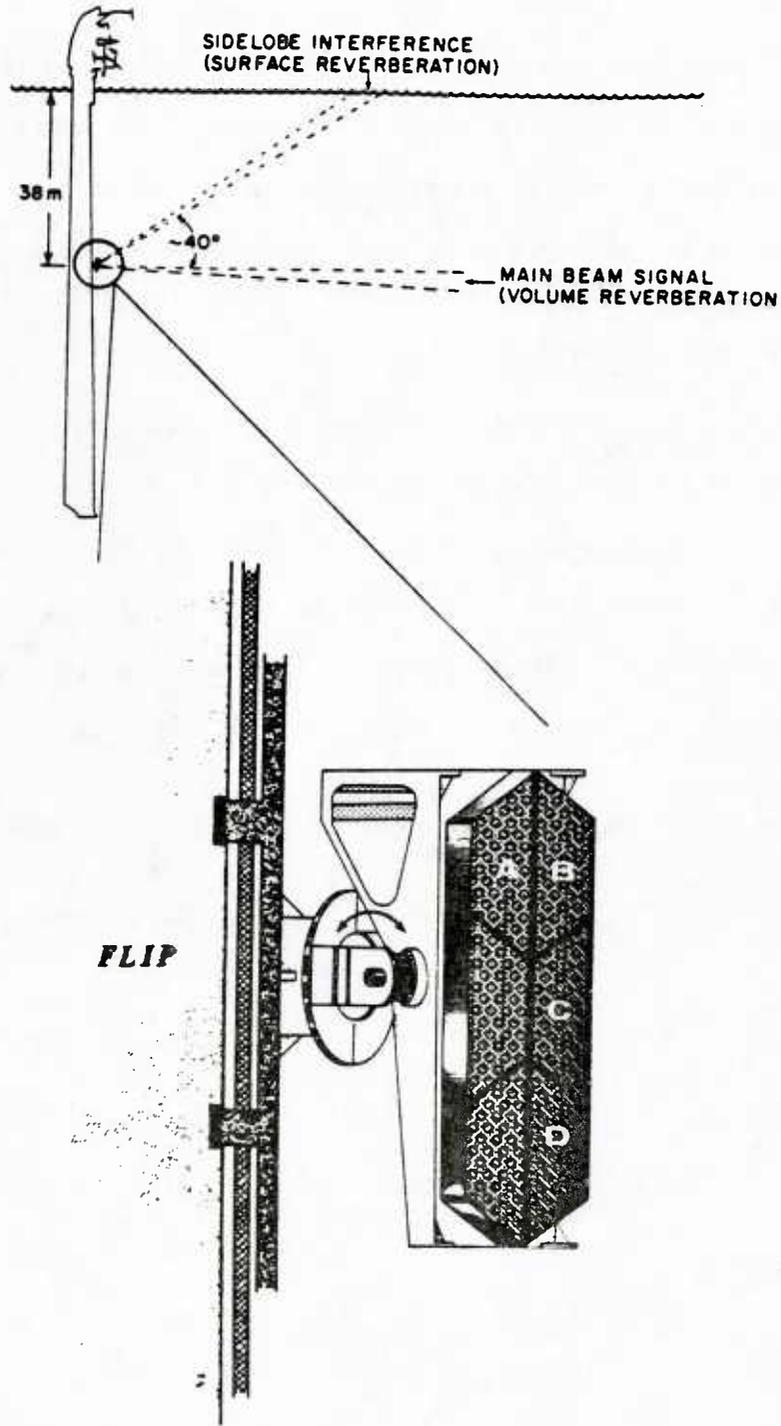
Figure 4.1 *FLIP experimental geometry.* Panel A was used to transmit and panels B, C, D to receive. Surface reverberation entering through the sidelobe contaminates the volume reverberation return.

FLIP sonar simulation

single panel beam pattern
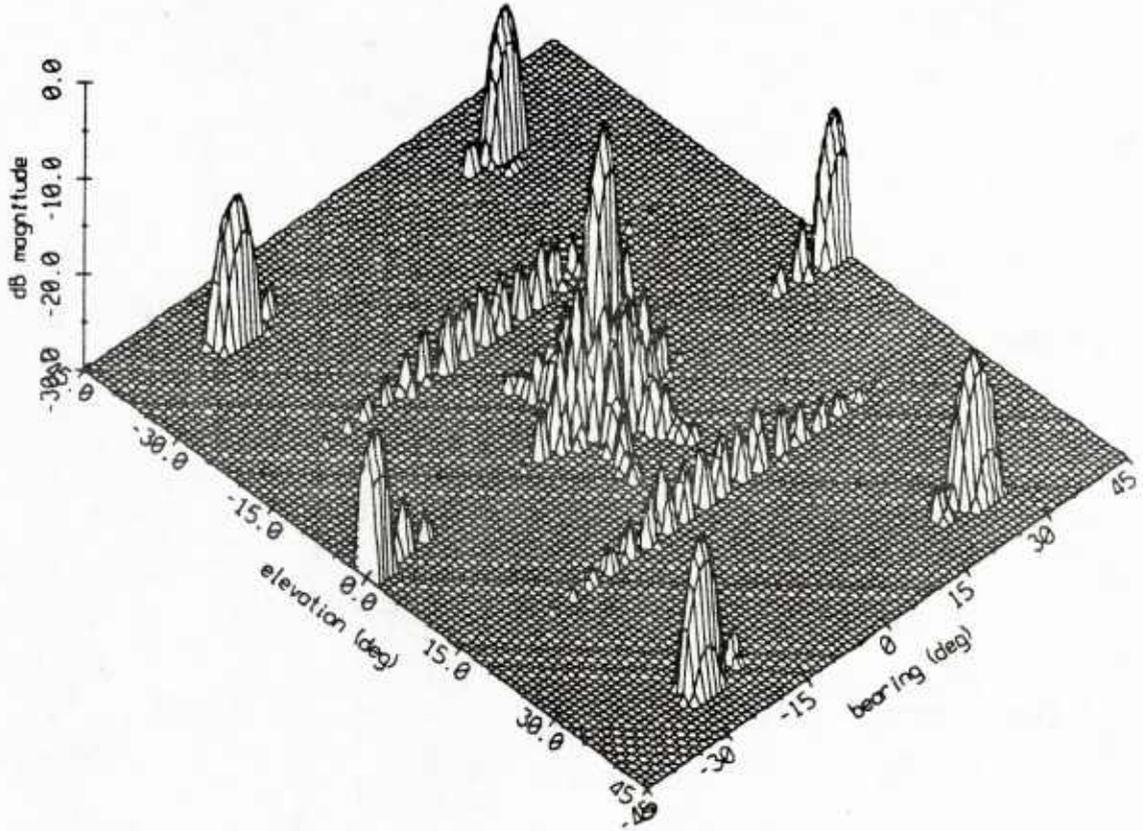
Figure 4.2 *Beam pattern of a single FLIP panel.* The upper two grating lobes at -37° elevation and ± 26° bearing are the surface reverberation outlets.
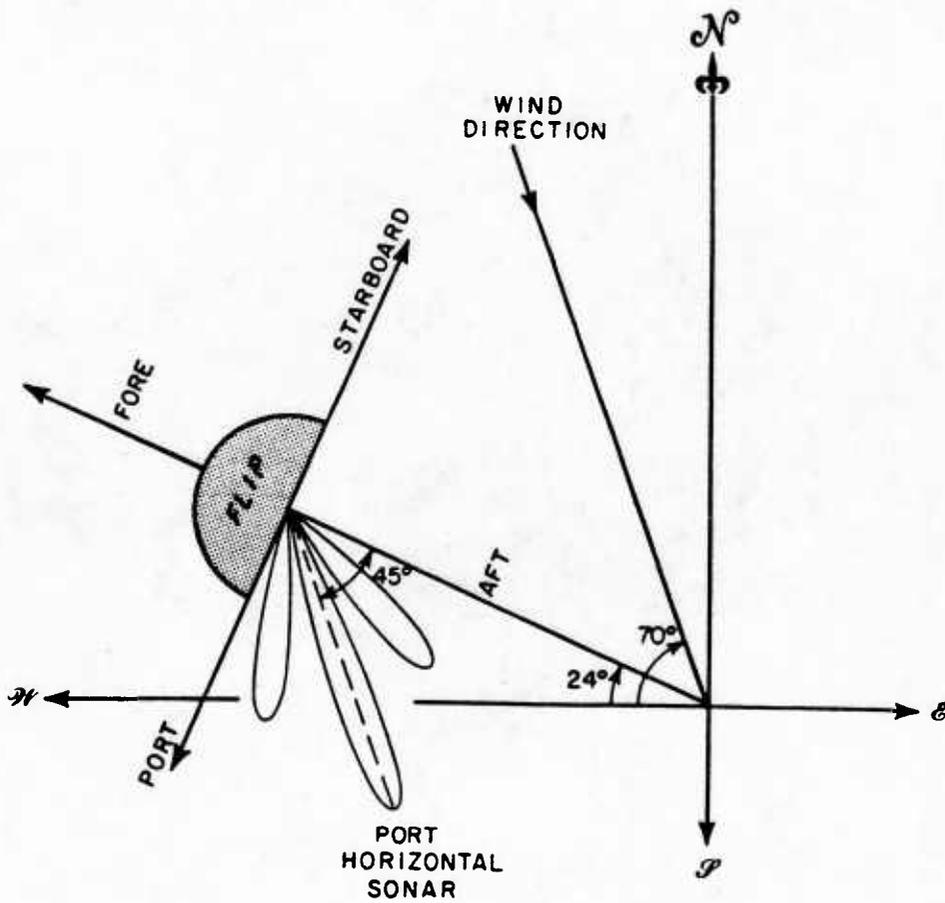
Figure 4.3 *FLIP orientation during data collection.* The main lobe axis nearly coincides with the wind direction.
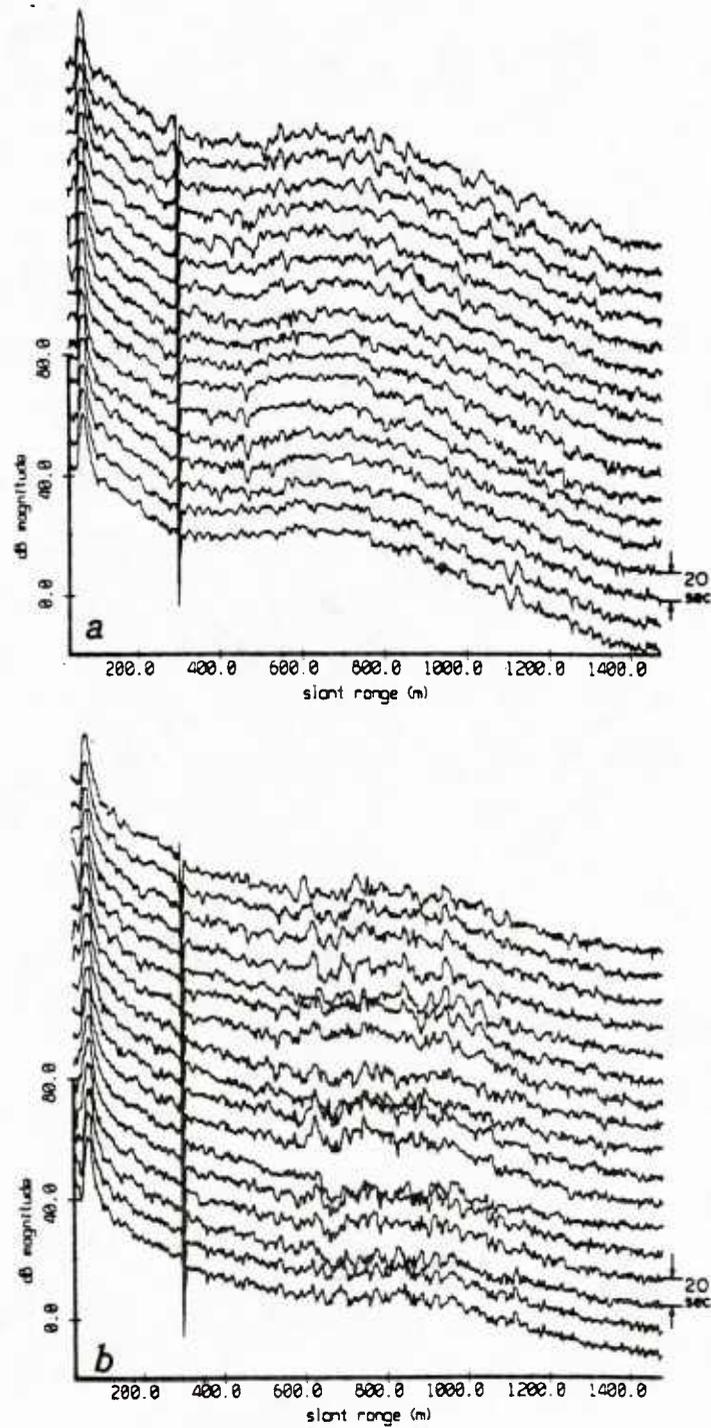
Figure 4.4 *Representative intensity profiles*; (a) run 11A, (b) run 12A. Each profile is a 20 ping average. The periodic intensity fluctuations in the far ranges reflect the motion of FLIP.
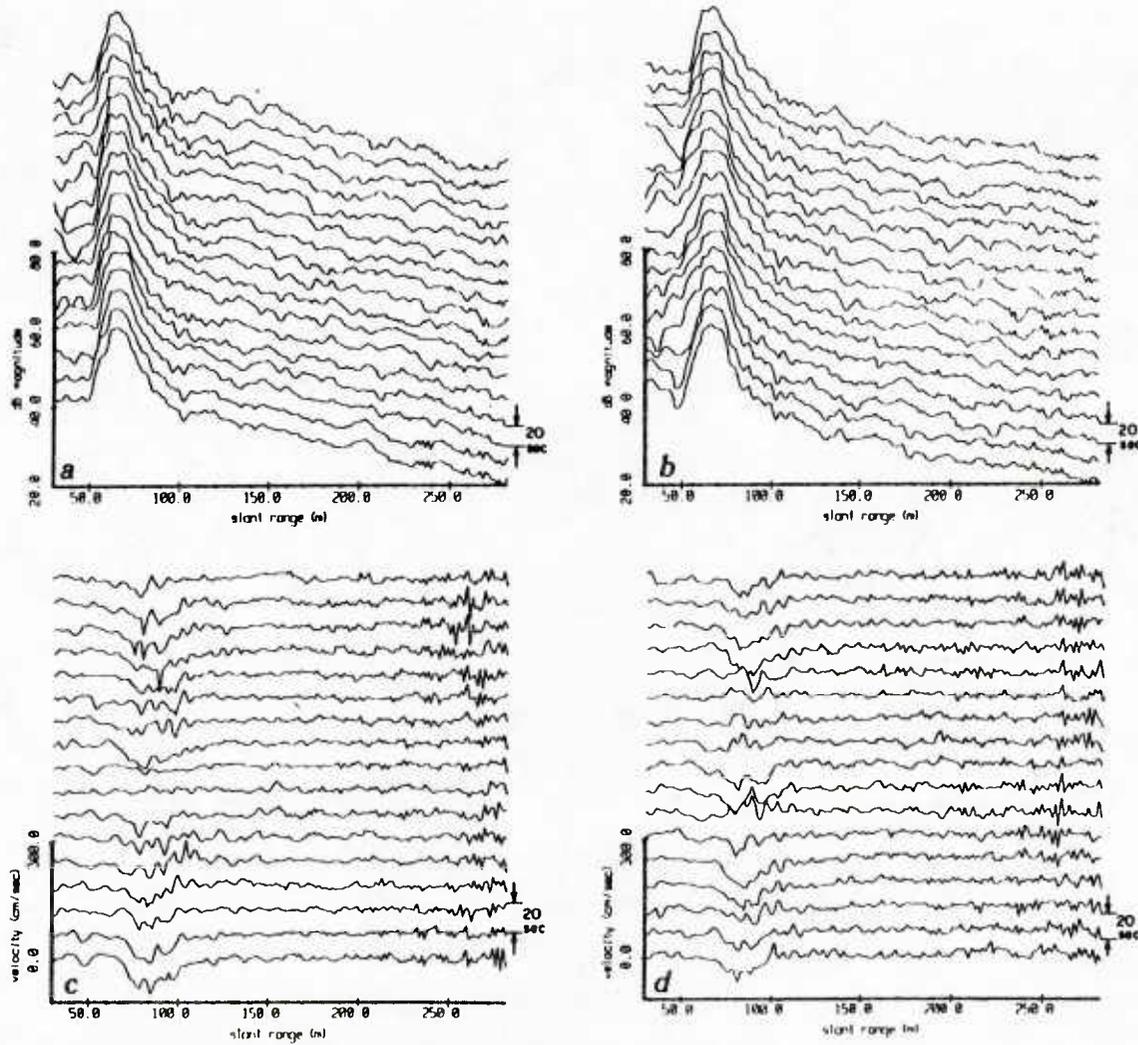
Figure 4.5 *Near-range intensity and velocity profiles;* (a,c) run 11A, (b,d) run 12A. A definite velocity "event" can be seen associated with the surface reverberation intensity feature.
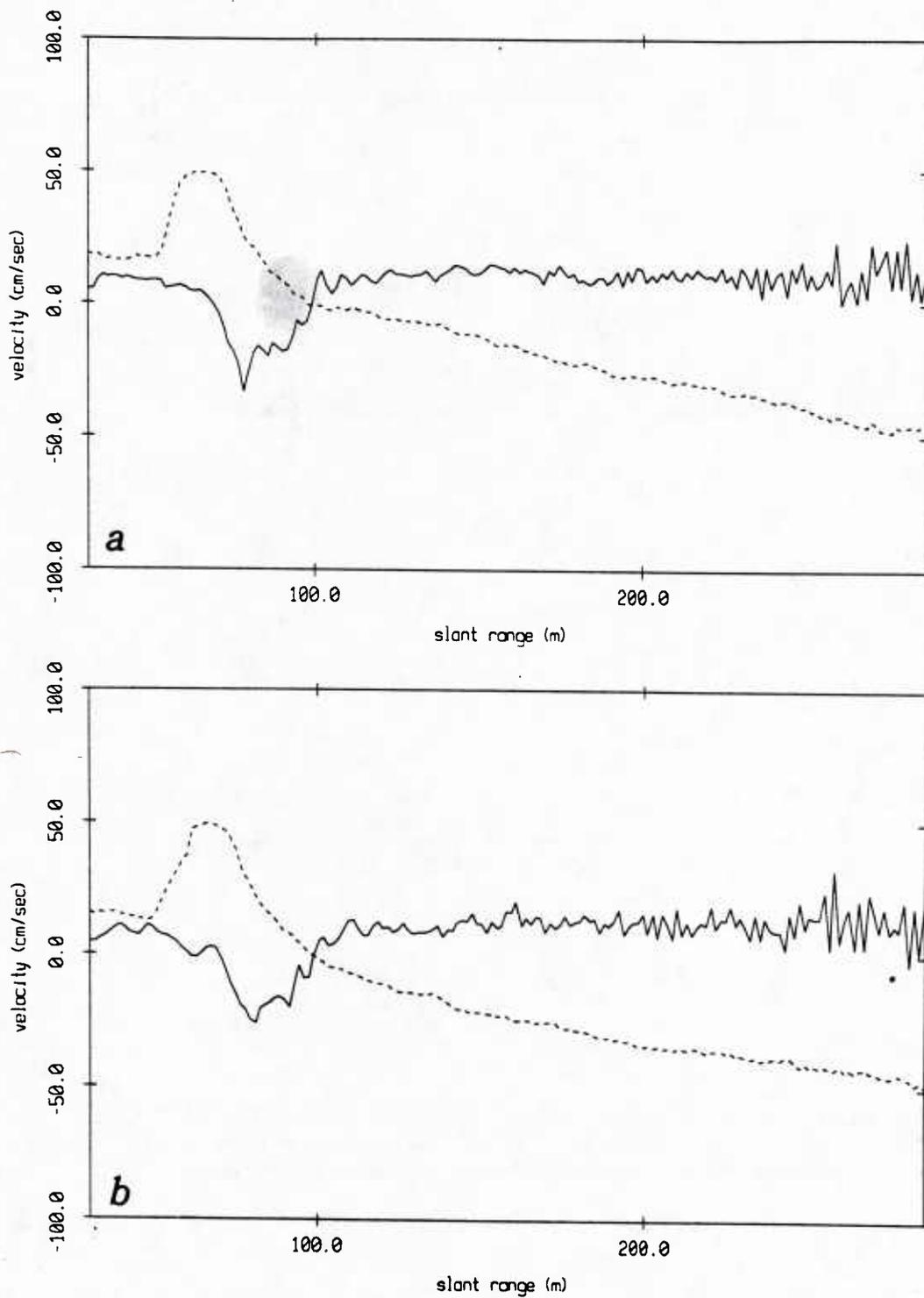
**Figure 4.6** *The near-range intensity/velocity " anomaly"*; (a) run 11A, (b) run 12A. The velocity feature is seen to develop during the second half of the intensity feature.
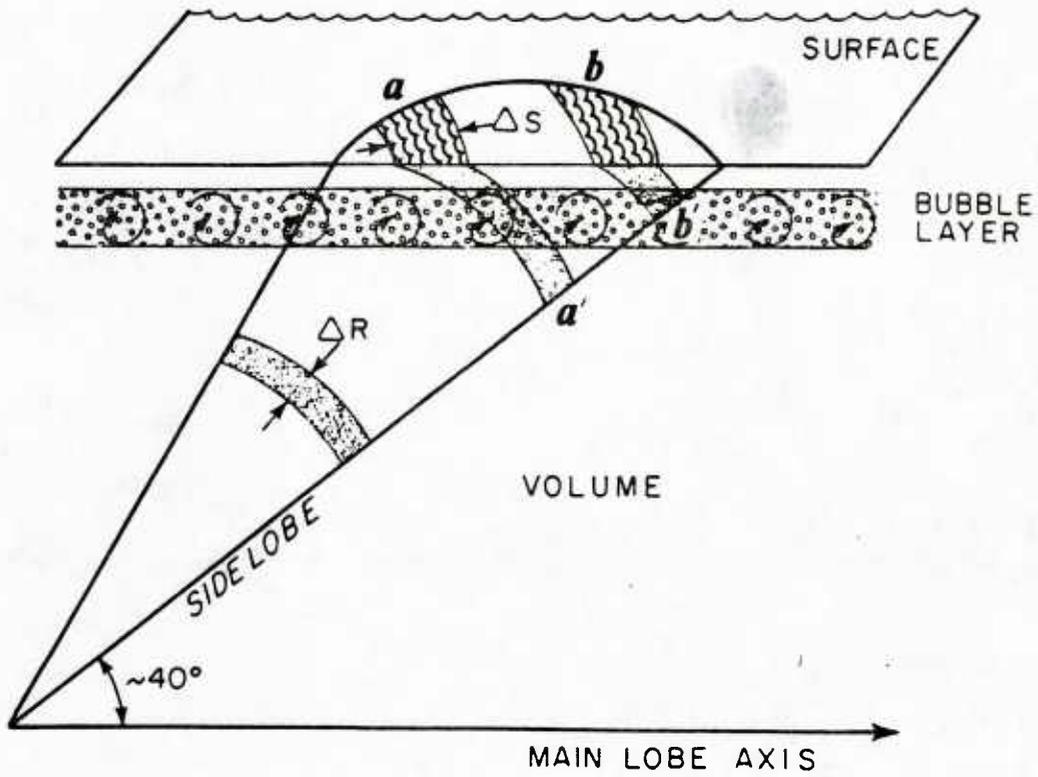
Figure 4.7 *Illustration of the " bubble layer" hypothesis.* Towards the end of the sidelobe sur-
face hit the volume part of the combined volume/surface scattering region
diminishes, allowing the surface velocity component to emerge.
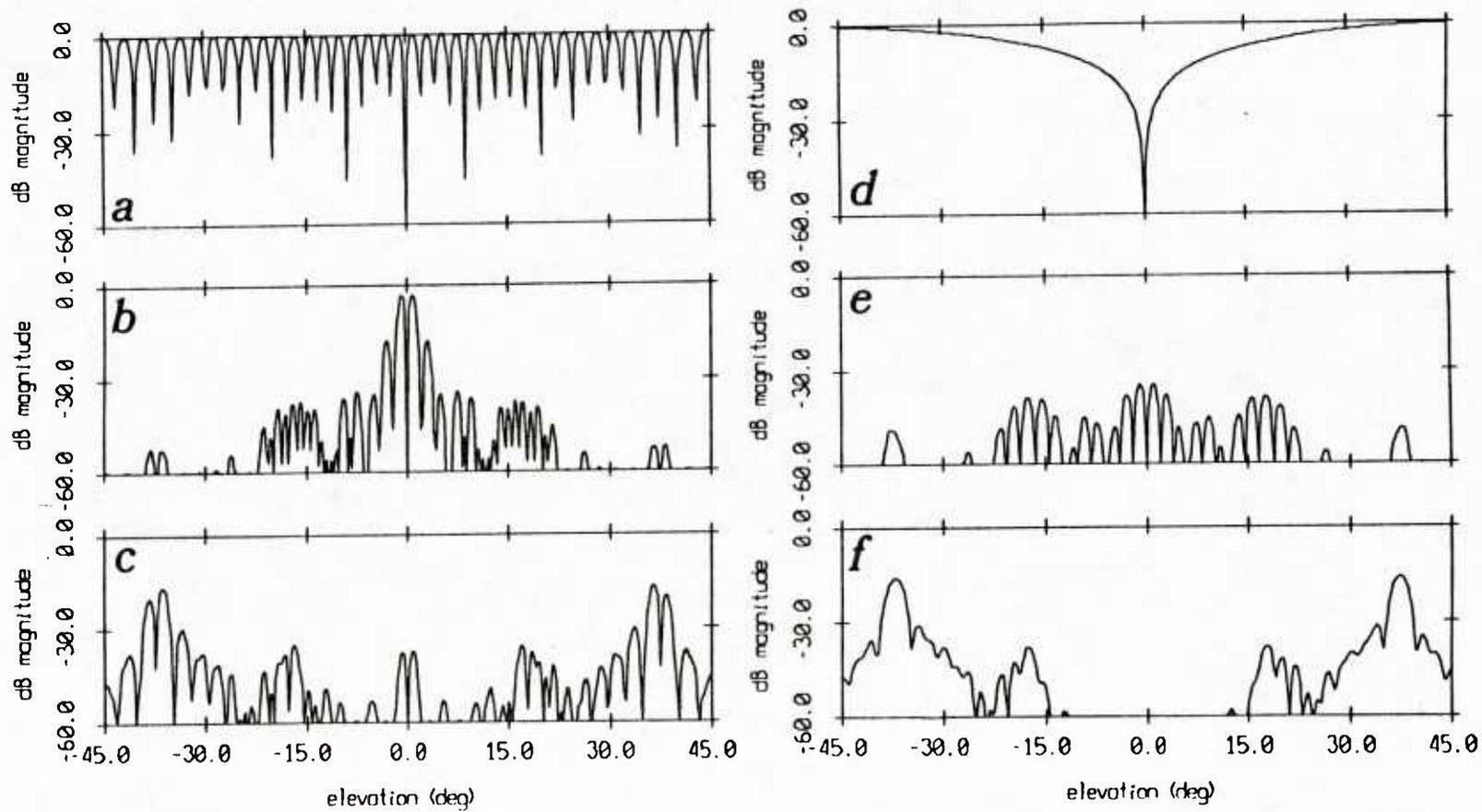
Figure 4.8 *Effect of panel separation on the reference beam.* The equivalent omnidirectional beam pattern for configuration C1 (a) is characterized by a multitude of grating nulls; in addition to the desired broadside null (b), more nulls are obtained in the reference beam, one of which disects the original grating lobe (c). The corresponding plots for configuration C2 show the single wide null (d) to completely eliminate the main lobe from the reference channel (e) while leaving the grating lobe unaffected (f).
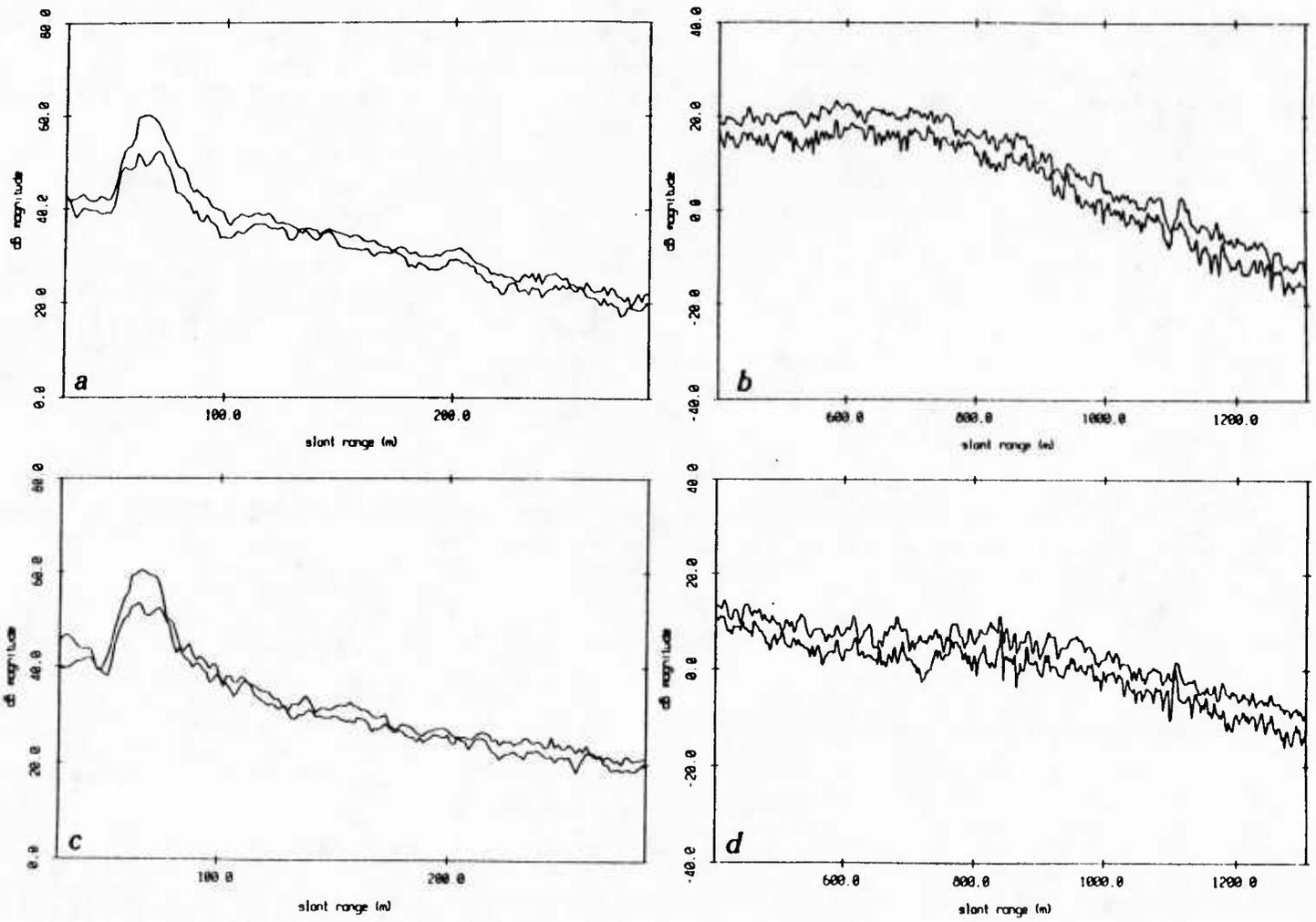
Figure 4.9 *ANC results for real FLIP data.* (a,b) Run 11A, (c,d) run 12A. Although a degree of cancellation is obtained, SRC is clearly not achieved with the experimental configuration (C1).
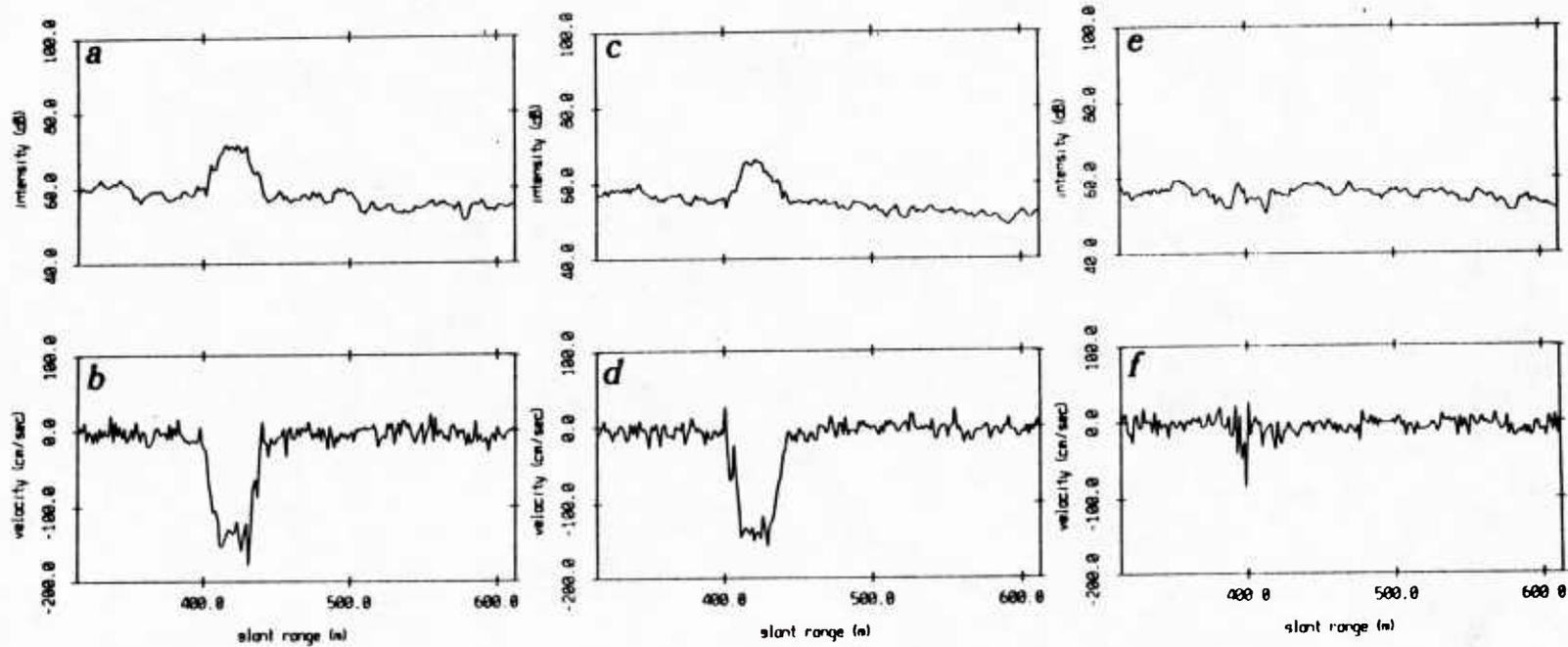
Figure 4.10 *ANC results for simulated data.* Intensity and velocity profiles of simulated data (a,b), data processed with configuration C1 (c,d) and data processed with "ideal" configuration C2 (e,f).

CHAPTER V

SEA BEAM SIDELOBE INTERFERENCE CANCELLATION

Sea Beam is a system developed by the General Instruments Corporation which uses time of arrival information obtained through a multibeam echo-sounder to produce high resolution contoured charts of the ocean floor. It transmits 7 ms pulses at a carrier frequency of 12.158 kHz with adjustable repetition rate. It employs a 20-element transmit array mounted along the ship's keel and a 40-hydrophone receive array which lies athwartships. The resulting transmit beam pattern is wide (54°) athwartships and narrow (2 2/3 °) in the fore-aft direction. The opposite is true for the receive beam (2 2/3° and 20°, respectively). A total of 16 receive beams is formed by electronically steering at athwartships intervals of 2 2/3°. An illustration of the overall system geometry is given in Figure 5.1a. The calculated transmit and receive beam patterns are displayed in Figures 5.1b and 5.1c, respectively.

Sea Beam is now widely in use within the oceanographic community and has contributed greatly in advancing the study of sea floor morphology by making large-scale, detailed surveys possible. It is generally considered to be a highly useful and reliable scientific tool. However, years of operational experience with the system installed on the R/V *Thomas Washington* of the Scripps Institution of Oceanography (SIO) have revealed a number of artifacts in the Sea Beam output which may be misinterpreted as seafloor features. Recently, de Moustier [1985a], using a data acquisition system developed by the Marine Physical Laboratory (MPL) of SIO, collected the acoustic envelope from all 16 receive channels. Through these data he was able to identify the underlying causes of artifacts such as the "omega" and "tunnel" effects. He concluded that the bathymetric artifacts result from echo detection and processing errors associated with certain characteristics of the sea floor such as a sudden change in slope, or caused by interference entering through the sidelobes of the

130

receive beams.

5.1   Sea Beam sidelobe interference

Sidelobe interference becomes a serious problem when the sea floor surveyed is relatively flat and highly reflective. In that case, the strong near-specular return entering the main lobe of the downlooking beam "leaks" through the sidelobes of all other beams (Figure 5.2a) and is present in all receive channels at levels comparable to the main lobe backscattered returns. The sidelobe interference "ridge," characterized by its simultaneous arrival in all receive channels, can be clearly observed in the typical Sea Beam acoustic record shown in Figure 5.2b. In certain operational states the system will track the sidelobe response and interpret it as a synchronous arrival from all beams. The resulting contoured output is a concave-up half cylinder (Figure 5.3). This is known as the "tunnel effect."

Perhaps a more serious consequence of the sidelobe interference is that it masks the backscattered acoustic return in the interior (near-vertical) beams. As a result, it seriously inhibits the process of extracting additional information, beyond bathymetry, from the Sea Beam acoustic signals. For example, the grazing angle dependence of the backscattered intensity may be an important indicator of the sea floor roughness characteristics. In attempting to estimate this function from Sea Beam data, de Moustier [1985b] noted that the interior beams were rendered useless by sidelobe interference. Unless the interference is removed, any potentially important information possesed by the interior beams will remain unexplored.

Here, we offer a possible remedy for the sidelobe interference problem through a simple application of Adaptive Noise Cancelling.

5.2   Sidelobe interference cancellation

The same mechanism responsible for creating the sidelobe interference problem offers the potential for its removal through ANC. Specifically, the downlooking beam is a natural reference channel which could be used to operate sequentially on the other 15 beams. Because the interference-to-signal ratio is high in both the main and reference channels, a substantial improvement in signal-to-interference ratio (SIR) is predicted by ANC theory (Equations 2.5a,b).

Application of this concept on real Sea Beam data is not currently possible because only the envelope of the acoustic return is recorded. A modification of the MPL data acquisition system is under way to allow the collection of amplitude and phase information through quadrature sampling of all 16 beams.

5.2.1   REVGEN simulation

Preliminary conclusions on the feasibility of this technique may be reached through a REVGEN simulation. A simulation run (RS5.1) was performed which retains all known Sea Beam system parameters including the calculated transmit and receive beam patterns. A summary of this REVGEN run (RS5.1) is given in Table 5.1.

Simulation parameter	Symbol	Value
Carrier frequency	f_c	12.158 kHz
Pulse length	τ	7 ms
Sampling rate	f_s	1000 samples/s
Shell slice thickness	T	5 m
No. of volume scatterers per slice	N_{vs}^o	300
No. of bottom scatterers per slice	N_{bs}^o	300
Layer height	H	4000 m
Sound velocity	c	1500 m/s
Volume reverberation coefficient	δ_v	-90 db
Bottom reverberation coefficient	δ_b	-50 db

Table 5.1 REVGEN simulation RS5.1

A total of 4 receive beams (steered at 0°, 3°, 6° and 9°) was deemed sufficient for the purpose of this simulation. The synthetic Sea Beam record is displayed in Figure 5.4.a. The sidelobe interference pattern is clearly visible and bears close resemblance to the corresponding real data feature.

The 3 outer beams (3°, 6°, 9°) were processed through the joint-process least-squares filter (p=3, $\alpha_{LSL} = 0.02$) with the 0° beam serving as the reference channel. The results (Figure 5.4.b) are promising. The sidelobe interference has been succesfully removed with no evidence of distortion in the remaining signal.

Remarks

i. The emergence of the sidelobe interference "spike" from a backround of volume reverberation represents an intensity "jump" of ~20-40 dB. According to Simulation 3 (scale change) of Chapter 2, the stochastic approximation algorithms (i.e. LMS and GRL) would be unsuccessful in this setting. During exploratory cancellation attempts with the LMS and GRL on the simulated Sea Beam data, the two filters were driven to instability as predicted by Simulation 3.

ii. If similar cancellation performance is obtained for real Sea Beam data, the "tunnel effect" can be eliminated. However, additional simulations are needed to determine the extent to which recovery of the interior beam back-scattered return can be achieved.

iii. An alternative operation which may be effective in removing the Sea Beam sidelobe interference involves the placement of appropriate spatial nulls in all receive beams. Essentially, an entirely new beamforming scheme must be implemented; it would require tapping the outputs of all 40 receiver elements and hence further modification of the current Sea Beam data acquisition sys-

tem.

5.3   Chapter summary

It was demonstrated through a REVGEN simulation that the same mechanism responsible for creating the Sea Beam sidelobe interference problem offers the potential for its removal through ANC, pending a minor modification in the Sea Beam data acquisition system.
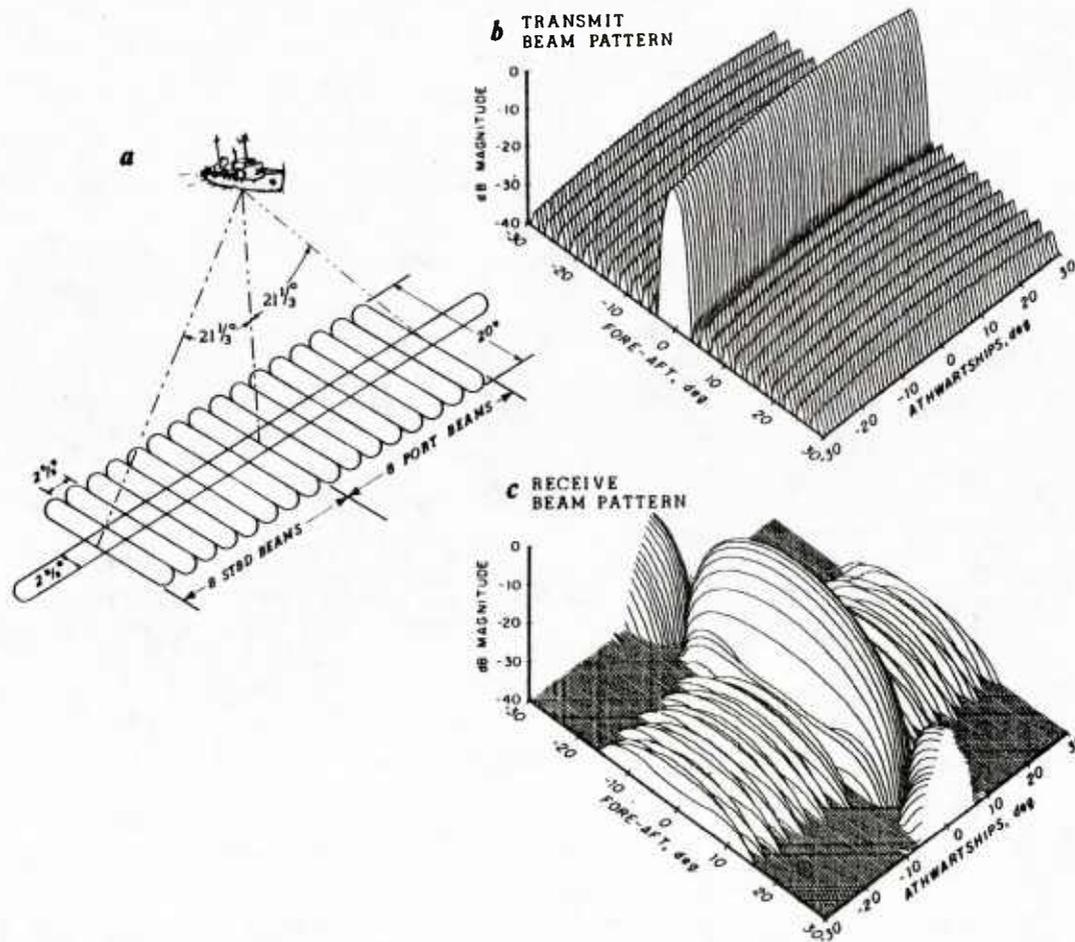
Figure 5.1 *Sea Beam experimental geometry and beam patterns.* (a) A schematic diagram showing the relationship between the transmit beam and the sixteen receive beams. The calculated transmit and receive beam patterns are displayed in (b) and (c) respectively.
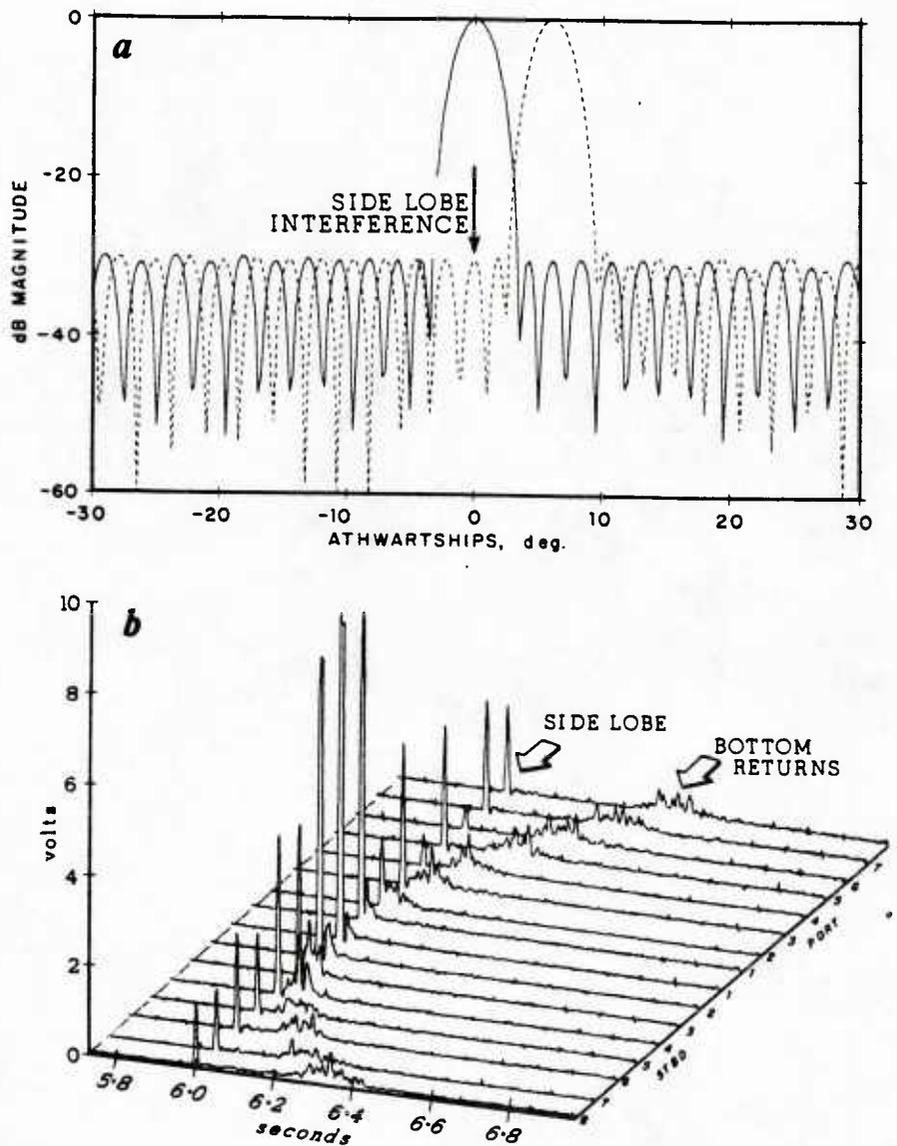
Figure 5.2 *Sea Beam sidelobe interference.* (a) Generating mechanism: The near-specular return entering the main lobe of the downlooking beam (solid line), "leaks" through the sidelobe structure of an outer beam (dotted line). (b) A typical Sea Beam record displaying the characteristic sidelobe interference "ridge" (from de Moustier, 1985a).
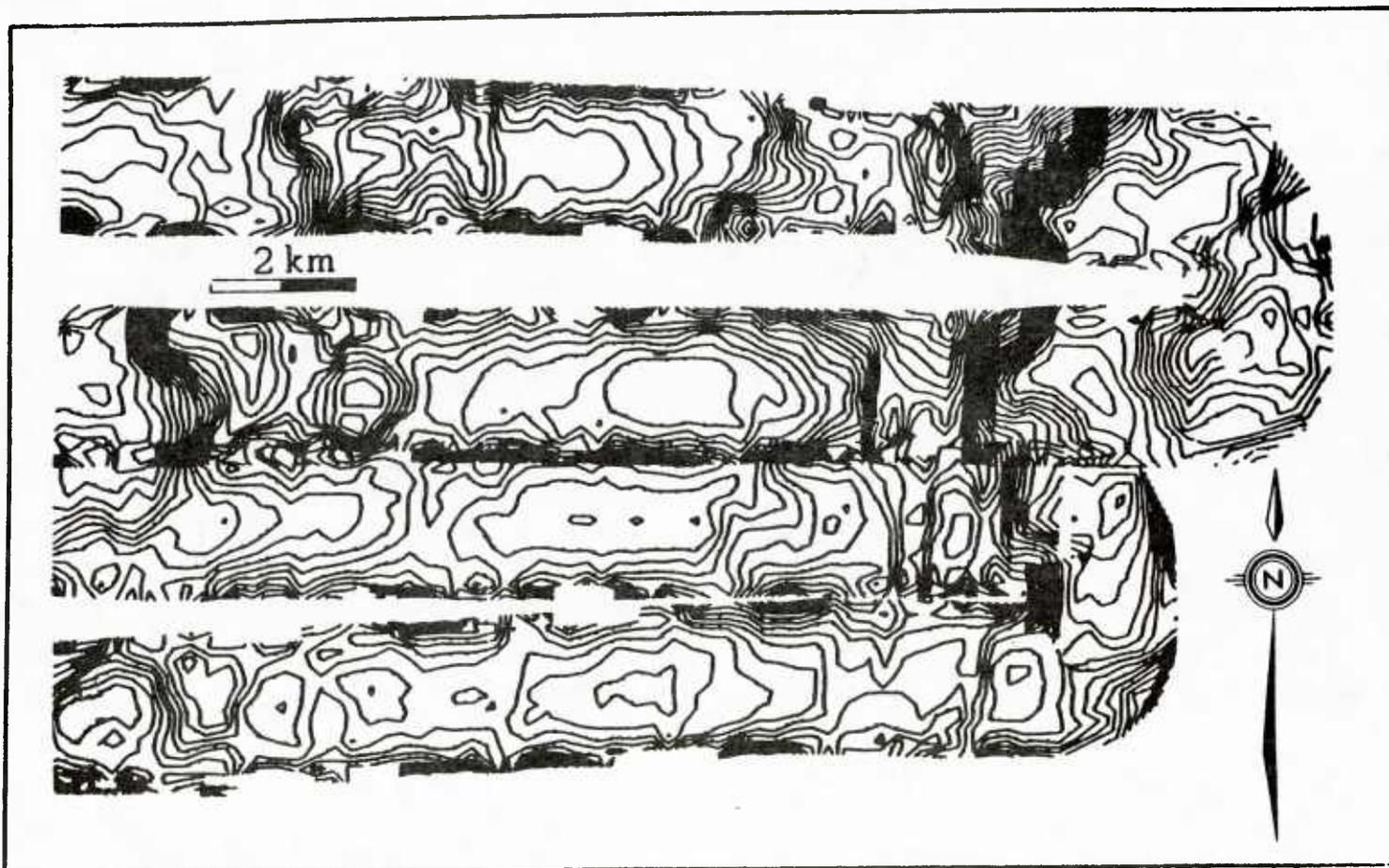
Figure 5.3 *The "tunnel effect"*. As a result of sidelobe interference, the contoured output of Sea Beam resembles a trough approximately centered on the ship's track (from de Moustier 1985a).

SEA BEAM Simulation
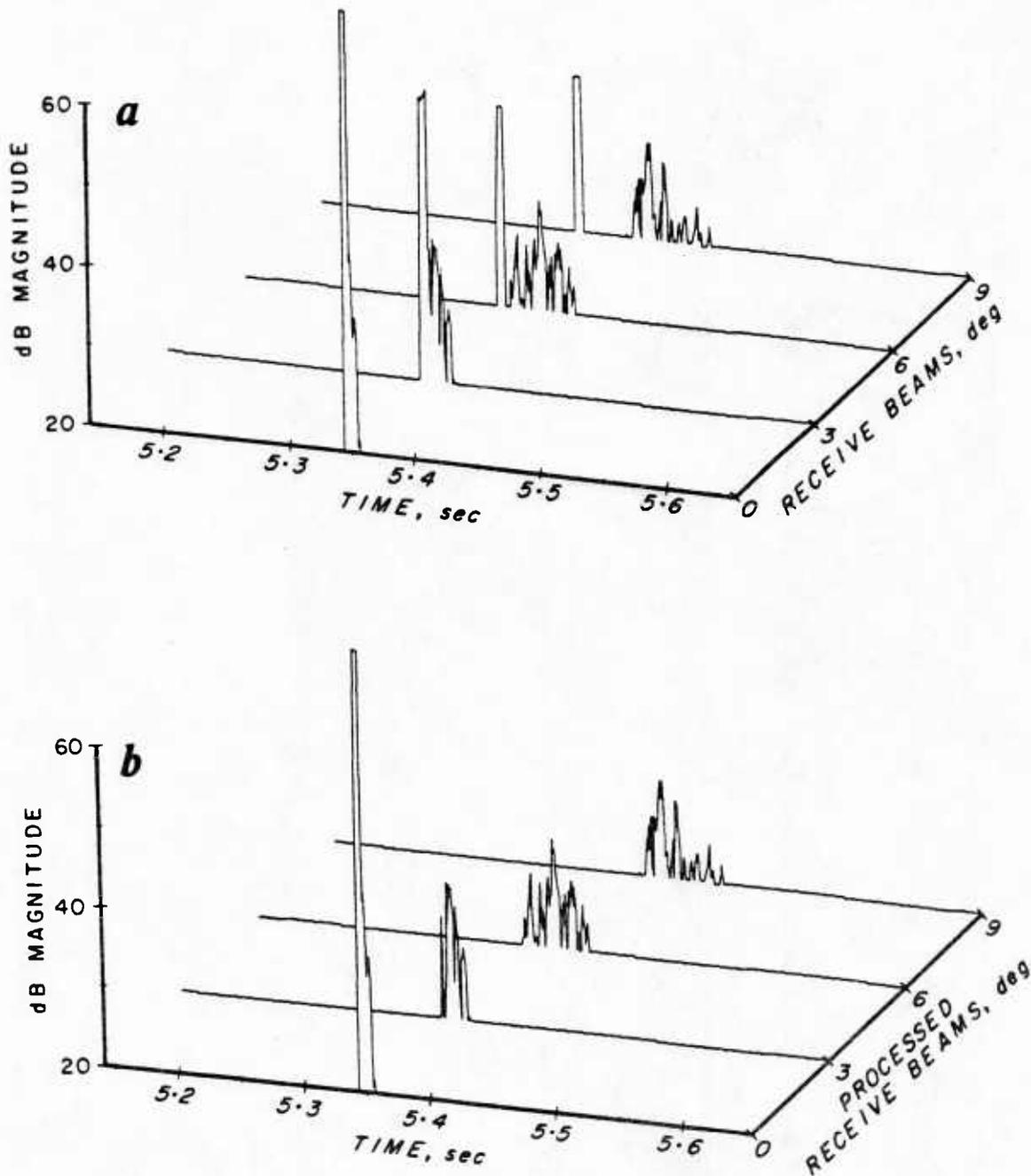
Figure 5.4 *Sea Beam sidelobe interference cancellation.* (a) REVGEN simulated data and (b) ANC processing results. By using the downlooking (0˚) beam as the reference channel, the sidelobe interference ridge is successfully removed from the outer beams of this simulated Sea Beam record.

CONCLUSIONS

The central theme of this thesis has been the application of the adaptive beamforming concept to the problem of selective reverberation cancellation. We have exposed relevant reverberation properties, evaluated a representative cross-section of adaptive algorithms and demonstrated experimentally the feasibility of selective reverberation cancellation through real and simulated data from three active sonar experiments.

The spatial correlation properties of reverberation predicted by the point-scattering model were shown to be directly applicable in a reverberation cancellation context. Specifically, the predicted disparities in vertical correlation between the boundary and volume returns provide a natural mechanism for the separation of the two components through adaptive noise cancelling.

Based on theoretical considerations substantiated by computer simulations, it was shown that lattice joint-process filters have superior convergence properties over direct tapped-delay-line implementations in the presence of power disparities in the reference channel. In addition, deterministic least-squares solutions were shown to perform better than stochastic approximation (gradient) solutions during drastic power transients in the reference channel.

Real and REVGEN-simulated composite reverberation data from a shallow-water experiment were used to determine the degree of cancellation obtainable through adaptive processing. It was shown that significant SNR enhancement can be achieved, for echoes embedded in a reverberation backround, through ANC with fixed, preformed reference beams. Morover, it was shown that the weak volume reverberation component can be extracted from a composite process through boundary reverberation cancellation obtained via constrained adaptive beamforming.

Data from a near-surface deployment of a Doppler sonar revealed an interesting "anomaly" in the intensity/velocity structure of surface reverberation which led to a hypothesis involving the presence of a thin layer of bubbles immediately below the surface. In addition, it was demonstrated through a REVGEN simulation that recovery of the volume velocity signal is possible through ANC if appropriate reference beams are constructed.

A REVGEN simulation of the Sea Beam bathymetric system was used to demonstrate that the sidelobe interference problem giving rise to the "tunnel effect" artifact can be aleviated through adaptive processing.

There are several directions in which the results developed here can be extended. Experimental measurements of the spatial correlation characteristics of oceanic reverberation under a variety of environmental conditions, would be very useful in assessing the reverberation cancellation potential of a given experimental arrangement. In addition, it would be of interest to pursue further the promising simulation results of Chapter III. If an appropriate reference beam can be constructed, it may indeed be possible to recover volume velocity information by selective removal of the surface reverberation component. Morover, significant potential benefits may be gained from the application of the sidelobe interference cancellation scheme suggested in Chapter IV to real Sea Beam data, pending a minor modification in the Sea Beam data acquisition system to allow the collection of both amplitude and phase information. Finally, recently developed algorithms based on the more general ARMA model [Morf and Lee, 1978; Lee, 1980] offer the potential for better representation of the reverberation process and may lead to improved cancellation performance.

APPENDIX

A.   Levinson's algorithm

This algorithm is an efficient solution of the linear prediction problem (Equation 2.4), when the autocorrelation matrix $\mathbf{R}_{ss}^p$ is Toeplitz. We begin with,

$$[I_m, A_p^{(1)},....,A^{p^{(p)}}]\mathbf{R}_{ss}^p = [E_p^c,0,....,0] \qquad (A.1)$$

The unknowns are the $\{A_p^{(i)}\}$ and E_p^c. The aim is to determine E_{p+1}^c and $\{A_{p+1}^{(i)}\}$ in a way that takes maximum advantage of the previous computations made to find E_p^c and $\{A_p^{(i)}\}$.

The method starts by trying an "obvious" solution, assuming that adding a zero to the previous solution may work. It would work if in the resulting equation

$$[I_m, A_p^{(1),....}A_p^{(p)},0]\mathbf{R}_{ss}^{p+1} = [E_p^c,0,...,0,\alpha_p] \qquad (A.2)$$

the term

$$\alpha_p = R_{ss}^{p+1} + \sum_1^{p-1} A_p^{(i)} R_{ss}^{p-i}$$

is zero. Since this will not happen in general, we have to find a way of forcing α_p to zero. For this we introduce the auxiliary (reversed) equations

$$[0,B_p^{(p)},...,B^{p^{(1)}}]\mathbf{R}_{ss}^{p+1} = [\beta_p,0,...,0,E_p^r] \qquad (A.3)$$

Next, we form a weighted combination of A.2 and A.3

$$[I_m, A_p^{(1)} + k_p^\alpha B_p^{(p)}, \ldots , k_p^\alpha]\mathbf{R}_{ss}^{p+1} = [E_p^c + k_p^\alpha \beta_p,0,...,\alpha_p + k_p^\alpha E_p^r]$$

from which it is easy to see that choosing

$$k_p^\alpha = -\alpha_p [E_p^r]^{-1}$$

gives a solution of the extended equation, i.e.

$$[I_m, A_{p+1}^{(1)}, \ldots , A_{p+1}^{(p+1)}] = [I_m, A_p^{(1)}, \ldots , A_p^{(p)},0] + k_p^\alpha[0,B_p^{(p)},...,B_p^{(1)},I_m].$$

Similarly, with the help of

$$k_p^\beta = -\beta_p [E_p^\epsilon]^{-1}$$

we can update the $\{B_p^{(i)}\}$ as

$$[B_{p+1}^{(p+1)},...,B_{p+1}^{(1)},I_m] = [0,B_p^{(p)},...,B_p^{(1)},I_m] + k_p^\beta [I_m,A_p^{(1)},...,A_p^{(p)},0]$$

The recursions for E_p^ϵ and E_p^r are

$$R_{p+1}^\epsilon = E_p^\epsilon - \alpha_p [E_p^r]^{-1}\beta_p$$

$$E_{p+1}^r = E_p^r - \beta_p [E_p^\epsilon]^{-1}\alpha_p$$

This concludes the multichannel prediction-error Levinson algorithm.

B. Joint multichannel complex least squares lattice (JMCLSL)

The multichannel least squares lattice algorithm is summarized as follows:

Initialization $(i = 0, 1,..., p)$

$$\mathbf{r}_i(-1) = 0 \ , \ i \neq p \tag{Ba}$$

$$\mathbf{E}_i^r(-1) = \epsilon I_m \ , \ i \neq p \tag{Bb}$$

$$\Delta_i(-1) = 0 \ , \ i \neq 0 \tag{Bc}$$

$$\gamma_{i-1}(-1) = 0 \ , \quad i \neq p \tag{Bd}$$

$$\mathbf{K}_i^f(i-1) = 0 \tag{Be}$$

Time update $(n \geq 0)$

$$e_o(n) = r_o(n) = x(n) \tag{Bf}$$

$$E_o^e(n) = E_o^r(n) = (1 - \alpha_{JCLSL}) E_o^r(n-1) + x(n)x^H(n) \tag{Bg}$$

$$\gamma_{-1}(n) = 0 \tag{Bh}$$

$$e_{-1}^d(n) = d(n) \tag{Bi}$$

Order update (i = 0,1,...,p)

Lattice

$$\Delta_i(n) = (1 - \alpha_{JCLSL}) \Delta_i(n-1) \tag{Bj}$$

$$- \frac{e_{i-1}(n)r_{i-1}^H(n-1)}{1 - \gamma_{i-2}(n-1)} \quad , \quad i \neq 0$$

$$K_i^e(n) = \Delta_i^H(n)E_{i-1}^{-1}(n) \quad , \quad i \neq 0 \tag{Bk}$$

$$K_i^r(n) = \Delta_i(n)E_{i-1}^{-1}(n-1) \quad , \quad i \neq 0 \tag{Bl}$$

$$e_i(n) = e_{i-1}(n) + K_i^r(n)r_{i-1}(n-1) \quad , \quad i \neq 0 \tag{Bm}$$

$$r_i(n) = r_{i-1}(n-1) + K_i^e(n)e_{i-1}(n) \quad , \quad i \neq 0 \tag{Bn}$$

$$E_i^e(n) = E_{i-1}^e(n) - \Delta_i(n)E_{i-1}^{-1}(n-1)\Delta_i^H(n) \quad , \quad i \neq 0 \tag{Bo}$$

$$E_i^r(n) = E_{i-1}^r(n-1) - \Delta_i^H(n)E_{i-1}^{-1}(n)\Delta_i(n) \quad , \quad i \neq 0 \tag{Bp}$$

$$\gamma_{i-1}(n) = \gamma_{i-2}(n) + r_{i-1}^H(n)E_{i-1}^r(n)r_{i-1}(n) \quad , \quad i \neq 0 \tag{Bq}$$

$$\Delta_i^d(n) = (1 - \alpha_{JCLSL})\Delta_i^d(n-1) - \frac{e_{i-1}^d(n)r_i^H(n)}{1 - \gamma_{i-1}(n)} \tag{Br}$$

$$K_i^q(n) = \Delta_i^q(n)E_i^{-\gamma}(n) \tag{Bs}$$

$$e_i^q(n) = e_{i-1}^q(n) + K_i^q(n)r_i(n) \tag{Bt}$$

Predictors

$$A_i^{(i)}(n) = K_i^r(n) \tag{Bu}$$

$$B_o^{(i)}(n) = K_i^c(n) \tag{Bv}$$

$$A_k^{(i)}(n) = A_k^{(i-1)}(n) + K_i^r(n)\ B_{k-1}^{(i-1)}(n-1) \tag{Bw}$$

$$1 \leq k \leq i-1$$

$$B_k^{(i)}(n) = B_{k-1}^{(i-1)}(n-1) + K_i^c(n)\ A_k^{(i-1)}(n) \tag{Bx}$$

REFERENCES

Alexandrou, D. and W.S. Hodgkiss (1981). "Preliminary processing of selected segments of the ARL/PSU FY80 field test data," Marine Physical Laboratory, Scripps Institution of Oceanography, San Diego, Ca., MPL TM-333.

Alexandrou, D. and W.S. Hodgkiss (1982a). "Initial processing of selected segments of the ARL/PSU FY80 field test data: Run ASP 3.1," Marine Physical Laboratory, Scripps Institution of Oceanography, San Diego, Ca., MPL TM-339.

Alexandrou, D. and W.S. Hodgkiss (1982b). "Initial processing of selected segments of the ARL/PSU FY80 field test data: Run ASP5.2," Marine Physical Laboratory, Scripps Institution of Oceanography, San Diego, Ca., MPL TM-340.

Alexandrou, D. and W.S. Hodgkiss (1982c). "Application of adaptive linear prediction structures to the prewhiteniing of the ARL/PSU FY80 field test data," Marine Physical Laboratory, Scripps Institution of Oceanography, San Diego, Ca., MPL TM-346.

Alexandrou, D. and W.S. Hodgkiss (1982d). "Complex adaptive one-step linear predictor algorithms," Marine Physical Laboratory, Scripps Institution of Oceanography, San Diego, Ca., MPL TM-341.

Alexandrou, D. and W.S. Hodgkiss (1982e). "Complex adaptive joint-process algorithms," Marine Physical Laboratory, Scripps Institution of Oceanography, San Diego, Ca., MPL TM-351.

Anderson, V.C. (1969). "DICANNE, a realizable adaptive process," Jour. Acous. Soc. Am. **45, no .2**, 398-405.

Anderson, V.C. and P. Rudnick (1969). "Rejection of a coherent arrival at an array," Jour. Acous. Soc. Am. **45, no. 2**, 406-410.

Anderson, W.B. (July 1981). "Volume reverberation characteristics of NUWES ranges," NUWES Report 1542.

Applebaum, S.P. and D.J. Chapman (Sept. 1976). "Adaptive arrays with main beam constraints," IEEE Trans. Antennas Propag. **AP-24**, 650-662.

Baker, B.B. and E.T. Copson (1939). *The mathematical theory of Huyghens principle* (Oxford Univ. Press, London).

Balakrishnan, A.V. "An adaptive non-linear data predictor," 1962 National Telemetry Conf. Proc., paper 6-5.

Balakrishnan, A.V. (Sept. 1964). "Effect of linear and non-linear signal processing on signal statistics," J. Res. NBS **68-D**, 953-965.

Barnard, G.R., C.W. Horton, M.K. Miller, and F.R. Spitznogle (1966). "Underwater sound reflection from a pressure-release sinusoidal surface," Jour. Acous. Soc. Am. **39**, 1162-1169.

145

146

Beckmann, P. (1965). "Scattering by composite rough surfaces," Proc. IEEE **53**, 1012-1015.

Bendat, J.S. and A.G. Piersol (1971). *Random data: Analysis and measurement procedures* (Wiley-Interscience, New York, N.Y.).

Brennan, L.E. and I.S. Reed (March 1973). "Theory of adaptive radar," IEEE Trans. Aerosp. Elec. Sys. **AES-9 No. 2**, 237-252.

Bruton, L.T. and D.A. Vaughnan-Pope (June 1976). "Synthesis of digital lattice filters from LC filters," IEEE Trans. Circ. Sys. **CAS-23, no. 6**, 395-402.

Buckley, J.P and R.J. Urick (1968). "Backscattering from the deep sea bed at small grazing angles," Jour. Acous. Soc. Am. **44 No. 2**, 648-650.

Burns, R.E. (1962). *A model of sedimentation in small sill-less embayed estuaries of the Pacific Nothwest* (Ph.D. Thesis, University of Washington, Seattle).

Chamberlain, S.G. and J.C. Galli (1983). "A model for numerical simulation of nonstationary sonar reverberation using linear spectral prediction," IEEE Jour. Ocean. Eng. **OE-8**, 21-36.

Chang, J.H. and F.B. Tuteur (1971). "A new class of adaptive array processors," Jour. Acous. Soc. Am. **49**, 639-649.

Chapman, R.P. and J.H. Harris (1962). "Surface backscattering strengths measured with explosive sound sources," Jour. Acous. Soc. Am. **34**, 1592-1597.

Clarke, G.L. (1970). "Light conditions in the sea in relation to the diurnal vertical migrations of animals," in *Proceedings of an international symposium on biological sound scattering in the ocean*, edited by G.B. Farquhar, pp. 41-48.

Clay, C.S. and H. Medwin (1964). "High frequency acoustical reverberation from a rough sea surface," Jour. Acous. Soc. Am. **36** (11), 2131-2135.

Clay, C.S. and H. Medwin (1977). *Acoustical Oceanography* (Wiley, New York, N.Y.).

Cox, C. and W. Munk (1954). "Measurement of the roughness of the sea surface from photographs of the sun's glitter," Jour. Opt. Soc. Am. **44**, 838.

Crombie, D.D. and J.M. Watts (1968). "Observations of coherent backscatter of 2-10 MHz radio surface waves from the sea," Deep-Sea Res. **15**, 81-87.

Cron, B.F. and C.H. Sherman (Nov. 1962). "Spatial correlation functions for various noise models," Jour. Acous, Soc. Am. **34, No.11**, 1732-1736.

Cushing, D.H. (1973). *The detection of fish* (Pergamon Press, New York, N.Y.).

Davisson, L.D. (April 1966). "A theory of adaptive filtering," IEEE Trans. Information Theory **IT-12**, 97-102.

Durbin, J. (1960). "The fitting of time series models," Rev. Inter. Statist. Inst. **28**, 233-244.

Ebbesmeyer, C.C. (1973). *Some observations of medium scale water parcels in a fjord: Dabob Bay, Washington* (Ph.D. Thesis, University of Washington, Seattle).

Eckart, C. (1953). "The scattering of sound from the sea surface," Jour. Acous. Soc. Am. **25**, 566-570.

Falconer, D.D. and L. Ljung (Oct. 1978). "Application of fast Kalman estimation to adaptive equilization," IEEE Trans. Communications **COM-26**, 1439-1446.

Faure, P. (1964). "Theoretical model of reverberation noise," Jour. Acous. Soc. Am. **36**, 259-266.

Fettweis, A., H. Levin, and A. Sedlmeyer (1974). "Wave digital lattice filters," Int. Jour. Circuit Theory Appl. **2**, 203-211.

Fisher, F.H. and E.D. Squier (1975). "Observation of acoustic layering and internal waves with a narrow-beam 87.5-kHz echo sounder," Jour. Acous. Soc. Am. **58**, 1315-1317.

Fortuin, L. (1970). "Survey of literature on reflection and scattering of sound waves at the sea surface," Jour. Acous. Soc. Am. **47**, 1209-1228.

Friedl, W.A. (1970). "Sonic scattering and its probable causes in two areas of Puget Sound," in *Proceedings of an international symposium on biological sound scattering in the ocean*, edited by G.B. Farquhar, pp. 527-548.

Friendlander, B., M. Morf, T. Kailath, and L. Ljung (1979). "New inversion formulas for matrices classified in terms of their distance from Toeplitz matrices," Linear algebra and its applications **27**, 31-60.

Friendlander, B. (Aug. 1982). "Lattice filters for adaptive processing," IEEE Proc. **70, No. 8**, 829-867.

Gabor, D., W.P.L. Wilby, and R. Woodcock (July 1960). "A universal non-linear filter, predictor and simulator which optimizes itself by a learning process," Proceedings IEE (London) **108, part B**, 422-435.

Gabriel, W.F. (Feb. 1976). "Adaptive arrays - An introduction," IEEE Proc. **64**, 239-272.

Gardner, R.R. (1973). "Acoustic backscattering from a rough surface at extremely low grazing angles," Jour. Acous. Soc. Am. **53 No.3**, 848-857.

Garrison, G.R., S.R. Murphy, and D.S. Potter (1960). "Measurements of the backscattering of underwater sound from the sea surface," Jour. Acous. Soc. Am. **32**, 104-111.

Gibbs, R.H. and C.F.E Roper (1970). "Ocean Acre preliminary report on vertical distribution of fishes and cephalopods," in *Proceedings of an international symposium*

on biological sound scattering in the ocean, edited by G.B. Farquhar, pp. 119-133.

Glaser, E.M. (April 1961). "Signal detection by adaptive filters," IRE Trans. Information Theory **IT-7**, 87-98.

Glover, J.R. Jr. (Dec. 1977). "Adaptive noise cancelling applied to sinusoidal interferences," IEEE Trans. Acous. Speech Sig. Proc. **ASSP-25, no.6**, 484-491.

Goddard, R.P (1985). "REVGEN, high-fidelity simulation of sonar signals," Applied Physics Laboratory, University of Washington, Seattle., APL-UW 8805.

Gray, A.H. Jr. and J.D. Markel (1975). "A normalized digital filter structure," IEEE Trans. Acous. Speech Sig. Proc. **ASSP-23, no. 3**, 268-277.

Greenblatt, P.R. (1980). *Observations of zooplankton patchiness using a high frequency sonar and a multiple sample plankton net* (Ph.D. thesis, University of California, San Diego).

Griffiths, L.J. (Oct. 1969). "A simple adaptive algorithm for real-time processing in antenna arrays," IEEE Proc. **57, No. 10**, 1696-1704.

Griffiths, L.J. (April 1975). "Rapid measurement of digital instantaneous frequency," IEEE Trans. Acous. Sp. Sig. Proc. **ASSP-23**, 207-222.

Griffiths, L.J. (May 1977). "A continuously adaptive filter implemented as a lattice structure," Proc. IEEE Int. Conf. Acous. Sp. Sig. Proc., 683-686.

Griffiths, L.J. (1978). "An adaptive lattice structure for noise-cancelling applications," IEEE Int. Conf. on Acous., Speech and Signal Proc., 87-90.

Hansen, D.S. (1984). *Considerations in upper ocean Doppler velocimetry* (Ph.D. thesis, University of California, San Diego).

Haykin, S., B.W. Carrie, and S.B. Kessler (1982). "Maximum entropy analysis of radar clutter," Proc. IEEE **70**, 953-962.

Hayre, H.S. and D.E. Kauffman (1965). "Plane-wave scattering from a rough surface with correlated large and small scale orders of roughness," Jour. Acous. Soc. Am. **41**, 599-603.

Helton, R.A. (Nov. 1976). "Ocenographic and acoustic characteristics of the Dabob Bay range," NAVTORPSTA Report 1300.

Hendershot, R.G. and W.C. Acker (1984). "Doppler techniques applied to fisheries hydroacoustics," Proc. OCEANS 84 conf., 15-20.

Hersey, J.B., R.H. Backus, and J. Hellwig (1962). "Sound scattering spectra of Deep Scattering Layers in the Western North Atlantic Ocean," Deep Sea Res. **8**, 196-210.

Hicks, B.L., N. Knable, J.J. Kovaly, G.S. Newell, J.P. Ruina, and C.W. Sherwin (March 1960). "The spectrum of X-band radiation backscattered from the sea surface," Jour. Geophys. Res. **65, no. 3**, 825-837.

Hodgkiss, W.S. and J.A. Presley (June 1981). "Adaptive tracking of multiple sinusoids whose power levels are widely separated," IEEE Trans. Circuits Syst. **CAS-28**, 550-561.

Holliday, D.V. (June 1974). "Doppler structure in echoes from schools of pelagic fish," Jour. Acous. Soc. Am. **55, No. 6**, 1313-1322.

Horton, C.W., S.K. Mitchell, and G.R. Barnard (1967). "Model studies on the scattering of acoustic waves from a rough surface," Jour. Acous. Soc. Am. **41**, 635-643.

Horton, C.W. and T.G. Muir (1967). "Theoretical studies on the scattering of acoustic waves from a rough surface," Jour. Acous. Soc. Am. **41**, 627-634.

Howells, P. "Intermediate frequency sidelobe canceller," U.S. Patent 2 202 990, Aug. 24 1965.

Igarashi, Y. and R. Stern (1971). "Observation of wind-wave-generated Doppler shifts in surface reverberation," Jour. Acous. Soc. Am. **49**, 802-809.

III, O.L. Frost (Aug. 1972). "An algorithm for linearly constrained adaptive array processing," IEEE Proc. **60, No. 8**, 926-935.

Isaacs, J.D., S.A. Tont, and G.L. Wick (1974). "Deep scattering layers: vertical migration as a tactic for finding food.," Deep-Sea Res. **21**, 651-656.

Itakura, F. and S. Saito (1971). "Digital filtering techniques for speech analysis and synthesis," Proc. 7th Int. Cong. Acous., 261-264.

Jackson, D.R. and K.Y. Moravan (Feb. 1984). "Horizontal spatial coherence of reverberation," Jour. Acous. Soc. Am. **75 no.2**, 428-436.

Jacobson, M.J. (July 1962). "Space-time correlation in spherical and circular noise fields," Jour. Acou. Soc. Am. **34, No. 7**, 971-978.

Jakowatz, C.V., R.L. Shuey, and G.M. White (Sept. 1960). "Adaptive waveform recognition," in *4 th London Symposium on Information Theory* (Butterworths, London), pp. 317-326.

Kailath, T. (March 1974). "A view of three decades of linear filtering theory," IEEE Trans. Inf. Th. **IT-20, No. 2**, 146-181.

Kampa, E. M. (1970). "Photoenvironment and sonic scattering," in *Proceedings of an international symposium on biological sound scattering in the ocean*, edited by G.B. Farquhar, pp. 51-58.

Kaye, G.T. (April 1978). "Backscattering from discrete targets at 87.5 kHz," Jour. Acous. Soc. Am. **64 no.2**, 556-562.

Kelly, J.L. Jr. and C.C. Lochbaum (1962). "Speech synthesis," Proc. 4th Int. Congress Acous., 1-4.

Kernighan, B.W. (1975). "RATFOR - A preprocessor for a rational fortran," Vol. 5, in *Software - Practice and experience*, pp. 395-406.

Kolmogorov, A.N. (April 1962). "Interpolation and extrapolation of stationary random sequences," Bull. Acad. Sci. USSR Ser. Math. **5**.

Lacoss, R.T. (May 1968). "Adaptive combining of wideband array data for optimal reception," IEEE Trans. Geosc. Elec. **GE-6, No. 2,** 78-86.

Lawson, C.L. and R.J. Hanson (1974). *Solving least squares problems* (Prentice-Hall, Englewood Cliffs, N.J.).

Levinson, N. (Jan. 1947). "The Wiener rms (root-mean-square) error criterion in filter design and prediction," Jour. Math. Phys. **25**, 261-278.

Lhermitte, R. (Jan. 1983). "Doppler sonar observation of tidal flow," Jour. Geophys. Res. **88, no.** C1, 725-742.

Liebermann, L.N. (1963). "Analysis of rough surfaces by scattering," Jour. Acous. Soc. Am. **35**, 932.

Lippmann, B.A. (1953). "Note on the theory of gratings," Jour. Opt. Soc. Am. **43**, 408.

Lucky, R.W. (April 1965). "Automatic equalization for digital communication," Bell Sys. Tech. Journal **24**, 547-588.

Lysanov, Y.P. (1958). "Theory of the scattering of waves at periodically uneven surfaces," Sov. Physics - Acoustics **4**, 1-10.

Makhoul, J. (April 1975). "Linear prediction: A tutorial review," Proc. IEEE **63**, 561-580.

Makhoul, J. (Oct. 1977). "Stable and efficient lattice methods for linear prediction," IEEE Trans. Acous. Sp. Sig. Proc. **ASSP-25**, 423-428.

Makhoul, J. (Aug. 1978). "A class of all-zero lattice digital filters: Properties and applications," IEEE Trans. Acous. Sp. Sig. Proc. **ASSP-26, No. 4**, 304-314.

Markel, J.D. and A.H. Gray, Jr. (1975). "Roundoff noise characteristics of a class of orthogonal polynomial structures," IEEE Trans. Acous. Speech Sig. Proc. **ASSP-23**, 473-486.

Markel, J.D. and A.H. Gray, Jr. (1978). *Linear prediction of speech* (Springer-Verlag, Berlin).

McKinney, C.M. and C.D. Anderson (1964). "Measurements of backscattering of sound from the ocean bottom," Jour. Acous. Soc. Am. **36 No.1**, 158-163.

Medwin, H. (1966). "Specular scattering of underwater sound from a wind-driven surface," Jour. Acous. Soc. Am. **41 No.6**, 1485-1495.

Middleton, D. (1967a). "A statistical theory of reverberation and similar first-order scattered fields, part I: Waveforms and the general process," IEEE Trans. Information Theory IT-13, 372-392.

Middleton, D. (1967b). "A statistical theory of reverberation and similar first-order scattered fields, part II: Moments, spectra and special distributions," IEEE Trans. Information Theory IT-13, 393-414.

Middleton, D. (1972a). "A statistical theory of reverberation and similar first-order scattered fields: part III: Waveforms and fields," IEEE Trans. Information Theory IT-18, 35-67.

Middleton, D. (1972b). "A statistical theory of reverberation and similar first-order scattered fields: part IV: Statistical models," IEEE Trans. Information Theory IT-18, 68-90.

Miller, K.S. and M.M. Rochwarger (Sept. 1972). "A covariance approach to spectral moment estimation," IEEE Trans. Inform. Theory IT-18, no. 5, 588-596.

Morf, M., D.T. Lee, J.R. Nichols, and A. Viera (April 1977). "A classification of algorithms for ARMA models and ladder realizations," Proc. IEEE Conf. on Acous. Speech and Sig. Proc., 13-19.

Morf, M., A. Viera, and D.T. Lee (Dec. 1977). "Ladder forms for identification and speech processing," Proc. IEEE Conf. D&C, 1074-1078.

Morf, M., B. Dickinson, T. Kailath, and A. Viera (Oct. 1977). "Efficient solution of covariance equations for linear prediction," IEEE Trans. Acous. Speech Sig. Proc. ASSP-25, no. 5, 429-433.

Morf, M. and D.T. Lee (Jan. 1978). "Recursive least-squares ladder forms for fast parameter tracking," Proc. IEEE Conf. Decision and Control, 1326-1367.

Moustier, C. de and M.C. Kleinrock (1985a). "Bathymetric artifacts in Sea Beam data: how to recognize them, what causes them," Jour. Geophys. Res. (in press).

Moustier, C. de (1985b). "Beyond bathymetry: mapping acoustic backscattering from the deep seafloor with Sea Beam," Jour. Acous. Soc. Am. (submitted).

Moustier, C.P. de (1985). "Inference of manganese nodule coverage from Seabeam acoustic backscattering data," Geophysics 50, 989-1001.

Ol'shevskii, V.V. (1967). *Characteristics of sea reverberation* (Colsultants Bureau, New York, N.Y.).

Oppenheim, A.V. and R.W. Schafer (1975). *Digital signal processing* (Prentice-Hall, Englewood Cliffs, N.J.).

Orr, M.H. and F.R. Hess (1978). "Remote acoustic monitoring of industrial chemical waste released at Deep Water Dumpsite 106," Jour. Geophys. Res. 83, 6145-6154.

Pidgeon, V.W. (Feb. 1968). "Doppler dependence of radar sea return," Jour. Geophys. Res. **73, no. 4,** 1333-1341.

Pincock, D.G. (1978). "The feasibility of Doppler sonar fish counting," IEEE Jour. Ocean. Eng. **OE-3 No.2,** 37-40.

Pinkel, R. (1980). "Acoustic doppler techniques," in *Air-Sea Interaction* (Plenum Publishing Corp., New York, N.Y.), pp. 171-199.

Pinkel, R. (1981). "On the use of Doppler sonar for internal wave measurements," Deep-Sea Res. **28A, no. 3,** 269-289.

Plemons, T.D., J.A. Shooter, and D. Middleton (1972). "Underwater acoustic scattering from lake surfaces. I. Theory, experiment and validation of the data," Jour. Acous. Soc. Am. **52 No.5 (part 2),** 1487-1502.

Plemons, T.D., J.A. Shooter, and D. Middleton (1972). "Underwater acoustic scattering from lake surfaces. II. Covariance functions and related statistics," Jour. Acous. Soc. Am. **52 No.5 (part 2),** 1503-1515.

Pollard, R.T. (1970). "On the generation by winds of inertial waves in the ocean," Deep-Sea Res. **17,** 795-812.

Princehouse, D.W. (1977). "REVGEN, a real time reverberation generator," Proc. IEEE Int. Conf. on Acoustics, Speech and Signal Processing., 827-835.

Proni, J.R., F. Ostapoff, and R.L. Sellers (1978). "Acoustic observations of high-frequency, near-surface internal wave groups in the deep ocean during GATE," Deep Sea Res. **23,** 299-307.

Proud, J.M., R.T. Beyer, and P. Tamarkin (1960). "Reflection of sound from randomly rough surfaces," Jour. Appl. Phys. **31,** 543-552.

Rayleigh, J.W. Strutt, Lord (1945). *Theory of sound* (Dover, New York, N.Y.).

Regier, L. (Aug. 1982). "Mesoscale current fields observed with a shipboard profiling acoustic meter," Jour. Phys. Oceanography **12,** 880-886.

Rice, S.O. (1951). "Reflections of electromagnetic waves from slightly rough surfaces," Commun. Pure Appl. Math **4,** 351.

Riegler, R.L. and R.T. Compton Jr. (June 1973). "An adaptive array for interference rejection," IEEE Proc. **61,** 748-758.

Rummler, W.D. (1968). "Introduction of a new estimator for velocity spectral parameters," Bell Telephone Laboratories, Whippany, New Jersey, Technical Memo MM-68-4141-5.

Satorius, E.H. and J.D. Pack (April 1979). "Least squares adaptive algorithms," Naval Ocean Systems Center (NOSC) TR-423.

Satorius, E.H. and S.T. Alexander (June 1979). "Channel equalization using adaptive lattice algorithms," IEEE Trans. Communications COM-27, NO. 6, 899-905.

Schade, C.M. (Aug. 1971). "Optimal regulation of physiological systems via real-time adaptive model synthesis," SEL-71-003. Stanford Electronics Laboratories, Stanford University.

Shor, S.W.W. (Jan. 1966). "Adaptive technique to discriminate against coherent noise in a narrow-band system," J. Acoust. Soc. Am. 39, 74-78.

Stewart, G.W. (1973). *Introduction to matrix computations* (Academic Press, London).

Swarts, R.L. (1972). "Doppler shift of surface reverberation," Jour. Acous. Soc. Am. 52, No.1, 457-461.

Szego, G. (1939). "Orthogonal polynomials," Amer. Math. Soc. Colloq. Publ. 23.

Theriault, K.B. (1981). "Bounds on pulsed-Doppler current profiler performance," Bolt, Benarek and Newman, Cambridge, Mass., Technical Memo 634.

Thomson, W.T. (Feb. 1950). "Transmission of elastic waves through a stratified solid medium," Jour. Applied Physics 21, 80-93.

Thorpe, S.A. (1982). "On the clouds of bubbles formed by breaking wind-waves in deep water, and their role in air-sea gas transfer," Phil. Trans. R. Soc. London A304, 155-210.

Twersky, V. (1951). "On the nonspecular reflection of sound from planes with absorbent bosses," Jour. Acous. Soc. Am. 23, 336-338.

Uretsky, J.L. (1965). "The scattering of plane waves from periodic surfaces," Ann. Phys. 33, 400-427.

Urick, R.J. and R.M. Hoover (1956). "Backscattering of sound from the sea surface; its measurement, causes and application to the prediction of reverberation levels," Jour. Acous. Soc. Am. 28, 1038-1042.

Urick, R.J. and G.R. Lund (Nov. 1964). "Vertical coherence of explosive reverberation," Jour. Acous. Soc. Am. 36 No.11, 2164-2170.

Urick, R.J. and G.R. Lund (1970). "Horizontal coherence of explosive reverberation," Jour. Acous. Soc. Am. 47 No.3 (part 2), 909-911.

Urick, R.J. and G.R. Lund (1970). "Vertical coherence of shallow-water reverberation," Jour. Acous. Soc. Am. 47 No.1 (part 2), 342-349.

Urick, R.J. (1975). *Priciples of underwater sound* (McGraw-Hill, New York, N.Y.).

Valenzuela, G.R. and M.B. Laing (Jan. 1970). "Study of Doppler spectra of radar sea echo," Jour. Geophys. Res., 551-563.

154

Van Trees, H.L. (1968). *Detection, estimation and modulation theory, part I* (John Wiley, New York, N.Y.).

Wakita, H. (Oct. 1973). "Direct estimation of the vocal tract by inverse filtering of acoustic speech waveforms," IEEE Trans. Audio Electroacoustics **AU-21**, 417-427.

Weller, R.A., J.P. Dean, J. Marra, J.F. Price, E.A. Francis, and D.C. Boardman (1985). "Three-dimensional flow in the upper ocean," Science **227**, 1552-1556.

Whittle, P. (1963). "On the fitting of multivariate autoregressions and the approximate canonical factorization of a spectral density matrix," Biometrica **50**, 129-134.

Widrow, B. and M. Hoff, Jr. (1960). "Adaptive switching circuits," IRE WESCON Conv. Rec., pt 4, 96-104.

Widrow, B., P.E. Mantey, L.J. Griffiths, and B.B. Goode (Dec. 1967). "Adaptive antenna systems," IEEE Proc. **55**, 2143-2159.

Widrow, B., J.R. Glover, J.M. McCool, J. Kaunitz, C.S. Williams, R.H. Hearn, J.R. Zeidler, E. Dong, Jr., and R.C. Goodlin (Dec. 1975). "Adaptive noise cancelling: Principles and applications," IEEE Proc. **63, No. 12**, 1692-1716.

Widrow, B., J.M. McCool, M.J. Larimore, and C.R. Johnson, Jr. (Aug. 1976). "Stationary and nonstationary learning characteristics of the LMS adaptive filter," IEEE Proc. **64, No. 8**, 1151-1162.

Wiener, N. (1949). *Extrapolation, interpolation and smoothing of stationary time series with engineering applications* (Technology Press and Wiley, New York).

Wiggins, R.A. and E.A. Robinson (April 1965). Jour. Geophys. Res. **70**, 1885-1891.

Wilson, G.R. (Dec. 1982). "Comparison of the measured covariance of surface reverberation for horizontal and vertical arrays," Jour. Acous. Soc. Am. **72 No. 6**, 1905-1910.

Wilson, G.R. and M.E. Frazer (March 1983). "Horizontal covariance of surface reverberation: Comparison of a point-scatterer model to experiment," Jour. Acous. Soc. Am. **73 No.3**, 749-760.

Wold, H. (1938). *A study in the analysis of stationary time series* (Almqvist and Wiksell, Uppsala, Sweden).

Zahm, C.L. (March 1973). "Application of adaptive arrays to suppress strong jammers in the presence of weak signals," IEEE Trans. Aerosp. Elec. Sys. **AES-9, No. 2**, 260-271.

Zedel, L.J. (1985). *Evaluation of an acoustic Doppler profiler and its application to the study of stratified flow in a fjord* (M.S. thesis, University of Victoria, Canada).

Chief of Naval Research
Department of the Navy
Arlington, Virginia 22217
    Code 12, 122(2), 102C
    111, 112, 113,
    1122PO, 425-AC, 460

ONRDET
NSTL Station
Bay St. Louis, Mississippi 39529
    Code 112, 1121, 1122CS, 422CB,
    1122PO, 1125GG

Director
Office of Naval Research
Branch Office
1030 East Green Street
Pasadena, California 91101

Commander
Naval Sea Systems Command
Washington, D. C. 20362
    Code 63, 63R, 63R-23

Defense Advanced Res. Proj. Agency
TTO - Tactical Technology Office
1400 Wilson Boulevard
Arlington, Virginia 22209
    Atten: CDR Kirk Evans

Commander
Naval Air Systems Command
Washington, D. C. 20361
    Code 370

Commander
Naval Ship Res. & Dev. Center
Bethesda, Maryland 20084

Director
Strategic Systems Proj. Ofc. (PM-1)
Department of the Navy
Washington, D. C. 20361
    Code NSP-2023

Commander
Naval Surface Combat Systems Center
White Oak
Silver Spring, Maryland 20910

Commanding Officer
Civil Engineering Laboratory
Naval Construction Battalion Center
Port Hueneme, California 93043
    Code L40, L42

Director of Research
U.S. Naval Research Laboratory
Washington, D. C. 20375
    Code 2620, 2627, 5000, 5100, 5800

Commanding Officer
Naval Ocean Research and
    Development Activity (NORDA)
NSTL Station
Bay. St. Louis, Mississippi 39529
    Code 100, 110, 300, 330,
    340, 350, 360, 500

Commander
U.S. Naval Oceanographic Office
NSTL Station
Bay St. Louis, Mississippi 39522
    Bill Jobst

Commander
Submarine Development Group ONE
Fleet Post Office
San Diego, California 92152

Commander
Naval Wafare Systems Command
Washington, D. C. 20360
    Code PME-124, 320A

Commanding Officer
U.S. Naval Air Development Center
Attention: Jim Howard
Warminister, Pennsylvania 18974

Executive Secretary, Naval Studies
    Board
National Academy of Sciences
2101 Constitution Avenue, N.W.
Washington, D.C. 20418

Commander
Naval Ocean Systems Center
San Diego, California 92152
    Code 00, 01, 16, 94, 531
    . 5301, 71, 72

Commanding Officer
Naval Underwater Systems Center
Newport, Rhode Island 20844
    John D'Albora

Officer in Charge
Naval Underwater Systems Center
New London Laboratory
New London, Connecticut 06320
    Code 900, 905, 910, 930, 960

Assistant Secretary of the Navy
(Research Engineering & Systems)
Department of the Navy
Washington, D. C. 20350

Commanding Officer
Naval Coastal Systems Laboratory
Panama City, Florida 32401

Director
Defense Documentation Center
(TIMA), Cameron Station
5010 Duke Street
Alexandria, Virginia 22314

Institute for Defense Analyses
400 Army-Navy Drive
Arlington, Virginia 22202

Chief Scientist
Navy Underwater Sound Reference Div.
U.S. Naval Research Laboratory
P.O. Box 8337
Orlando, Florida 32806

Supreme Allied Commander
U.S. Atlantic Fleet
ASW Research Center, APO
New York, New York 09019
    Via: ONR 100 M, CNO OP092D1,
    Secretariat of Military,
    Information Control, Committee

Director
College of Engineering
Department of Ocean Engineering
Florida Atlantic University
Boca Raton, Florida 33431

Director
Applied Research Laboratory
Pennsylvania State University
P.O. Box 30
State College, Pennsylvania 16802

Director
Lamont-Doherty Geological Observatory
Torrey Cliff
Palisades, New York 10964

Director
The Univ. of Texas at Austin
Applied Research Laboratory
P.O. Box 8029
Austin, Texas 78712

Director
Woods Hole Oceanographic Institution
Woods Hole, Massachusetts 02543

National Science Foundation
Washington, D. C. 20550

STOIAC
Battelle Columbus Laboratories
505 King Avenue
Columbus, Ohio 43201

National Oceanic & Atmospheric
    Administration
Ocean Engineering Office
6001 Executive Boulevard
Rockville, Maryland 20852

Superintendent
U.S. Naval Postgraduate School
Monterey, California 93940

Director
Institute of Marine Science
University of Alaska
Fairbanks, Alaska 99701

Director
Applied Physics Laboratory
Johns Hopkins University
Johns Hopkins Road
Laurel, Maryland 20810
    Atten: J. R. Austin

Director
Marine Research Laboratories
c/o Marine Studies Center
University of Wisconsin
Madison, Wisconsin 53706

Director
Applied Physics Laboratory
University of Washington
1013 East 40th Street
Seattle, Washington 98105

Director
Inst. of Ocean Science Engineering
Catholic University of America
Washington, D.C. 20017

Office of Naval Research
Resident Representative
c/o Univ. of California, San Diego
La Jolla, California 92093

University of California, San Diego
Marine Physical Laboratory Branch Office
La Jolla, California 92093

December 1985